On the spin-Peierls phase transition of frustrated Heisenberg chains

Inaugural-Dissertation
zur
Erlangung des Doktorgrades
der Mathematisch-Naturwissenschaftlichen Fakultät
der Universität zu Köln

vorgelegt von
Rainer Raupach
aus Berlin

Köln 2000

Contents

Chapter 1

Introduction

One-dimensional systems (1-d) provide a fascinating and challenging area of activity from a theoretical point of view. There are basically three reasons. First, 1-d systems show interesting phenomena and rich phase diagrams[1] due to strong quantum fluctuations. Second, the topological structure allows several analytical approaches such as for instance Bethe-Ansatz (BA) [see e.g. [1]] and conformal field theory (CFT) [see e.g. [2]] as well as numerical studies. Besides techniques as exact diagonalization and quantum Monte-Carlo [3] the density matrix renormalization group (DMRG) [4] plays a crucial role. Particularly, this holds for non-integrable systems. Thus, several tools are available to access one-dimensional systems. Third, many compounds exhibit distinct chain structures as microscopic interactions along a certain direction dominate in comparison to the perpendicular couplings. They can be modeled appropriately by 1-d systems. Hence, in contrast to naive expectations theoretical results can be compared directly to experimental measurements in many cases.

Since the discovery of $CuGeO_3$ as the first inorganic spin-Peierls (SP) compound [5, 6] this substance has played a key role among the quasi 1-d systems. The SP phase transition, which is the analogue of the well known Peierls transition [7], is of particular interest. The quantum

[1] This has to be understood in the sense of zero temperature quantum phase transitions. Note that phase transitions at finite temperature are only possible if the pure 1-d system couples to a higher dimensional background.

mechanical effects manifest in its driving force. Since the ground state of quantum antiferromagnets is a singlet the system tends to form local spin-singlets each of two adjacent spins. This is the basic prerequisite to explain the instability towards modulations. Phenomenologically, spin-Peierls systems show rich phase diagrams and complex phenomena which can be understood within one-dimensional approaches.

The first experimental observation of the SP transition in *organic* materials was already obtained in the 1970s [8–13]. The discovery of $CuGeO_3$, however, as the first and up to now only *inorganic* SP compound has renewed the interest in this phenomenon. Large crystals of high quality can now be synthesized allowing for a variety of very precise experimental studies. The relevant magnetic moments are aligned in chains embedded in the 3-d lattice. The magnetic interactions are interceded by microscopic exchange mechanisms and prove to be dominant along the chain direction. As a consequence, one-dimensional systems are suitable to model $CuGeO_3$ and to perform detailed analysis of several phenomena. Therefore, $CuGeO_3$ has attracted much attention in experimental as well as in theoretical works.

An experimental survey of the structure of $CuGeO_3$ suggets a description by modulated Heisenberg chains with an additional next-nearest-neighbour interaction, usually referred to as frustration. Within an adiabatic treatment of the phonons zero temperature as well as finite temperature properties were shown to be consistent [14–20]. As these models are non-integrable one has to fall back on numerical methods to obviate perturbative approaches. Especially the finite temperature physics are a sophisticated task. With respect to this, the recently developed transfer-matrix DMRG (TMRG) on the basis of transfer-matrices provides an exceedingly powerful tool. It is based on an idea of S.R. White [4] and was extended to finite temperatures subsequently [21, 22]. Since then, the potential of TMRG has been demonstrated in several applications [23]. The attained accuracy explicitly exceeds that of other numerical techniques.

The purpose of the present thesis is twofold. First, frustrated and dimerized Heisenberg chains are studied. The qualitative behaviour of thermodynamical quantities, particularly susceptibilities, is strongly depending on the frustration parameter which affects the phase transition with respect to microscopic parameters. This is important from a theoretical point of view. The TMRG allows the calculation of several properties for the given microscopic model circumventing perturbative methods. On the other hand, the theoretical findings are compared to experiments on $CuGeO_3$. This affects thermodynamical data as well as predictions on the phase transitions. Within this quasi one-dimensional approach involving adiabatic phonons a remarkable agreement is obtained in many cases.

In the next chapter the basic ideas of the DMRG are presented. Thereupon, chapter 3 illustrates the extension to finite temperatures. An adiabatic description of the SP phase transition and a review of important properties of $CuGeO_3$ are given in chapter 4. The SP transition at finite temperature is investigated on the basis of the TMRG. We focus on thermodynamics in the dimerized phase, non-universal effects of the dimerization susceptibility and the influence of an external pressure on the critical temperature and microscopic parameters. Chapter 5 is dedicated to the investigation of static dimer-dimer correlation functions which allows to access the transition from the high temperature into the incommensurate phase. In particular, the effect of an external magnetic field and the phase diagram are analyzed. Finally, summary and outlook onto open questions are given in chapter 6.

Chapter 2

Density-matrix-renormalization-group

The formulation of the density-matrix-renormalization-group (DMRG) by S.R. White in 1992 [4] was an important achievement in renormalization group (RG) methods. Apart from analytical applications [see [24,25] and references therein] it has turned out to be a very powerful numerical tool to analyze quasi one-dimensional quantum lattice systems with short range interaction [see e.g. [26] as a general reference]. The main task of this "standard" DMRG is the investigation of properties of the ground state, e.g. ground state energy, low lying excitations and zero temperature correlations. The recently developed quantum transfer-matrix DMRG (TMRG) allows to study thermodynamic quantities such as thermodynamical potentials, specific heat and susceptibilities [21,22]. In general, the attained accuracy exceeds that of other numerical methods like exact diagonalization especially at low temperatures. Of course, this temperature region is of highest interest with respect to strong quantum effects. Recently, variants of the DMRG have also been applied to classical systems, stochastic problems and questions of molecular physics [27].

2.1 Renormalization group

The basic idea of RG techniques in general is to integrate out unimportant degrees of freedom progressively using a sequence of renormalization group transformations. The RG was proposed by Wilson [28] to study the critical behaviour of any desired system justified by the hypothesis that critical phenomena are characterized by the physics on large length scales. Typically, the renormalization procedure can be carried out in real-space [29] or momentum-space [30].

In the context of DMRG the main objective is to find the ground state and the corresponding energy for a very large system. The procedure starts with a numerical representation of a small system which can be diagonalized exactly. Subsequently, the system is enlarged, then reduced to a fixed number of basis states in the renormalization step. An iterative application increases the effective system size yielding approximate results for the thermodynamic limit. Obviously, the crucial problem is to select an appropriate basis for the truncation procedure. Wilson formulated a numerical real-space RG to solve the (one-dimensional) Kondo problem [31]. The conducting electrons are mapped to a semi-infinite quantum lattice model with exclusively nearest-neighbour interaction where the first site represents the impurity. Starting from a system with length L the hamiltonian H_L is diagonalized. Then, the operator H_L is projected onto the m lowest eigenvalues and a site is added in order to build H_{L+1} [see Fig. 2.1]. The interaction beetween the block of length L and the additional site has to be reconstructed. Finally, H_L is substituted by H_{L+1} and the procedure is repeated starting from the diagonalization. Due to the truncation the Hilbert space never exceeds a certain size and the computational effort, i.e. memory and CPU-time, is of order $\mathcal{O}(L)$.

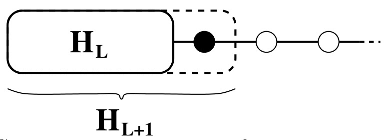

Figure 2.1: Schematic diagram of Wilson's RG algorithm.

The principal assumption in this approach is that the energetically lowest eigenstates in the block are relevant to represent the final ground state. In the Kondo problem studied this situation is realized since each site along the chain corresponds to an exponentially decreasing energy scale [31] due to localization. Other interesting one-dimensional quantum models, such as the Heisenberg or the Hubbard model, do not provide this advantageous feature. Therefore, the accuracy declines considerably after a few iterations [32,33]. Hence, in general the energy of the block states is not an appropriate measure. The obvious problem is to choose convenient boundary conditions in the diagonalization step. However, this difficulty is automatically solved by using a density matrix, which optimizes the vectors of the reduced basis with respect to the representation of the ground state. The concept of DMRG combines the optimal truncation with an iterative enlargement of the system.

2.2 Density matrix

The problem how to find the optimal truncated basis was solved by White [4]. For illustration we consider a one-dimensional quantum system with an arbitrary length. The system is devided into two *blocks* $\mathbf{B}$ ($\mathbf{B}'$) labeled by orthonormalized sets of eigenstates $\{|i\rangle_l, i = 1, ..., k_l\}$ and $\{|i\rangle_r, i = 1, ..., k_r\}$.

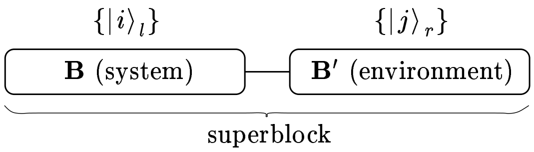

For numerical purposes $\mathbf{B}$ and $\mathbf{B}'$ are often chosen to be identical for practical reasons, i.e. $\mathbf{B}$=$\mathbf{B}'$. We restrict ourselves to this case for simplicity, i.e. $k_l = k_r =: k$. The complete system, the so-called *superblock*, is assumed to be in the pure (normalized) *target state*

$$|\psi\rangle = \sum_{i,j} \psi_{i,j} \, |i\rangle_l \, |j\rangle_r \, . \tag{2.1}$$

Typically, $|\psi\rangle$ represents the ground state or the eigenstate corresponding to a low lying excitation. The *system block* is considered to be embedded in the superblock whereas the rest acts as *environment.* We now ask for the probability $p(i_0)$ that the system block is in the state

$|i_0\rangle_l$. Using the projector

$$P_{i_0} = |i_0\rangle_l\,{}_l\langle i_0| \sum_j |j\rangle_r\,{}_r\langle j| \tag{2.2}$$

this probability reads

$$p(i_0) = \langle\psi|P_{i_0}|\psi\rangle = \sum_j \psi^*_{i_0,j}\psi_{i_0,j}, \tag{2.3}$$

where eq. (2.1) was used for the explicit expression. We notice that $p(i_0)$ is a diagonal element of the matrix

$$\rho_{i,i'} = \sum_j \psi^*_{i,j}\psi_{i',j}. \tag{2.4}$$

Eq. (2.4) defines a reduced density matrix with respect to the system block. Obviously, ρ is a hermitian operator and the condition $\mathrm{Tr}\,\rho = 1$ is fulfilled due to normalization of the target state. Let ρ have the eigenstates $|u^\alpha\rangle$ $(\alpha = 1, ..., k)$ with eigenvalues w_α. Then

$$w = \langle u|\,\rho\,|u\rangle = \sum_{i,i'} u^*_i\rho_{i,i'}u_{i'} = \sum_j \left|\sum_i u_i\psi_{i,j}\right|^2 \geq 0, \tag{2.5}$$

i.e. all eigenvalues are positive semi-definite. We assume the eigenvaues to be sorted by magnitude, i.e. $w_0 \geq w_1 \geq ... \geq w_k$. If $\hat{\mathcal{O}}$ denotes an arbitrary operator acting on the system block the expectation value with respect to $|\psi\rangle$ reads

$$\langle\psi|\hat{\mathcal{O}}|\psi\rangle = \mathrm{Tr}\left\{\rho\,\hat{\mathcal{O}}\right\} = \sum_\alpha w_\alpha\,\langle u^\alpha|\,\hat{\mathcal{O}}\,|u^\alpha\rangle\,. \tag{2.6}$$

This result was expected since w_α is nothing else than the probability of the system block being in the state $|u^\alpha\rangle$ from (2.3). To approximate this expectation value by a truncated basis we can neglect eigenstates with $w_\alpha \ll 1$ without appreciable loss of accuracy. More precisely, we want to represent $|\psi\rangle$ in a reduced subsystem with $m \leq k$ states optimally. First, we construct an approximation of the target state, which can be written as

$$|\psi\rangle \approx |\tilde{\psi}\rangle = \sum_{i,j=1}^{m} \widetilde{\psi}_{i,j} \, |i\rangle_l \, |j\rangle_r \tag{2.7}$$

without loss of generality. This expansion is not exact, if m is actually smaller than the number of states in the system block. In order to find the optimal truncated basis we have to minimize

$$S = \left\| |\psi\rangle - |\tilde{\psi}\rangle \right\|^2 \tag{2.8}$$

by varying $|i\rangle_l$, $|j\rangle_r$ and $\widetilde{\psi}_{i,j}$ under the constraint $\sum_{i,j} |\widetilde{\psi}_{i,j}|^2 = 1$. The matrix notation of eq. (2.8) then reads

$$S = \sum_{i,j} \left| \psi_{i,j} - \widetilde{\psi}_{i,j} \right|^2 = \mathrm{Tr}\left\{ (\psi - \widetilde{\psi})^\dagger (\psi - \widetilde{\psi}) \right\}, \tag{2.9}$$

where we have to vary $|i\rangle_l$, $|j\rangle_r$ (defining $\psi_{i,j}$) and $\widetilde{\psi}_{i,j}$ with $\widetilde{\psi}_{i,j} = 0$ for i or $j = m+1, ..., k$. This minimization procedure succeeds using the singular value decomposition (SVD) from linear algebra. The SVD-theorem yields the representation

$$\psi = UDV^\dagger, \tag{2.10}$$

where U, V are unitary and D is a diagonal matrix with non-negative elements, the so-called singular values of ψ. Inserting eq. (2.10) into the definition of the density matrix [cf. eq. (2.4)] leads to

$$\rho = UD^2U^\dagger. \tag{2.11}$$

Therefore, the squares of the singular values of ψ are the eigenvalues of the density matrix. The transformation matrix U simply contains the eigenvectors of ρ in the rows. We apply the SVD transformation also to the approximated state, which defines $\widetilde{D} := U^\dagger \widetilde{\psi} V$. Now, we rewrite eq. (2.9) using the properties of the trace,

$$\begin{aligned} S &= \mathrm{Tr}\left\{ (D - \widetilde{D})^\dagger (D - \widetilde{D}) \right\} \\ &= \sum_{i,j} \left| D_{i,j} - \widetilde{D}_{i,j} \right|^2. \end{aligned} \tag{2.12}$$

Since D is a diagonal matrix, the minimization directly implies $\widetilde{D}_{i,j} = 0$ for $i \neq j$, i.e. $\widetilde{D}$ must also be diagonal. Due to the representation (2.7) at least $k - m$ of the diagonal entries of $\widetilde{D}$ have to be zero, say $\widetilde{D}_{i,i} = 0$ for $i = m + 1, ..., k$. Finally, the truncated basis set is optimal if $\widetilde{D}_{i,i}$ for $i = 1, ..., m$ are the m largest singular values of ψ which correspond to the m largest eigenvalues of the density matrix. The explicit representation of the optimally approximated state thus reads

$$\widetilde{\psi}_{\mathrm{opt}} = U \begin{pmatrix} \sqrt{w_0} & & & & & \\ & \ddots & & & & \\ & & \sqrt{w_m} & & & \\ & & & 0 & & \\ & & & & \ddots & \\ & & & & & 0 \end{pmatrix} V^{\dagger}, \tag{2.13}$$

where U, V are defined by the SVD of ψ [cf. eq. (2.10)] and the (diagonal) entries are sorted by magnitude. We like to note that the SVD does not play a role in numerics but is used formally for a dressy formulation to find the optimal truncated basis. Practically, relevant operators are projected onto this certain basis which refers to (2.6) in a sense [see the DMRG algorithm in section 2.3]. However, the formal proof shows that the density matrix succeds also in a more general context, namely showing a norm of an operator to be optimized.

The probability interpretation of the eigenvalues w_α of ρ allows an estimation of the so-called *discarded weight* P_m which measures the error due to the cutoff,

$$P_m = 1 - \sum_{\alpha=1}^{m} w_\alpha. \tag{2.14}$$

Accordingly, the distribution of the weights plays a crucial role. For some integrable models the eigenvalues of the density matrix can be obtained exactly [34]. The distribution shows an exponential decay of the weights w_α. Therefore, the discarded weight falls rapidly with the number m. We will not perform a quantitative analysis here. As the method mainly used in this work is the TMRG the magnitude of errors will be studied in the dedicated chapter.

A generalization of the "simple" density matrix is to use *multiple target states* $|\psi_1\rangle, ..., |\psi_N\rangle$, for instance a mixed state. Let W_μ be the probability that the superblock is in the state $|\psi_\mu\rangle$. If ρ_μ is the density matrix for the pure target state $|\psi_\mu\rangle$, then the complete density matrix of the mixed state reads [35]

$$\rho = \sum_\mu W_\mu \rho_\mu, \tag{2.15}$$

if we optimize <u>one common</u> reduced basis. A typical application is to assume the superblock at finite temperature, i.e. W_μ represents the (normalized) Boltzmann weight corresponding to the energy of the state $|\psi_\mu\rangle$. Of course, the accuracy declines as the error due to the cutoff for a fixed m grows. This can easily be understood if we consider very large temperatures, i.e. $T \to \infty$. Then, every eigenstate is realized with the same probability. We would have to represent all system block states in a reduced basis which never succeeds. The low temperature region may be accessible if only a few low lying excitations are relevant for the thermodynamics. In particular, critical quantum systems do not show this property. We shall see in chapter 3 that the TMRG poses a more powerful method for finite temperatures which allows to opimize only a single target state. The TMRG results prove to excel the "thermodynamic DMRG" [36].

2.3 DMRG algorithm

We want to focus on the so-called *infinite size algorithm* which is more similar to the TMRG method later used than the *finite size algorithm* [35]. A quantum system with nearest-neighbour interaction is considered. We assume n states per site, e.g. $n = 2S + 1$ for a spin-S system. The standard DMRG algorithm with open boundary conditions proceeds as follows:

0. Take a block **B** of a certain length[1] L with hamiltonian $\mathcal{H}_B = \sum_{i=1}^{L-1} \hat{h}_{i,i+1}$.[2]

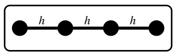

1. Enlarge the block by one site, forming the block **B-s**, hamiltonian $\mathcal{H}_{B-s} = \mathcal{H}_B + h^{(\mathrm{int.})}$ and other operators A_{B-s}.

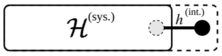

2. Form the superblock **B-s-s-B** and diagonalize the Hamiltonian[3] $\mathcal{H}_{B-s-s-B} = \mathcal{H}^{(\mathrm{sys.})}_{B-s} + \mathcal{H}^{(\mathrm{env.})}_{s-B} + h^{(\mathrm{int.})}$ numerically, calculating only the target state $|\psi\rangle$. If desired, calculate expectation values for arbitrary operators A_{B-s} defined on the enlarged system block, $\langle\psi|A_{B-s}|\psi\rangle$.

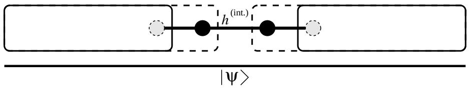

3. Build the reduced density matrix ρ and compute the complete eigensystem $\{w_\alpha, |u^\alpha\rangle\}$. Write the eigenstates corresponding to the m largest weights into the columns of the matrix U.

4. Project onto the reduced basis[4], i.e. $\bar{\mathcal{H}}_{B-s} = U^\dagger \mathcal{H}_{B-s} U$ and $\bar{A}_{B-s} = U^\dagger A_{B-s} U$.

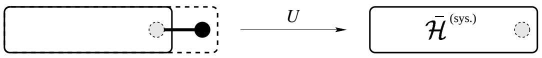

---

[1] L has to be chosen small enough such that the superblock **B-s-s-B** [cf. step 2] can be diagonalized exactly.

[2] The hamiltonian only contains the intra-block interactions.

[3] We assume the quantum system having reflection symmetry. Therefore, the environment is simply the reflected system.

[4] The information on the last site of the block has to be stored in order to define the interaction with an additional site in the next pass of step 3.

$\boxed{5.}$ Rename the enlarged system block, **B-s** $\to$ **B**, and restart with step 1, substituting $\bar{\mathcal{H}}_{B-s} \to \mathcal{H}_B$ and $\bar{A}_{B-s} \to A_B$.

2.4 Comments and computational improvements

In each iteration step the effective size of the system obviously grows by two sites. The calculated quantities converge to their values in the thermodynamic limit. The linear dimension of the matrix, which we have to diagonalize in step 2, is n^{2L+2} at the beginning and $n^2 \cdot m^2$ in the following runs. For a spin-1/2 system and a typical $m = 100$ the memory used is ≈ 10 GByte and increases as m^4! The density matrix, in contrast, is much smaller, namely $n^{L+1} \times n^{L+1}$ at the beginning and $nm \times nm$ in the following runs, and does not raise a computational problem.

There are two possibilities to reduce the necessary size of memory and, hence, to increase the speed of the algorithm.

- Due to the nearest-neighbour interaction most of the matrix-elements of the superblock hamiltonian are zero. Therefore, we deal with a **sparse matrix** and only the non-vanishing matrix-elements have to be stored. However, the sparseness of the matrix is reduced during the iterative procedure since the RG generates couplings between spins with larger distances.

- Most of the considered systems provide **conserved quantities**, for instance the total magnetization. The hamiltonian decomposes into blocks with constant quantum number.

These properties reduce memory requirement to only an order of hundreds of megabytes which allows running the algorithm on usual workstations. The numerical diagonalization methods typically used are Davidson [37] or Lanczos [38, 39].

Chapter 3

Transfer-matrix DMRG

Thermodynamics of any quantum system is determined by the complete spectrum of the hamiltonian. In principle, the partition function as the sum over all Boltzmann weights yields any thermodynamical quantity. Though the Bethe ansatz gives all eigenvalues for exactly solvable models, it is difficult to study the thermodynamic properties analytically. With regard to numerical studies of non-integrable models there is no reasonable chance to succeed on this direct way, especially in the thermodynamic limit.

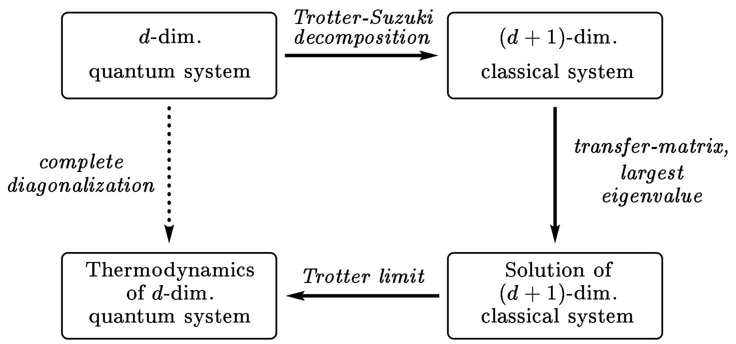

A promising detour was proposed by Trotter [40] and Suzuki [41, 42], the so-called *Trotter-Suzuki (TS) transformation approach* [see section 3.1]. Basically, the d-dimensional quantum system is mapped to a classical system in $d+1$ dimensions. The equivalent classical model can be solved using a transfer-matrix where the *quantum transfer-matrix* [see section 3.2] is particularly suited for determining the thermodynamics. The largest eigenvalue on its own already yields the partition function in the thermodynamic limit according to quantum space. The transfer-matrix DMRG (TMRG) combines the Trotter-Suzuki decomposition with a density-matrix-renormalization-group calculation of the dominating eigenvalue. Returning to the previous discussions this method can be applied here because only one target state has to be taken into account. Furthermore, this approach does not involve any finite size effects with respect to quantum space. The inaccuracies caused by a finite virtual (or Trotter) dimension are of a higher order and therefore easier to control.

3.1 Trotter-Suzuki transformation

We consider a one-dimensional quantum system of length L with nearest-neighbour interaction $\hat{h}_{i,i+1}$ and periodic boundary conditions,

$$\mathcal{H} = \sum_{i=1}^{L} \hat{h}_{i,i+1}, \tag{3.1}$$

where $L+1 \equiv 1$. First, the hamiltonian is decomposed into an even (odd) part $\mathcal{H}_{e(o)}$ which contains only the interactions starting on an even (odd) site, $\mathcal{H} = \mathcal{H}_e + \mathcal{H}_o$. The partition function is expressed by means of the Trotter formula,

$$Z_L = \mathrm{Tr}\; e^{-\beta\mathcal{H}} = \lim_{M\to\infty} \underbrace{\mathrm{Tr}\;\left\{\left[e^{-\epsilon\mathcal{H}_e} e^{-\epsilon\mathcal{H}_o}\right]^M\right\}}_{=\mathcal{Z}_{L,M}}, \tag{3.2}$$

where $\epsilon = \beta/M$ and $\beta = 1/T$ is the inverse temperature. Commonly, M is labeled as *Trotter number.* $\mathcal{Z}_{L,M}$ is the partition function of the mapped classical system with quantum (virtual or Trotter) dimension

L (M) which can be written explicitly as

$$\mathcal{Z}_{L,M} = \sum_{\alpha_1,\dots,\alpha_{2M}} \langle\alpha_1|e^{-\epsilon\mathcal{H}_o}|\alpha_2\rangle\langle\alpha_2|e^{-\epsilon\mathcal{H}_e}|\alpha_3\rangle \times \dots$$
$$\times\langle\alpha_{2M-1}|e^{-\epsilon\mathcal{H}_o}|\alpha_{2M}\rangle\langle\alpha_{2M}|e^{-\epsilon\mathcal{H}_e}|\alpha_1\rangle. \tag{3.3}$$

The states $|\alpha_i\rangle = |s_i^1\rangle \otimes |s_i^2\rangle \otimes \dots \otimes |s_i^L\rangle$, varying the classical spin variables $s_i^1, \dots, s_i^L$, represent a complete basis of the quantum space. This insertion of unity operators in the virtual space looks similar to the path-integral formalism of quantum mechanics. Actually, eq. (3.3) is obtained by applying the same formalism to the quantum lattice model and, hence, often referred to as lattice path-integral representation. Each matrix-element $\langle\alpha_i|e^{-\epsilon\mathcal{H}_{e(o)}}|\alpha_{i+1}\rangle$ factorizes into $L/2$ local matrices of type

$$\tau(s_i^j s_i^{j+1}|s_{i+1}^j s_{i+1}^{j+1}) = \langle s_i^j s_i^{j+1}|e^{-\epsilon\hat{h}_{i,i+1}}|s_{i+1}^j s_{i+1}^{j+1}\rangle \tag{3.4}$$

which denotes a plaquette interaction in the classical model. Therefore, the local transfer-matrix τ can be represented graphically as

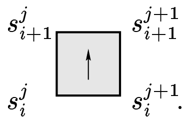

Fig. 3.1 shows the partition function [cf. eq. (3.3)] translated to this graphical language. The spins at two adjacent corners have to be identified and summed over. The boundary spins are thought of being connected periodically.

3.2 Quantum transfer-matrix

The classical checkerboard model [cf. Fig. 3.1] is dressily solved using a transfer-matrix. There are several possibilities of defining a transfer-matrix. We choose the so-called quantum transfer-matrix (QTM) which is most appropriate for calculating thermodynamical properties. The QTM corresponding to a certain Trotter-number M is defined by the

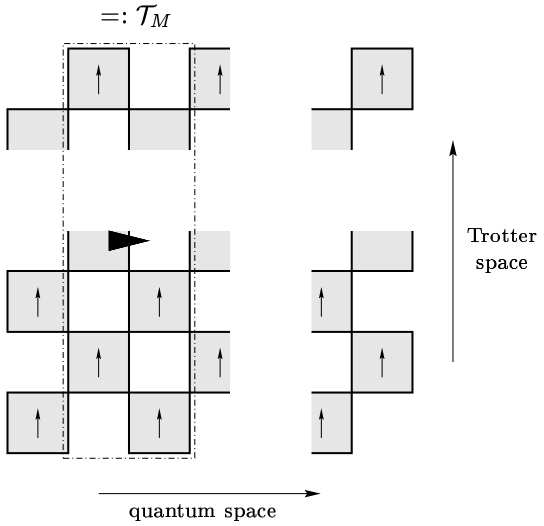

Figure 3.1: Graphical representation of the mapped classical checkerboard model and the quantum transfer-matrix.

matrix-elements,

$$\langle \sigma_1 \ldots \sigma_{2M} | \mathcal{T}_M | \sigma'_1 \ldots \sigma'_{2M} \rangle =$$
$$\sum_{\{\tilde{\sigma}_k\}} \prod_{k=1}^{M} \tau(\sigma_{2k}\tilde{\sigma}_{2k}|\sigma_{2k+1}\tilde{\sigma}_{2k+1})\tau(\tilde{\sigma}_{2k+1}\sigma'_{2k+1}|\tilde{\sigma}_{2k+2}\sigma'_{2k+2}). \quad (3.5)$$

This operator obviously shifts virtual space states along the quantum direction. We rewrite the partition function,

$$\mathcal{Z}_{L,M} = \mathrm{Tr}\ \mathcal{T}_M^{L/2} = \sum_{\mu} \Lambda_\mu^{L/2}, \quad (3.6)$$

where Λ_μ are the eigenvalues of the QTM. Note that the eigenvalues are still depending on M. Some important features of the spectrum of $\mathcal{T}_M$ are given by simple arguments. Consider the temperature approaching infinity, $T \to \infty$. Then the local transfer-matrix tends to a local unity operator, $\tau(\alpha_1\beta_1|\alpha_2\beta_2) = \delta_{\alpha_1,\alpha_2}\delta_{\beta_1,\beta_2}$, or graphically

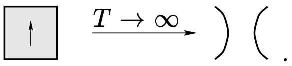

Let the classical spin variables have n possible values, i.e. states $|1\rangle$, $\ldots$, $|n\rangle$. The QTM in a rotated view reads

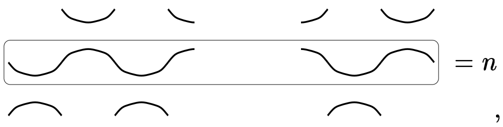

where the sum over the interior Kronecker δ's yields a factor n. Therefore, the entries of $\mathcal{T}_M$ are n or zero. From thermodynamics we already know that the largest eigenvalue of the QTM has the value $\Lambda_0 = n^2$ in order to satisfy $s \to \ln n$ for the entropy per site [cf. eq. (3.6)]. For every finite value of M the spectrum is discrete and the eigenvalues can be sorted by magnitude, $\Lambda_0 > \Lambda_1 \geq \Lambda_2 \geq \ldots$, where the largest eigenvalue is unique and separated from the next leading eigenvalue.[1] In particular, we are interested in the thermodynamic limit with respect to the quantum direction, i.e. $L \to \infty$. Due to the structure of the spectrum only the largest eigenvalue of the QTM determines the thermodynamics. Reanalyzing eq. (3.6) yields

$$\mathcal{Z}_{L,M} = \Lambda_0^{L/2} \left\{ 1 + \left(\frac{\Lambda_1}{\Lambda_0} \right)^{L/2} + \left(\frac{\Lambda_2}{\Lambda_0} \right)^{L/2} + \ldots \right\} \stackrel{L\to\infty}{\longrightarrow} \Lambda_0^{L/2}, \qquad (3.7)$$

or for the free energy per site

$$f_{\infty,\epsilon} = -T \lim_{L\to\infty} \frac{1}{L} \ln \Lambda_0^{L/2} = -\frac{T}{2} \ln \Lambda_0. \qquad (3.8)$$

We must keep in mind that this thermodynamical potential describes a classical system with dimensions $\infty \times M$ and still not the bulk limit of the quantum chain, equivalent to a non-vanishing ϵ. More precisely, the finite size corrections due to M appear as

$$f_{\infty,\epsilon} = f_{\text{bulk}} + \mathcal{O}(\epsilon^2), \qquad (3.9)$$

[1]The gap beetween Λ_0 and Λ_1 does not vanish even in the Trotter-limit $M \to \infty$. Since a level crossing indicates a discontinuity in the partition function and therefore a phase transition a degeneracy is not possible for a one-dimensional quantum system at any finite temperature.

where the next leading terms can be read off from eq. (3.2). Hence, the limit $\epsilon \to 0$ (or $M \to \infty$) formally leads to the desired results for the quantum chain. A crucial question in the above formalism is of course if the two limits in quantum and Trotter direction are interchangeable. The answer was given in the interchangeability theorem by Suzuki [41]. The chosen order is irrelevant for quantum systems with short range interaction and the deduced results can be applied to the latter problems.

Another important physical quantity can directly be obtained using the spectrum of the QTM. Within this transfer-matrix approach the correlation length ξ is given by [see e.g. [43]]

$$\xi^{-1} = \ln \frac{\Lambda_0}{\Lambda_1}, \tag{3.10}$$

where Λ_1 is the next leading eigenvalue. Again, we recognize that no phase transition takes place, i.e. the correlation length remains finite, at finite temperature since the spectrum of $\mathcal{T}_M$ is gapped.

3.3 TMRG algorithm

In principle, the major numerical problem is the same as in the standard DMRG, namely to find the largest eigenvalue and the corresponding eigenstate(s). However, there are a couple of important differences which do not allow to apply the algorithm previously presented directly.

- As pointed out above, the thermodynamic limit with respect to quantum direction, $L \to \infty$, was performed exactly within the QTM approach. The task of the TMRG method is to increase the Trotter-number M. For technical reasons the parameter ϵ has to be fixed. Consequently, the temperature given by

  $$T = \frac{1}{\epsilon M} \tag{3.11}$$

  is decreased by enlarging the virtual dimension.

- The structure of the QTM is different compared to a hamiltonian. Instead of a sum over local operators we have to perform multiplications of tensors. The blocks therefore have to be handled suitably.

- The quantum transfer-matrix is not hermitian. Since the largest eigenvalue Λ_0 is unique we know that eigenstates exist but differ depending on whether being applied from left or right. Hence, a single target state doubles to a left and a right vector, $\langle\psi^L|$ and $|\psi^R\rangle$.

First, the system and the environment block have to be determined. The QTM which is identified as superblock is splitted into two equal parts. Obviously, we have to distinguish between the cases M odd and even. The system blocks are exemplarily shown for (a) $M = 3$ and (b) $M = 4$. We may take one of these blocks as initial configuration for the TMRG procedure.

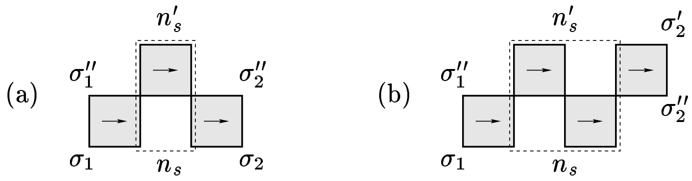

$\mathcal{S}_o(\sigma''_1, n'_s, \sigma''_2|\sigma_1, n_s, \sigma_2)$ $\qquad$ $\mathcal{S}_e(\sigma''_1, n'_s, \sigma'_2|\sigma_1, n_s, \sigma''_2)$

Again, the corner spins of two adjacent local transfer-matrices have been identified and summed out. The external spins in the middle of each block are combined to block-spin variables n_s or n'_s respectively. Henceforth, the objects $\mathcal{S}_{o(e)}$ will be called *renormalized system blocks*. Intrinsically, the local transfer-matrices are considered symmetric as an operator acting in arrow direction since $\hat{h}_{i,i+1}$ is hermitian. If we additionally assume a spatial reflection symmetry of the local interaction, i.e. $\hat{h}_{i,i+1} = \hat{h}_{i+1,i}$, which is satisfied for most of the interesting one-dimensional quantum models the environment blocks are constructed by rotating the system,

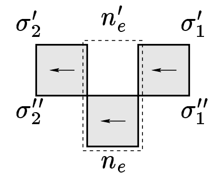

(a)

$$\mathcal{E}_o(\sigma_2', n_e', \sigma_1' | \sigma_2'', n_e, \sigma_1'') \; = \; \mathcal{S}_o(\sigma_1'', n_e, \sigma_2'' | \sigma_1', n_e', \sigma_2') \tag{3.12}$$

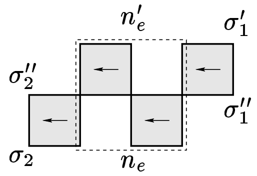

(b)

$$\mathcal{E}_e(\sigma_2'', n_e', \sigma_1' | \sigma_2, n_e, \sigma_1'') \; = \; \mathcal{S}_e(\sigma_1'', n_e, \sigma_2 | \sigma_1', n_e', \sigma_2'').$$

The superblock in both cases reads

$$\mathcal{T}_M(\sigma_1', n_s', \sigma_2', n_e' | \sigma_1, n_s, \sigma_2, n_e) =$$
$$\begin{cases} \sum\limits_{\sigma_1'', \sigma_2''} \mathcal{S}_o(\sigma_1'', n_s', \sigma_2'' | \sigma_1, n_s, \sigma_2) \; \mathcal{E}_o(\sigma_2', n_e', \sigma_1' | \sigma_2'', n_e, \sigma_1'') \\ \sum\limits_{\sigma_1'', \sigma_2''} \mathcal{S}_e(\sigma_1'', n_s', \sigma_2' | \sigma_1, n_s, \sigma_2'') \; \mathcal{E}_e(\sigma_2'', n_e', \sigma_1' | \sigma_2, n_e, \sigma_1'') \end{cases}, \tag{3.13}$$

which means connecting the system and the environment and summing over the two conjoint spins. We now have to calculate the largest eigenvalue and its eigenstates numerically. An appropriate way is the projection or *power method*. However, the idea is to project out states orthogonal to the dominating eigenstate similar to eq. (3.7). Since $\mathcal{T}_M$ is non-symmetric we have to be careful with the definition of orthogonality which will be specified later on. Let $\{|\mu\rangle\}$ be a right set of eigenstates corresponding to the eigenvalues from eq. (3.6). Applying the QTM k-times to a randomly chosen initial state $|\phi_{\text{rand}}\rangle = \sum_\mu a_\mu |\mu\rangle$ yields

$$\frac{\mathcal{T}_M{}^k}{a_0 \Lambda_0{}^k} |\phi_{\text{rand}}\rangle = \sum_\mu \frac{a_\mu}{a_0} \left(\frac{\Lambda_\mu}{\Lambda_0}\right)^k |\mu\rangle \stackrel{k\to\infty}{\longrightarrow} |0\rangle \equiv |\psi^R\rangle, \tag{3.14}$$

assuming that $|\phi_{\text{rand}}\rangle$ contains the highest weight state $|0\rangle$, i.e. $a_0 \neq 0$. As we have already identified the correlation length in section 3.2 the convergence of the power method obviously is $\exp(-k/\xi)$. More precisely, the number of iterations needed for attaining an accuracy of δ is of order

$$k \sim \xi |\ln \delta|. \tag{3.15}$$

As the correlation length is increasing for larger Trotter-numbers (or equivalently lower temperatures), k also grows. To reach a relative error of about $\delta = 10^{-16}$ less then $k = 20$ iterations are typically needed for high temperatures.

The left target state is calculated equivalently. However, having the spatial refection symmetry the wave function of $\langle\psi^L|$ can be obtained directly from that of $|\psi^R\rangle$. Due to the symmetry involved in (3.13) we have

$$\psi^L(\sigma_1, n_s, \sigma_2, n_e) = \psi^R(\sigma_1, n_e, \sigma_2, n_s), \tag{3.16}$$

where e.g. $\psi^R(\sigma_1, n_e, \sigma_2, n_s)$ is the coefficient of $|\sigma_1\rangle \otimes |n_e\rangle \otimes |\sigma_2\rangle \otimes |n_s\rangle$. Note that $\langle\psi^L| \neq (|\psi^R\rangle)^\dagger$ in general. The normalization is chosen to be $\langle\psi^L|\psi^R\rangle = 1$.

The thermodynamic density matrix in Trotter direction is expressed by means of the QTM, $\rho_{\text{th}} = \mathcal{T}_M^{L/2}/\text{Tr}\{\mathcal{T}_M^{L/2}\}$. Fortunately, due to the structure of the spectrum of $\mathcal{T}_M$ this expression simplifies to $\rho_{\text{th}} = |\psi^R\rangle\langle\psi^L|$ in the quantum thermodynamic limit $L \to \infty$. We are particularly interested in a reduced density matrix in order to renormalize the enlarged system blocks. Therefore, a partial trace with respect to the environment is performed yielding

$$\rho = \text{Tr}_{\sigma_1, n_e} |\psi^R\rangle\langle\psi^L|, \tag{3.17}$$

or written in terms of the matrix-elements

$$\rho(\underbrace{n_s', \sigma_2'}_{=\tilde{n}_s'} | \underbrace{n_s, \sigma_2}_{=\tilde{n}_s}) = \sum_{\sigma_1, n_e} \psi^R(\sigma_1, n_s', \sigma_2', n_e)\psi^L(\sigma_1, n_s, \sigma_2, n_e). \tag{3.18}$$

The reduced density matrix obviously is also non-symmetric. From a physical point of view ρ_{th} and hence ρ should be positive semi-definit. A rigorous proof, however, has not yet been found, only in a few special cases the reduced density matrix has been shown to be positive semi-definit [23]. Numerically we find that the eigenvalues of ρ are real and larger than or equal to zero as already pointed out by the authors of ref. [23]. A practical solution of the numerical diagonalization problem will be discussed in the next section. Let $\mathcal{W}$ be a diagonal matrix which contains the eigenvalues w_α of ρ. The corresponding left (right) eigenstates are defined by $\rho\, \mathcal{U}^R = \mathcal{W}\, \mathcal{U}^R$ ($\mathcal{U}^L \rho = \mathcal{U}^L \mathcal{W}$). Hence, the columns (rows) of $\mathcal{U}^R$ ($\mathcal{U}^L$) contain the coefficients of each eigenstate with respect to the basis $\{|\widetilde{n}\rangle\}$ [cf. eq. (3.18)]. The eigenstates are normalized satisfying the condition $\mathcal{U}^L\, \mathcal{U}^R = \mathbf{1}$.

To enlarge the system we add one local transfer-matrix as depicted examplarily starting from $\mathcal{S}_o$.

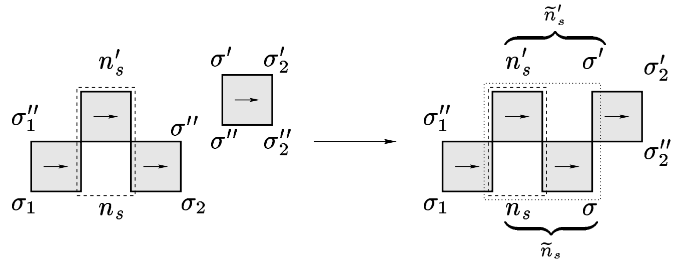

As two virtual space slices are appended in the superblock the Trotter-number is increased by one, changing from even to odd M or vice versa.

$$
\begin{aligned}
(a)\quad & \widetilde{\mathcal{S}}_e(\sigma''_1, \widetilde{n}'_s, \sigma'_2|\sigma_1, \widetilde{n}_s, \sigma''_2) \\
&\qquad = \sum_{\sigma''} \mathcal{S}_o(\sigma''_1, n'_s, \sigma''|\sigma_1, n_s, \sigma_2)\ \tau(\sigma', \sigma''|\sigma'_2, \sigma''_2) \\
(b)\quad & \widetilde{\mathcal{S}}_o(\sigma''_1, \widetilde{n}'_s, \sigma''_2|\sigma_1, \widetilde{n}_s, \sigma_2) \\
&\qquad = \sum_{\sigma''} \mathcal{S}_e(\sigma''_1, n'_s, \sigma'_2|\sigma_1, n_s, \sigma'')\ \tau(\sigma'', \sigma|\sigma''_2, \sigma_2)
\end{aligned}
\tag{3.19}
$$

The combined variable $\widetilde{n}_s$ is defined by the tensor product of the involved states, i.e. $|\widetilde{n}_s\rangle = |n_s\rangle \otimes |\sigma\rangle$. In the last step of the TMRG procedure the enlarged blocks $\widetilde{\mathcal{S}}_{o(e)}$ are renormalized, i.e. projected onto the highest weight states. If $\dim(\{|\widetilde{n}_s\rangle\})$ exceeds a certain dimension m we construct the matrix U^R (U^L) as a block of $\mathcal{U}^R$ ($\mathcal{U}^L$) which contains only the m right (left) eigenstates corresponding to the largest eigenvalues w_α in the columns (rows).

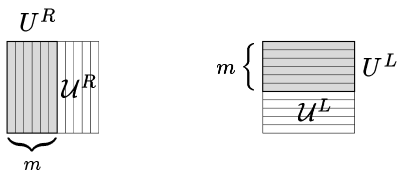

The renormalization reads

$$
\begin{aligned}
(a)\quad & \mathcal{S}_e(\sigma_1'', n_s', \sigma_2' | \sigma_1, n_s, \sigma_2'') \\
&= \sum_{\widetilde{n}_s, \widetilde{n}_s'} U^L(n_s', \widetilde{n}_s')\, \widetilde{\mathcal{S}}_e(\sigma_1'', \widetilde{n}_s', \sigma_2' | \sigma_1, \widetilde{n}_s, \sigma_2'')\, U^R(\widetilde{n}_s, n_s) \\
(b)\quad & \mathcal{S}_o(\sigma_1'', n_s', \sigma_2'' | \sigma_1, n_s, \sigma_2) \\
&= \sum_{\widetilde{n}_s, \widetilde{n}_s'} U^L(n_s', \widetilde{n}_s')\, \widetilde{\mathcal{S}}_o(\sigma_1'', \widetilde{n}_s', \sigma_2'' | \sigma_1, \widetilde{n}_s, \sigma_2)\, U^R(\widetilde{n}_s, n_s)
\end{aligned}
\tag{3.20}
$$

Graphically, the block is transformed to the known renormalized block with a single (maximum) m-valued block-spin $|n_s\rangle$, shown for $\widetilde{\mathcal{S}}_e \longrightarrow \mathcal{S}_e$.

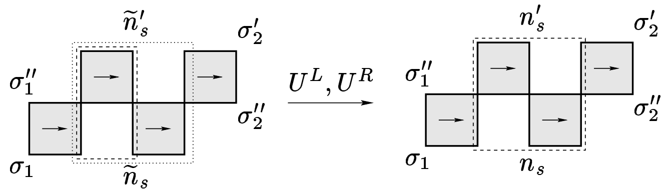

Since the environment block $\mathcal{E}_{o(e)}$ can be constructed using the symmetries of the system we only have to enlarge and renormalize $\mathcal{S}_{o(e)}$. The TMRG loop is repeated constructing the environment block and the transfer-matrix $\mathcal{T}_{M+1}$.

3.4 Implementation

The transfer-matrix DMRG was programmed[2] using the language C^{++}. A crucial problem of the TMRG is to handle the superblock whose dimension is n^4m^4 on a workstation. Similar to the standard DMRG conserved quantities can be used. The total magnetization of all investigated quantum chains within the scope of this thesis is conserved. Locally we find $s_i^j + s_i^{j+1} = s_{i+1}^j + s_{i+1}^{j+1}$. Defining new spin variables by adding a phase factor $\sigma_i^j = (-1)^{i+j} s_i^j$ which means inverting the spins on one sublattice of the checkerboard model yields $\sigma_i^j + \sigma_{i+1}^j = \sigma_i^{j+1} + \sigma_{i+1}^{j+1}$. Therefore, the QTM decomposes into blocks with constant $\mathcal{Q} = \sum_i \sigma_i^{j+1}$. Returning to section 3.2 the largest eigenvalue is localized in the sector $\mathcal{Q} = 0$ for every temperature since there is no level crossing. A proof was also given by the authors of ref. [44]. The numerical effort reduces to calculating the relevant block of $\mathcal{T}_M$.

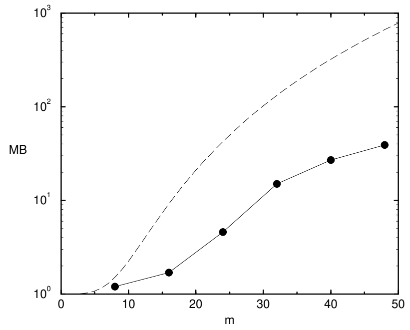

Figure 3.2: Used memory for the free fermion model ($n = 2$) in megabytes as a function of the size m of the reduced basis (symbols) compared to the theoretically calculated effort without storage enhancement (dashed line).

The total memory typically needed for a spin-1/2 model, i.e. $n = 2$, as a function of m is shown in Fig. 3.2. The increase is obviously less than that of the non-enhanced version ($\propto m^4$ for larger m) and the actual size differs by a factor of approximately 10.

The memory measurement already contains an important property of ρ. Due to the quantum number of $\mathcal{T}_M$ the reduced density matrix also consists of subblocks with a constant total spin which can be diagonalized separately. As mentioned before, for small M we numerically find

[2]Friedhelm Schönfeld was also involved in writing the program code.

the eigenvalues of ρ being real and non-negative. However, due to the truncation error after several iterations small imaginary parts arise especially when using numerical libraries as for instance LAPACK (Linear Algebra Package) and BLAS (Basic Linear Algebra Routines). If two eigenvalues are (almost) degenerate, the commonly used QR algorithm applied to non-symmetric matrices becomes instable and certain eigenvalues split up into complex conjugated pairs. We solve this problem by diagonalizing ρ externally using MAPLE which can handle any arbitrary precision while LAPACK routines are limited to double precision, i.e. floating point numbers with 16 digits. Nevertheless, if a complex conjugated pair $\{w_{\mathrm{r}} \pm i w_{\mathrm{i}}, |u_{\mathrm{r}}\rangle \pm i|u_{\mathrm{i}}\rangle\}$ appears, the real part w_{r} is taken as eigenvalue and the two eigenvectors are chosen as $|u_{\pm}\rangle = |u_{\mathrm{r}}\rangle \pm |u_{\mathrm{i}}\rangle$. This has to be carried out for both left and right eigenstates. The orthonormalization reads $\langle u^L_\alpha | u^R_\beta\rangle = \delta_{\alpha\beta}$. The m dominant eigenvectors, i.e. the matrices U^R/U^L, are returned to the main C^{++} program. This idea does not improve the performance but the numerical stability.

Another variant of the TMRG is to use a symmetric transfer-matrix. With regard to Fig. 3.1 the QTM has the structure $\mathcal{T}_M = T_1 T_2$ where the T_i are disjunct products of local transfer-matrices. We can formally define a square root of T_i and write the partition function in terms of the alternative quantum transfer-matrix $\widetilde{\mathcal{T}}_M = {T_1}^{1/2} T_2 {T_1}^{1/2}$. If T_1 and T_2 are symmetric then $\widetilde{\mathcal{T}}_M$ is complex symmetric. Assuming additionally a semi-positive spectrum of T_1 the symmetrized QTM is also real. Left and right target states are identical and the reduced density matrix turns out to be (complex) symmetric which simplifies numerical diagonalization. However, constructing $\widetilde{\mathcal{T}}_M$ numerically involves an additional matrix multiplication which reduces the performance significantly. The obtained accuracy is actually not better than in the original asymmetric version. We therefore retain the presented TMRG algorithm as in section 3.3.

3.5 Accuracy analysis

For demonstrating the potential of TMRG we apply the algorithm to the usual spin-1/2 XXZ chain whose hamiltonian is defined by

$$\mathcal{H}_{\text{XXZ}} = \sum_i \big[\underbrace{J\big(\hat{S}_i^x \hat{S}_{i+1}^x + \hat{S}_i^y \hat{S}_{i+1}^y + \Delta \hat{S}_i^z \hat{S}_{i+1}^z\big) + h\hat{S}_i^z}_{\hat{h}_{i,i+1}} \big]. \tag{3.21}$$

$\hat{S}_i^x$, $\hat{S}_i^y$, $\hat{S}_i^z$ denote the components of usual spin-1/2 operators, h is the external magnetic field and Δ the anisotropy parameter. We shall set $J = 1$ for simplicity, i.e. temperatures are given in the unit T/J. This has already been done by Wang and Xiang [21] and by Shibata [22] simultaneously. Since exact results are available, this quantum model allows (a) to check that the program is working correctly and (b) to measure the accuracy by reproducing exactly known results.

We expect the discarded weight [see section 2.2] being a good estimate of the error with respect to truncation in each renormalization step. We already find $P_m < 10^{-5}$ for the small number of $m = 16$ states kept. The discarded weight is decreasing very rapidly by increasing m. Of course, P_m is depending on the temperature, generally increasing for small T. To attain a similiar situation in the standard DMRG hundreds of states are necessary. The reason for this bonhomie in the TMRG method is the structure of the $\mathcal{T}_M$ spectrum: the largest eigenvalue is always separated from the next leading one yielding a strong exponential decrease of the weights w_α. However, the calculated thermodynamic quantities involve cumulative errors which can only be measured by comparison with exactly known results.

Let us focus on the free energy which is closely related to the largest eigenvalue [cf. eq. (3.8)]. In the case $\Delta = 0$ we have the free fermion model. It is easily solved using spinless fermions connected to the spin operators by the Jordan-Wigner transformation [45, 46]. Although the fermions are detected as non-interacting this model comprises a gapless spectrum and non-trivial quantum effects due to fermionic symmetry. Therefore, it is a suitable probational model. Fig. 3.3 shows the error of the TMRG free energy for a constant $m = 24$ as a function of ϵ for different temperatures. As expected from eq. (3.9) the deviation scales with ϵ^2 for large temperature where the cutoff error is negligible. The

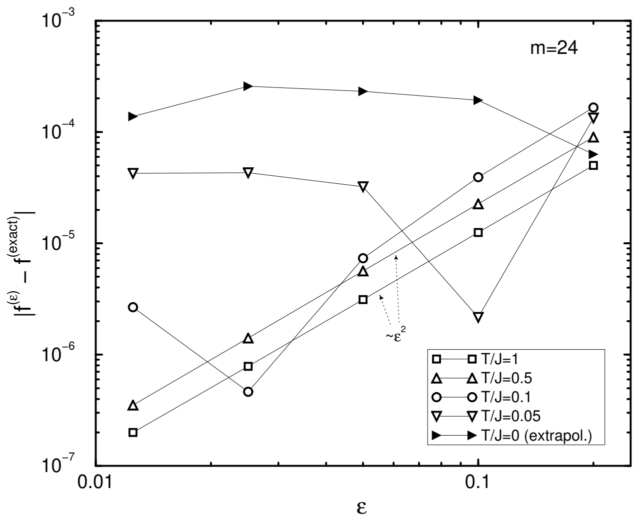

Figure 3.3: Accuracy of the free energy. Comparison of TMRG results and exact free fermion calculations as a function of ϵ.

lower the temperature the larger is the cumulative error of the renormalization procedure. As different numbers of iterations are necessary for different values of ϵ to reach the same temperature, no clear scaling behaviour can be detected in the low temperature regime. However, choosing $\epsilon = 0.05$, for instance, the deviations from the exact results are smaller than 10^{-4} down to $T/J \approx 1/20$. The low temperature behaviour of the free energy is known to be $f(T) - e_o \simeq T^2$. This allows to determine the groundstate energy by fitting a quadratic function to the TMRG data. Although the transfer-matrix DMRG is not intended to calculate zero temperature properties the extrapolated ground state energy is better than 10^{-3} for $m = 24$ only. Next, we want to study the influence of m on the accuracy. Fig. 3.4 depicts deviations as a func-

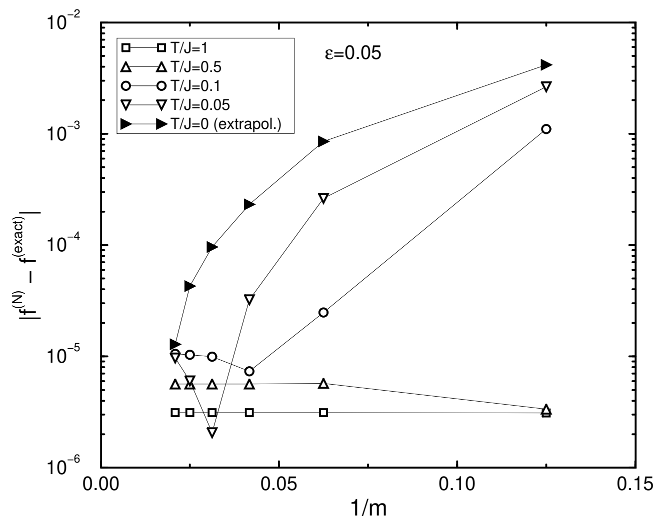

Figure 3.4: Effect of m on the accuracy of the free energy.

tion of $1/m$ for a constant value $\epsilon = 0.05$. While the accuracy for high temperatures is mainly determined by the finite ϵ, the low temperature values can crucially be improved by increasing the number of states kept. In conclusion, there is a competition between the number of iterations and the value of ϵ since the temperature is defined by $T = 1/\epsilon M$. A smaller ϵ increases the accuracy with respect to Trotter decompostion, but enlarges the cumulative error with respect to truncation for a given temperature. In principle, a sytematic extrapolation with respect to m and ϵ is possible [21]. We do not want to go into details here since the accuracy with a suitable fixed ϵ and a certain number of states kept is high enough for our purpose.

3.6 Expectation values of local operators

In principle, all thermodynamical quantities can be derived by the parameter dependences, e.g. T, h, of the free energy. Nevertheless, as this context involves calculating derivatives numerically it is more convenient to measure expectation values directly. Let $\hat{o}$ be an operator acting locally, say, at most on two sites. The thermal expectation value of $\hat{o}$ can be calculated within the QTM formalism using a transfer-matrix $\mathcal{T}_{\hat{o}}$ of the local operator. Switching to the "graphical language" again we define $\mathcal{T}_{\hat{o}}$ as

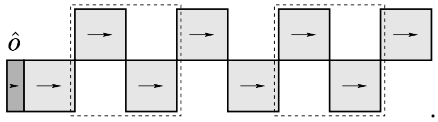

Hence, the local operator is added at one end of the QTM with open boundaries with respect to virtual space and subsequently closed periodically. Fortunately, the operator $\mathcal{T}_{\hat{o}}$ can be constructed from the renormalized blocks such that no new operators have to be added to the renormalization scheme. The expectation value explicitly reads [43]

$$o = \langle \hat{o} \rangle_{\text{th}} = \frac{1}{\Lambda_0} \langle \psi^L | \mathcal{T}_{\hat{o}} | \psi^R \rangle. \tag{3.22}$$

Useful operators are $\hat{h}_{i,i+1}$ and $\hat{S}_i^z$ in order to calculate the internal energy $u = \langle \hat{h}_{i,i+1} \rangle_{\text{th}}$ and magnetization $m = \langle \hat{S}_i^z \rangle_{\text{th}}$[3]. Now, we are able to derive other thermodynamical potentials, for instance the entropy, $s = (u - f)/T$.

The specific heat and susceptibilities are of a more particular interest. In principle, they could be obtained from expectation values by calculating correlation functions but implying non-local operators. We will discuss this problem later [see section 4.7]. A straightforward method actually is the use of numerical derivatives. We approximate

[3]To improve the numerical accuracy we rather use a symmetrized magnetization operator $(\hat{S}_i^z + \hat{S}_{i+1}^z)/2$.

the specific heat $C = \partial u/\partial T$ by the formula

$$C\left(\frac{T_1 - T_2}{2}\right) \approx \frac{u(T_1) - u(T_2)}{T_1 - T_2}, \tag{3.23}$$

where the accuracy is of order $(T_1 - T_2)^2$. On the other hand the TMRG errors are enforced by a factor $\frac{1}{T_1 - T_2}$. As the energy function is not obtained for arbitrary temperatures we have to use the values given by eq. (3.11). For large M the available temperatures are close one to another and the errors, therefore, can be controlled by choosing suitable intervals. Fig. 3.5 compares the numerical findings ($m = 48$) with exact results for the Heisenberg ($\Delta = 1$) and the free fermion model ($\Delta = 0$). A detailed analysis of the accuracy is shown in the inset. Obviously,

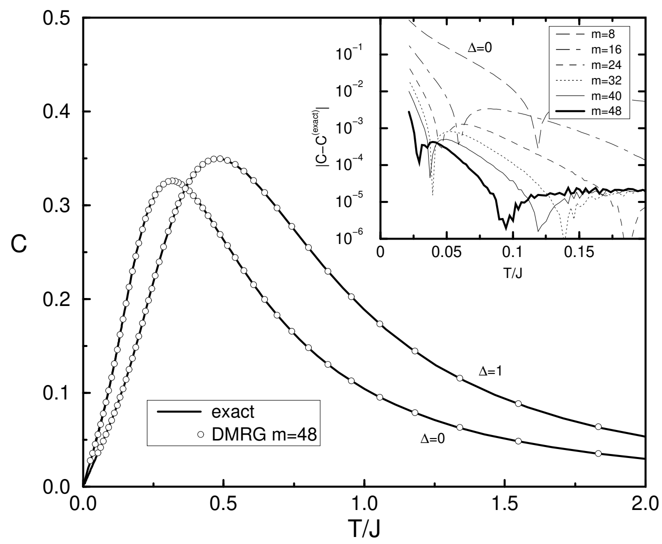

Figure 3.5: Specific heat: TMRG results versus exact data [52] for the spin-1/2 Heisenberg model ($\Delta = 1$) and the free fermion model ($\Delta = 0$). The inset shows the low temperature deviations exemplarily for free fermions for different values of m.

increasing the number of states kept improves the quality of our data. Alternatively, we could calculate the specific heat using the relation $C = T\, \partial s/\partial T$ which yields comparable deviations from the exact data.

To study the response of the system on external magnetic fields we have to calculate the magnetic susceptibility which is defined by

$$\chi(T,h) = \frac{\partial}{\partial h} m(T,h) \approx \frac{m(T,h+\Delta h) - m(T,h-\Delta h)}{2\Delta h}. \qquad (3.24)$$

Numerically, we calculate the magnetization for two different magnetic fields deviating by $\pm\Delta h$ from the desired h. Again, the accuracy with respect to the approximated derivative is of the order $(\Delta h)^2$ while the TMRG errors are amplified by $\frac{1}{\Delta h}$. Typically, we set $\Delta h = 0.01J$.

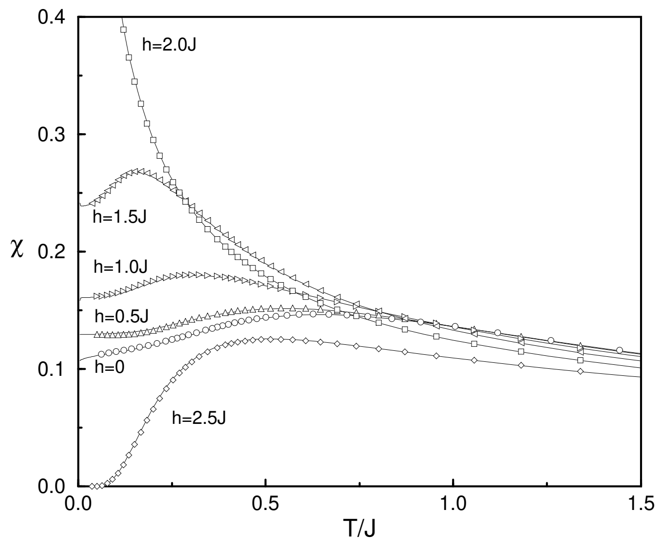

Figure 3.6: Magnetic susceptibility: TMRG results ($m = 32$, $\epsilon = 0.05$) versus exact data for spin-1/2 Heisenberg model with different magnetic fields.

Fig. 3.6 depicts the numerical data (symbols) versus exact results (lines)

[52] for different magnetic fields. As stated above, the deviations are expected to be of the order 10^{-4}. The accuracy, of course, can be improved by using a larger m and a smaller Δh simultaneously.

Concluding, the TMRG emerges as a very powerful method and improves over other numerical techniques particularly affecting the low temperature properties. While the finite size gap in exact diagonalization calculations becomes visible already for $T/J \simeq 1/10$, the transfer-matrix DMRG is at least able to reach temperatures of order $1/100$. Therefore, a lot of distinct quantum effects are only accessible by means of the TMRG.

3.7 Frustrated and dimerized spin models

With regard to the study of the spin-Peierls phase transition for realistic substances we investigate spin-1/2 Heisenberg models with a modulated magnetic exchange and an additional interaction of next-nearest-neighbours (NNN),

$$\mathcal{H}_{\alpha,\{\delta_i\}} = J \sum_i \left[(1+\delta_i)\hat{\mathbf{S}}_i \hat{\mathbf{S}}_{i+1} + \alpha \hat{\mathbf{S}}_i \hat{\mathbf{S}}_{i+2} \right], \qquad (3.25)$$

where $\hat{\mathbf{S}}_i$ denotes the usual spin-1/2 operator. Since $\sum_i \delta_i = 0$ a single δ_i signifies the deviation of the i-th coupling strength from the mean value J. The NNN interaction is commonly referred to as *frustration*[4], where α denotes the frustration parameter. The last term represents the Zeeman energy. The easiest way defining a non-trivial modulation is to set $\delta_i = (-1)^i \delta$, i.e. the presence of a *dimerization* of strength δ. Hence, the unit cell of the spin chain is doubled.

The spectrum of the elementary excitations significantly depends on the parameters α and δ. Fig. 3.7 shows the general phase diagramm of frustrated and dimerized Heisenberg chains. The spectrum is gapped,

[4]We would like to remark that the term “frustration” is somewhat deceptive. Only a classical antiferromagnetic system shows a frustration in a proper sense by adding a next-nearest-neighbour interaction. In general, eigenstates of a quantum antiferromagnet with only nearest-neighbour interaction are already frustrated using this classical definition.

if an arbitrarily small dimerization $\delta > 0$ is present. The system also shows a gap in the case $\delta = 0$ for an overcritical frustration $\alpha > \alpha_c$ subject to a spontaneous symmetry breaking due to the tendency of forming local singlets. This critical value was determined being $\alpha_c \approx 0.2412$ [14, 47, 48] by a numerical scaling analysis.

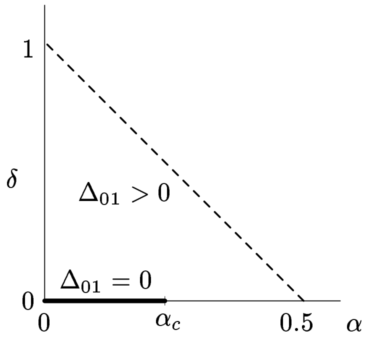

Figure 3.7: Phase diagram of the frustrated and dimerized Heisenberg chain characterized by the singlet-triplet gap Δ_{01}.

In particular, the structure becomes clear on the Shastry-Sutherland line $2\alpha + \delta = 1$ [dashed line in Fig. 3.7] where the ground state is exactly known to be a product of singlets of neighbouring spins [14, 49, 50]. Note, that this configuration is often denoted as dimer state because the expectation values $\langle \hat{\mathbf{S}}_i \hat{\mathbf{S}}_{i+1} \rangle$ are alternating, not to be confused with the alternation of the exchange couplings introduced in (3.25) by hand. The singlet-triplet gap decomposes into two parts, $\Delta_{01} = \Delta_\alpha + \Delta_\delta$, a spontaneous gap Δ_α due to frustration and an additional dimerization gap $\Delta_\delta \simeq \delta^{2/3}$ [51, 52]. In the thermodynamics the gap appears as the typical activated behaviour.

The application of the presented TMRG technique to the model requires a nearest-neighbour interaction and translational invariance. In order to satisfy these requirements we combine each two spin 1/2 to an effective four state object. A similiar strategy has been adopted in Ref. [53] to cast a system with next-nearest-neighbour interaction in a form suitable for application of the TMRG algorithm. Practically, the size of the transfer-matrix $\mathcal{T}_M$ and also of local operators, $\mathcal{T}_{\hat{o}}$, increases by a factor $2^4 = 16$. The free energy reads $f = -\frac{T}{4} \ln \Lambda_0$ as a local transfer-matrix stretches over four original spins. Eq. (3.22) intrinsically contains the enlarged unit cell and is still valid. Local operators can be extended up to four spin-1/2, e.g. $\frac{1}{4}h_i + \frac{1}{2}h_{i+1} + \frac{1}{4}h_{i+2} \to u$ and $\frac{1}{4}(\hat{S}^z_i + \hat{S}^z_{i+1} + \hat{S}^z_{i+2} + \hat{S}^z_{i+3}) \to m$, which has a positive effect on the accuracy. However, note that the model (3.25) does not provide a spatial reflection symmetry even when formulated as a four state problem. The environment block [see section 3.3] therefore has to be stored and renormalized expilicitly.

In order to verify that the TMRG is highly accurate in this modified case we consider the Majumdar-Ghosh point, i.e. $\alpha = 0.5$, $\delta = 0$.

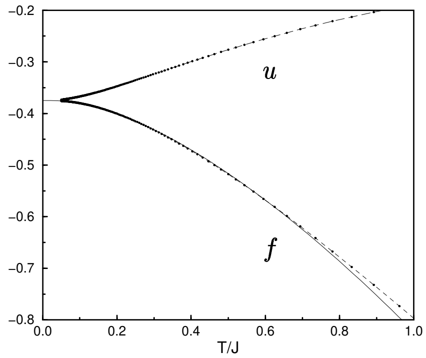

Figure 3.8: TMRG results ($\epsilon = 0.05$, $m = 24$) for the free and internal energy of the Majumdar-Ghosh model ($\alpha = 0.5$, $\delta = 0$). The solid line shows a low temperature fit of the free energy [see text].

The ground state is known to be a product of local singlets of neighboured spins [49]. We therefore have a twofold degeneracy. The exact value of the ground state energy reads $e_0 = -\frac{3}{8}J$. Assuming a quadratic dispersion in lowest order the density of states can be written as[5]

$$\mathcal{D}(\omega) - \delta(\omega - e_0) \simeq \frac{\Theta(\omega - e_0 - \Delta)}{\sqrt{\omega - e_0 - \Delta}} \tag{3.26}$$

which shows the typical van-Hove singularity for one-dimensional systems. The partition function per site for $T \ll \Delta$ therefore obeys

$$z - e^{-e_0/T} \simeq \int_{e_0+\Delta}^{\infty} \mathcal{D}(\omega) e^{-\omega/T} d\omega \simeq T^{1/2} e^{-(e_0+\Delta)/T}, \tag{3.27}$$

[5]We neglect normalization factors.

such that the singular part of the free energy scales according to

$$f(T) - e_0 \simeq T^{3/2} e^{-\Delta/T}. \tag{3.28}$$

We can use this formula to determine the ground state energy and the excitation gap from the finite temperature data [see Fig. 3.8]. Choosing the interval $0.05 \leq T \leq 0.2$ we derive $e_0 = -0.37500(3)J$, excellently confirming the exact value, and $\Delta = 0.115(5)J$. The error was estimated by varying the fit interval. We expect the gap appearing in thermodynamic quantities to be half the (spectroscopic) singlet-triplet gap, i.e. $\Delta = \Delta_{01}/2$ where the origin of this factor $1/2$ can be understood as follows. The elementary excitations are spinons each with gap Δ, however, occuring pairwise. For the usual thermodynamic data like the free energy the activated behaviour shows a characteristic energy corresponding to the gap of the individual elementary excitations whether these occur in arbitrary numbers or restricted to even numbers does not matter [see e.g. Ref. [54]]. Hence, our estimate for the singlet-triplet gap is $\Delta_{01} \approx 0.23(1)J$ which compares fairly well to the value $0.2338(6)J$ [55, 56] calculated e.g. by means of a perturbative approach extrapolated to infinite order using an analytic Lanczos technique.

A different situation is realized for $\delta > 0$ due to the confinement of spinons in pairs. Here a crossover in the activated behaviour sets in at temperatures of the order of the binding energy $E_{\mathrm{B}} \leftrightarrow T_{\mathrm{B}}$. At temperatures above T_{B} the gap in the activated behaviour is $\Delta_{01}/2$, below T_{B} it is Δ_{01}. However, it is notedly difficult to detect these two regimes in the numerical data.

Chapter 4

The spin-Peierls phase transition

The well known Peierls transition [7] describes the instability of electrons in a periodic potential towards a modulation. As the potential couples to the phonons there is a competition between a gain of energy in the modulated potential and the loss of distortion energy. The situation for the spin-Peierls (SP) phase transition is slightly different. We consider spins localized on a lattice which interact due to a magnetic exchange. Naturally, the coupling constants depend on the present lattice deformation. Hence, the phonon degrees of freedom couple to the spin system. By changing the exchange couplings the spin system may gain energy, on the other hand distorting the lattice costs energy due to the creation of phonons. If this situation is present, we expect a mode with a certain momentum $\mathbf{k}$ to become unstable, where $\mathbf{k}$ is depending on the magnetic field and other model parameters. The SP transition therefore is a structural phase transition. This new phase is denoted as *commensurate* if $k = \pi/n$ or *incommensurate* else.

The investigation of the SP transition was stimulated by the discovery of quasi one-dimensional materials with distinct magnetic properties. Unfortunately, up to about 1993 the known substances were organic which complicated experimental studies. Since the discovery of the inorganic compound $CuGeO_3$ the field of the SP transition has attracted much interest, in experimental as well as in theoretical works. Although $CuGeO_3$ was already analyzed in 1954 by Ginetti [57] the structural phase transition was found in 1993 by Hase *et al.* [6]. Due to the fact that single crystals of very high quality and a sufficient size can be synthesized the experimental results are exceedingly meaningful. The magnetic interaction in $CuGeO_3$ turned out to be an antiferromagnetic Heisenberg exchange where an additional frustration is present [see section 4.1 and 4.2].

With regard to a theoretical description the theory of Cross and Fisher (CF) [51] is by now commonly accepted for the description of the SP transition within an adiabatic approach. However, an unfrustrated Heisenberg model is considered there, approximating the relevant response function within a continuum treatment [see section 5.2.1 for details]. Several important experimental observations can not be understood within this scope. The TMRG allows accessing the necessary low temperature region even for frustrated spin models without using any perturbative method or approximation, still with a mean-field like treatment of the phonons. For the first time, the SP transition and the low temperature phases in $CuGeO_3$ can be investigated directly. Neither other numerical methods, e.g. exact diagonalization, nor available exact results are able to succeed here.

4.1 Structure and phase diagram of $CuGeO_3$

Compared to the earlier known organic spin-Peierls compounds the structure of $CuGeO_3$ is simple [see fig. 4.1]. The magnetic properties are subjected to the spin-1/2 moments of the Cu^{2+}-ions which form chains along the c-direction. The copper ions are located in the middle of CuO_4 plaquettes which are placed along the c-direction sharing two common edges.

The relevant chain structure with respect to a theoretical modelling is shown in Fig. 4.2 where the dominant magnetic intrachain coupling is subjected to the super-exchange path (bond bending mechanism [59, 60]) over the bridging oxygens. As the Cu-O-Cu bond angle $\gamma \approx 99^\circ$ is close to the value 90° the coupling is expected to be ferromagnetic by Goodenough-Kanamori rules. However, side group effects due to a hybridization of O and Ge orbitals yield a small antiferromagnetic (AF) exchange interaction J which is believed to be

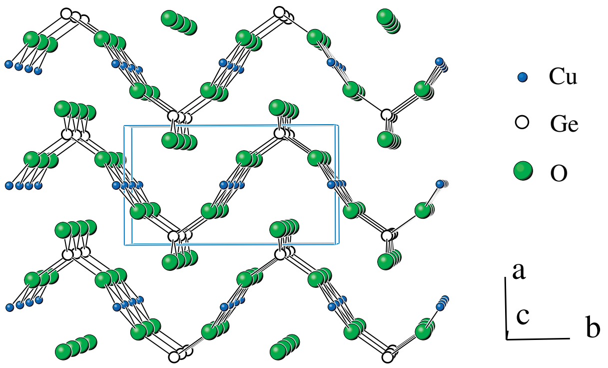

Figure 4.1: Crystal structure of $CuGeO_3$. The one-dimensional structure formed by the Cu^{2+}-ions is aligned along the c-direction.

almost isotropic. An additional exchange path Cu-O-O-Cu leads to a non-negligible AF next-nearest-neighbour (NNN) interaction J' of the Cu^{2+}-ions [60]. Fig 4.1 already visualizes that the interchain coupling

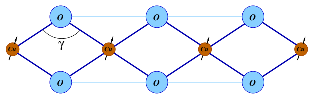

Figure 4.2: Cu^{2+} chains along the c-direction. The nearest neighbour (NN) AF spin exchange arises from a super-exchange path over the oxygen in between. NNN copper ions are additionally coupled antiferromagnetically (thin lines).

J_a along the a-direction is very weak ($J/J_a \approx 100$) which is confirmed by measuring the dispersion by inelastic neutron scattering. A comparison of the dispersion relation along the Cu^{2+} chain with that of the perpendicular b-axis leads to a ratio $J/J_b \approx 10$ [61–63]. Obviously, the experimental findings justify the desription of the magnetic properties of $CuGeO_3$ by frustrated Heisenberg chains.

The phase diagram shown by $CuGeO_3$ is typical for all spin-Peierls substances [see Fig. 4.3]. For high temperatures the compound resides in the undistorted uniform (spin liquid) phase (U). Decreasing the temperature the structure changes to dimerization (D) or incommensurate (I) modulation depending on the magnetic field. For low magnetic fields a non-magnetic dimerized state becomes stable whereas in the high field regime the lattice distortion is stabilized by the Zeeman energy. The main focus in the present thesis is on the U/D and the U/I transitions which take place at finite temperature.

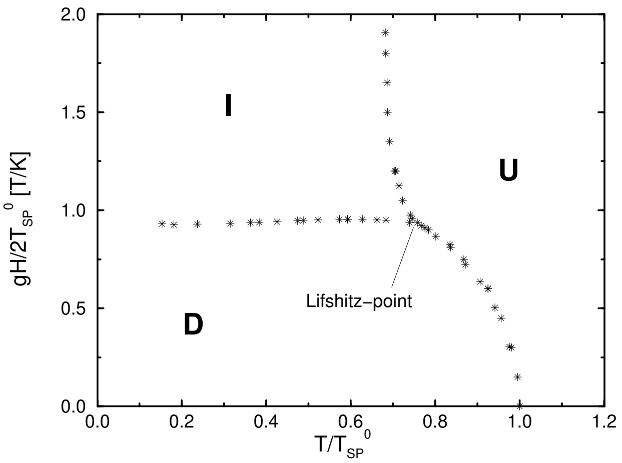

Figure 4.3: Phase diagram of $CuGeO_3$ [64], temperature versus magnetic field in reduced units. U: uniform phase; D: dimerized phase; I: incommensurate phase. The coexistence of all three phases is labeled as Lifshitz-point.

4.2 Mean-field approximation approach to the spin-Peierls phase transition

The NN exchange coupling constant affecting the sites i and $i+1$ depends linearly on their local displacements due to the bond bending mechanism. In lowest order the exchange coupling reads

$$J(\mathbf{u}_i, \mathbf{u}_{i+1}) = J + \sum_s \lambda_s \left(\mathbf{u}_{(i,s)} - \mathbf{u}_{(i+1,s)}\right), \qquad (4.1)$$

where λ_s is the microscopic *spin-phonon coupling* constant of the mode s and

$$\mathbf{u}_{(i,s)} = \sum_{\mathbf{q}} \sqrt{2Nm_s\,\Omega(\mathbf{q},s)}^{-1/2} e^{i\mathbf{q}\mathbf{R}_i}\mathbf{e}_{\mathbf{q},s}(b^\dagger_{-\mathbf{q},s} + b_{\mathbf{q},s}) \qquad (4.2)$$

denotes the local displacement operator[1] of the i-th copper atom with respect to the phonon branch s. As usual, m_s is the effective mass, N the number of unit cells and $\mathbf{R}_i$ the equilibrium position of the i-th atom, $\mathbf{e}_{\mathbf{q},s}$ denotes the polarization vector of the phonon s. The operator $b^\dagger_{\mathbf{q},s}(b_{\mathbf{q},s})$ creates (annihilates) a phonon with momentum $\mathbf{q}$ in the branch s. A detailed discussion of the relevant phonon modes is given in [65] where actually four modes turn out to be involved in the structural transition. We assume that the instability at momentum $\mathbf{k}$ occurs close to the value π such that the NNN interaction J' is independent of the modulation to lowest order[2]. Therefore, the hamiltonian reads

$$\mathcal{H} = \sum_i \left[J(\mathbf{u}_i, \mathbf{u}_{i+1})\hat{\mathbf{S}}_i\hat{\mathbf{S}}_{i+1} + J'\hat{\mathbf{S}}_i\hat{\mathbf{S}}_{i+2}\right] + \sum_{\mathbf{q},s} \Omega(\mathbf{q},s)\, b^\dagger_{\mathbf{q},s} b_{\mathbf{q},s} \qquad (4.3)$$

up to additional constants. The model [cf. eq. (4.3)] can be simplified significantly by treating the phonons adiabatically which is equivalent to a mean-field approximation (MFA) or the random-phase-approximation (RPA) which is used in the CF theory [51]. The displacement operators are replaced by their expectation values. Subsequently, the resulting order parameter has to be determined self-consistently. Rewriting

[1] We set $\hbar = 1$.

[2] A more detailed discussion is given in section 5.3.2.

eq. (4.3) yields

$$\mathcal{H} = \mathcal{H}_{\alpha,\{\delta_i\}} + E_{\text{elast}} + \mathcal{H}_{\text{Zeeman}}, \tag{4.4}$$

where the first term is the hamiltonian given by (3.25) containing the spin-spin and the spin-phonon interaction. The parameters are related by

$$\delta_i = \frac{1}{J} \sum_s \lambda_s \left(\langle \mathbf{u}_{(i,s)} \rangle - \langle \mathbf{u}_{(i+1,s)} \rangle \right), \quad \alpha = \frac{J'}{J}. \tag{4.5}$$

Note, that the lattice distortion is static due to the mean-field approach which leads to a classical elastic energy

$$E_{\text{elast}} = \frac{K}{2} \sum_i \delta_i^2 \text{ with } K = \frac{J^2}{2} \left(\sum_s \frac{\lambda_s^2}{m_s \Omega(\mathbf{q}, s)} \right)^{-1}. \tag{4.6}$$

The last term in eq. (4.4) denotes the Zeeman energy associated with an external magnetic field H,

$$\mathcal{H}_{\text{Zeeman}} = g\mu_{\text{B}} H \sum_i \hat{S}_i^z. \tag{4.7}$$

The ground state energy of $\mathcal{H}_{\alpha,\{\delta_i\}}$ is known to decrease as $\delta^{4/3} \times$ logarithmic corrections [51, 52] for $\alpha < \alpha_c$ and δ for $\alpha > \alpha_c$.[3] As the elastic energy grows proportionally to δ^2 a modulation of the couplings can lower the total ground state energy of (4.4) which indicates the possibility for a phase transition at finite temperature. However, although the model seems to be strictly one-dimensional the eleastic energy is the effective part of three-dimensional phonons which enables a phase transition.

Since the discovery of $CuGeO_3$ there have been numerous studies of appropriate sets of microscopic couplings. The microcopic parameters can be obtained, for instance, by fitting the theoretical magnetic susceptibility data to experimental results for temperatures well above the

[3] This is clear because of the spontaneous gap leading to a classical-like behaviour in first order perturbation.

transition temperature T_{SP}, i.e. in the uniform phase $\delta = 0$. Commonly used parameters are $J = 160\text{K}$[4] and $\alpha = 0.35$ [15, 16, 47]. They agree with results derived by adapting the singlet-triplet gap [17].

Since the lowest phonon energy with approximately 150K equals the magnetic energy scale the MFA is not justified a priori. However, many experimental features can be explained in the scope of the chosen quasi one-dimensional approach. Furthermore, results of Uhrig [66] show that a dynamical treatment of the magnetoelastic problem is equivalent to an effective magnetic problem, only implying renormalized coupling constants which are weakly depending on the temperature. Particularly, a frustration of the spin system is induced by dynamical phonons.

4.3 Non-universality of the dimerization response function

We first concentrate on the U/D phase transition, i.e. set $\delta_i = (-1)^i\delta$ in the model (4.4). An appropriate order parameter obviously is δ where the uniform (dimerized) phase is characterized by $\delta = 0$ ($\delta > 0$). For every finite temperature we expect the free energy of the model to behave analytically. Due to the obvious symmetry ($\delta \to -\delta$) an expansion with respect to the magnetic dimerization is given by

$$f(T,\delta) = f(T,0) + \frac{1}{2!}a(T)\delta^2 + \frac{1}{4!}b(T)\delta^4 + O(\delta^6). \tag{4.8}$$

The coefficient $a(T)$ of δ^2 is the reciprocal of the static "dimerization susceptibility". Hence, a zero in this coefficient signals a structural transition. Numerically we determine the coefficient by analyzing

$$A(T,\delta) = \frac{1}{J}\left[-\frac{1}{\delta}\frac{\partial f(T,\delta)}{\partial\delta} + K\right] = \frac{\langle\hat{\mathbf{S}}_1\hat{\mathbf{S}}_2\rangle - \langle\hat{\mathbf{S}}_2\hat{\mathbf{S}}_3\rangle}{2\,\delta} \tag{4.9}$$

which in the limit $\delta \to 0$ is simply denoted by $A(T)$[5]. Note that A is independent of K. In fig. 4.4 we show TMRG results for the temperature dependence of $A(T,\delta)$ for various δ in the case $\alpha = 0$. The TMRG

[4] The Boltzmann constant is set to $k_{\text{B}} = 1$.

[5] In a more general context the function $A(T)$ proves to be the dimer-dimer correlation function at momentum $k = \pi$ up to a factor [see section 4.7].

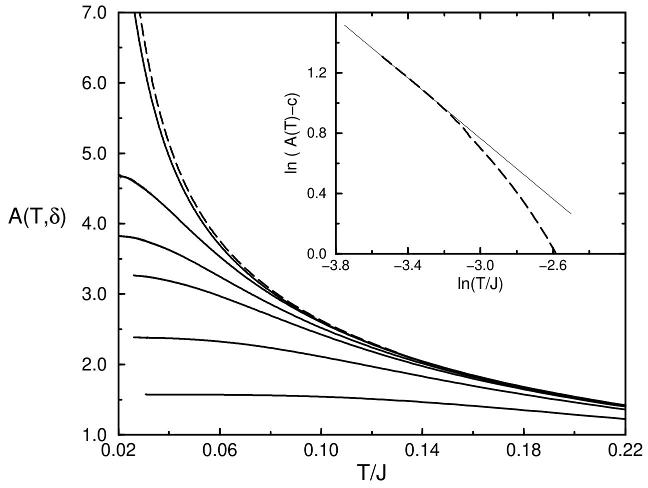

Figure 4.4: $A(T,\delta)$ as defined in the text versus temperature for $\alpha = 0$ and $\delta = 0.15, 0.1, 0.05, 0.04, 0.03, 0.01$ (from bottom to top) and the extrapolated $A(T)$ (dashed line). The inset shows a log-log plot of $(A(T) - c)$ with $c = -1.14$ (dashed line) together with a line with slope -1 (thin solid line).

parameters are $\epsilon = 0.05$ and $m = 24$ which are always utilized henceforth, if nothing different is specified. A detailed accuracy analysis with respect to exact results for free fermions is given in appendix B.2.

The relation $a(T) = K - JA(T)$ holds exactly, but we are restricted to finite δ in our numerics since the error in $A(T,\delta)$ scales with $1/\delta$. Determining $A(T)$ directly from $f(T,\delta) - f(T,0)$ would even involve an error of order $1/\delta^2$. In the sense of a multipoint formula we can assume an expansion like (4.8) up to order δ^{2n} to hold exactly, and calculate the corresponding n coefficients by considering the function $A(T,\delta)$ for n different values of δ. In this way we obtain reliable approximations for the functions $a(T), b(T), ...$ In the present work we employed a $n = 3$ point formula and used the three smallest dimerizations accessible. Here we are particularly interested in $A(T)$ at low temperature showing a divergence at $T = 0$. This singularity is caused by the failure of (4.8) at zero temperature. From [51] and also from scaling relations of the quantum critical Heisenberg chain [52] we know for $\alpha < \alpha_c$ that $f(0,\delta) - f(0,0) \simeq \delta^{4/3}$, neglecting logarithmic corrections. For $\alpha > \alpha_c$ the quantum chain shows a spontaneous magnetic dimerization as well as an excitation gap which leads to $f(0,\delta) - f(0,0) \simeq \delta$. More quantitatively, we first define a temperature variable $t = f(T,0) - f(0,0)$. The singular part of the free energy in dependence on t and δ is denoted by $\tilde{f}(t,\delta) = f(T,\delta) - f(0,0)$. Then, we expect the following scaling relation

$$\tilde{f}(t,\delta) = \frac{1}{l}\tilde{f}(tl^x, \delta l^y). \tag{4.10}$$

[See e.g. [67] as a general reference.] The exponents x and y are to be determined. From (4.10) we derive in the usual manner $\tilde{f}(t,\delta) = t^{1/x}\tilde{f}(1, \delta/t^{y/x})$. Fixing $\delta = 0$ directly implies $x = 1$ due to the definition of t. Next we use the fact that $\tilde{f}(0,\delta) \simeq \delta^\eta$ which implies $f(1,z) \simeq z^\eta$ for large z and furthermore $y = 1/\eta$. Lastly we note

$$A(T) = \frac{\partial^2}{\partial\delta^2}\tilde{f}(t,0) = t\frac{1}{t^{2/\eta}}\frac{\partial^2}{\partial\delta^2}\tilde{f}(1,0) \simeq t^{1-\frac{2}{\eta}}. \tag{4.11}$$

Fig. 4.4 displays $A(T,\delta)$ for $\alpha = 0$ and various δ and $A(T)$ (dashed line) derived from the curves with the lowest dimerization. As expected the low-temperature behavior of the free energy for a vanishing dimerization is found to be $t = T^2$ with an extrapolated groundstate energy $e_0 = -0.443(2)$. Here we have $\eta = 4/3$, thus we should observe $A(T) \simeq 1/T$ at sufficiently low T. This is excellently confirmed by our numerics [see inset of Fig. 4.4]. As the scaling relations only apply to the divergent terms we are allowed to subtract regular terms. For instance an additive constant for $A(T)$ does not change the scaling, but enlarges the temperature range where this sets in.

For overcritical frustration $\alpha > \alpha_c$ a similar scaling analysis can be performed. The main difference is the absence of quantum criticality due to the gap Δ of the elementary excitations. Fig. 4.5 shows $A(T,\delta)$ for $\alpha = 0.5$ and various δ. The coefficient $A(T)$ (dashed line) is deduced

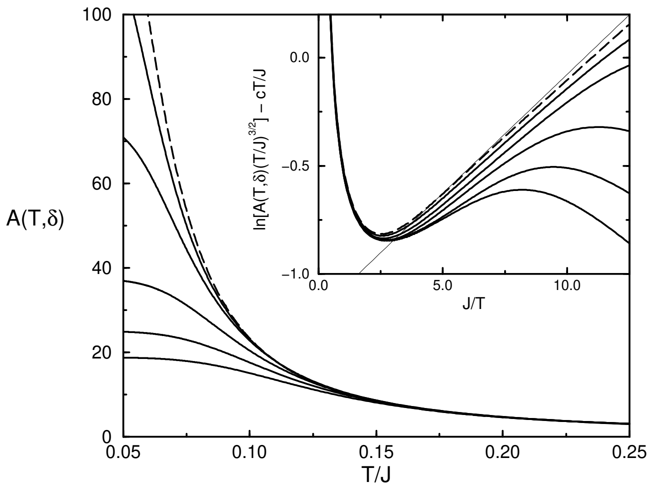

Figure 4.5: $A(T,\delta)$ versus temperature for $\alpha = 0.5$ and $\delta = 0.02, 0.015, 0.01, 0.005, 0.003$ (from bottom to top) as well as the extrapolated $A(T)$ (dashed line). The inset shows $\ln(A(T,\delta)(T/J)^{3/2}) - cT/J$ with $c = -0.56$ (solid lines) versus J/T, the same transformation applied to the extrapolated $A(T)$ (dashed line) and a line with slope $\Delta_{01}/2$ (thin solid line).

as before. The temperature variable is $t = T^{3/2}\exp(-\Delta/T)$ where $\Delta = \Delta_{01}/2$ [cf. section 3.7]. Here we have to set $\eta = 1$, which implies $A(T) \simeq t^{-1}$. Indeed we find a linear regime for $\ln(A(T)(T/J)^{3/2})$ as a function of $1/T$ [see inset of Fig. 4.5], which confirms the prediction of the scaling ansatz (4.11). Again, the subtraction of regular terms is admissible. The slight deviations from slope $\Delta_{01}/2$ must be attributed to an inaccuracy in the extrapolated $A(T)$.

To underline the significant differences in the divergent behaviour the function $T{\cdot}A(T)$ is shown for Heisenberg models with different frustrations and the free fermion model [see appendix B]. The behaviour in the case of free fermions is $A(T) \simeq \ln T$. As already seen, the singularity

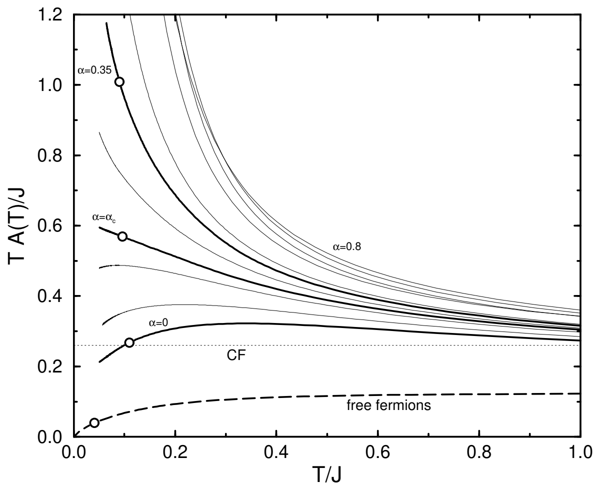

Figure 4.6: $T \cdot A(T)$ versus temperature: TMRG results for Heisenberg models with $0 \leq \alpha \leq 0.8$ in steps $\Delta\alpha = 0.1$ and exact calculation for the free fermion model. Additional α-values are marked. The open circles denote the relevant values for $CuGeO_3$ [see section 4.5]. The thin dotted line represents the prediction for $\alpha = 0$ by the CF theory.

for $\alpha < \alpha_c$ is $1/T$ where we expect $\lim_{T\to 0} T \cdot A(T) = 0$ due to the logarithmic corrections. The CF theory predicts the response function in the unfrustrated case to have the global behaviour $T \cdot A(T) = \chi_0 \approx 0.26$ [shown in fig. 4.6], however, based on a bosonization approach which is believed to capture only the long distance asymptotics of correlation functions. The enormous progress achieved by the numerical analysis is the correct treatment of the spin system on the lattice at practically all length scales. This improves over the continuum limit approach in which the asymptotics of correlation functions is incorrectly extended to short distances. For the unfrustratd Heisenberg model, i.e. $\alpha = 0$, we are able to observe directly the deviations between the continuum limit and a lattice treatment of the spin degrees of freedom. At the critical frustration $\alpha = \alpha_c$ the logarithmic corrections vanish where the fitted low temperature asymptotics reads $A(T) = \gamma J/T + c$ with parameters $\gamma = 0.623(2)$ and $c = -0.57(3)$. For overcritical frustration, i.e. $\alpha > \alpha_c$, the function $T{\cdot}A(T)$ is diverging due to the essential singularity in $A(T)$ caused by the spin gap. It is known that the gap opens exponentially at α_c, grows for increasing α and starts decreasing at $\alpha \approx 0.7$ [68–70]. Therfore, the strictly monotonous behaviour as a function of α disappears for larger α-values in the low temperature regime.

4.4 Critical temperature and order parameter

Up to now, we have considered static dimerized systems. If δ is treated as a thermodynamical degree of freedom, the system favors the dimerization which minimizes the free energy. The spontaneous dimerization $\delta(T)$ as function of temperature can either be calculated by comparing the free energies for different dimerizations δ ($K > 0$ fixed) or due to (4.9), $\delta(T)$ is implicitly defined by

$$A(T, \delta(T)) = \frac{K}{J}, \tag{4.12}$$

i.e. the intersection of $A(T, \delta)$ for fixed δ with the constant K/J. The transition temperature T_{SP} is defined by $\delta(T_{\text{SP}}^-) = 0$. For higher (lower) temperatures the free energy is increased (lowered) for a non-vanishing δ corresponding to the uniform (dimerized) phase. For determining the spontaneous dimerization we use (4.12) rather than the free energy intersection whose accuracy is lowered by a factor $1/\delta$.

In Fig. 4.7 the temperature dependence of the spontaneous dimerization ($\delta(T)$) is depicted exemplarily for $\alpha = 0, K = 1.6J$ and $\alpha = 0.35, K = 2.4J$. The exponents at the critical temperature T_{SP} are close to $1/2$ which is expected due to the mean-field treatment of the elastic degrees of freedom. The numerical analysis has been performed for a discrete set of parameters δ with a maximum value 0.15 which appears to be an upper bound for the actual $\delta(T = 0)$ for both examples. The value is in agreement with earlier self-consistent calculations by means of the DMRG for zero temperature [71]. Moreover, the critical

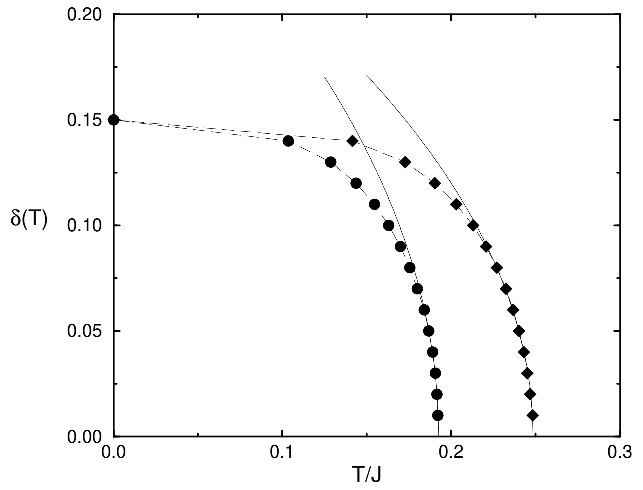

Figure 4.7: Spontaneous dimerization versus temperature for $\alpha = 0$, $K = 1.6J$ (circles) and $\alpha = 0.35$, $K = 2.4J$ (diamonds). The lines show fitted functions of type $c \cdot (T_c - T)^{\beta}$ with β fixed at 1/2.

temperature as a function of the elastic constant as well as a function of the dimerization $\delta(T = 0)$ can be deduced from $A(T, \delta)$. An application to $CuGeO_3$ is given in the following section.

4.5 The U/D transition in $CuGeO_3$

Within the one-dimensional adiabatic approach commonly used parameters are: $J \approx 160K$ and $\alpha \approx 0.35$. We focus on a brief comparison to experimental data. In order to fix the critical temperature at the experimentally determined value $T_{\text{SP}} = 14.4K$ for $CuGeO_3$ [see e.g. [72–74]] we have to use an elastic constant of $K = 11J$. Fig. 4.8 shows experimental and theoretical susceptibility data. The agreement for $T > 35K$ has already been proven in Ref. [16] utilizing exact diagonalization with $L = 16$. The finite size gap crops up already for temperatures below

$0.2J$. In our calculations we find agreement also in the region between T_{SP} and $35K$. The deviation close above the phase transition may be interpreted as a precursor due to fluctuations in the real system while our theoretical calculations indicate a sharp transition point. Below T_{SP} the susceptibility is systematically overestimated. With $K = 10.2J$, the TMRG results perfectly coincide with the experiment (see Fig. 4.8), but the transition takes place at about $15.2K$. Of course, this is a natural effect due to the mean-field approximation[6]. A similar overestimation of T_{SP} is observed by adjusting a square root behavior to the experimentally measured lattice dimerization [75].

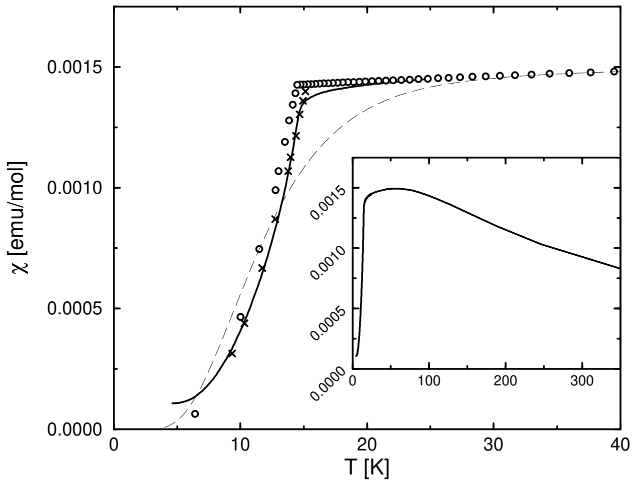

Figure 4.8: Zero field susceptibility of $CuGeO_3$. Comparison of experimental data (solid line) for the c-axis ($g_c = 2.05$) with exact diagonalization ($L = 16$) of the non-dimerized frustrated Heisenberg chain (dashed line) and TMRG results using $K = 11J$ (circles), $K = 10.2J$ (crosses).

[6]The critical exponent observed in experiments is Ising-like, i.e close to the value $\beta = 1/3$ [73, 76–78].

The spin-Peierls transition is also indicated by a cusp in the specific heat. However, a direct comparison of the experimental measurements to the numerically calculated data is inappropriate since $C = \frac{du}{dT} = \frac{\partial u}{\partial T} + \frac{\partial u}{\partial \delta}\frac{\partial \delta}{\partial T}$ involves another numerical derivative. Instead, the magnetic part of the experimental specific heat can be integrated yielding bounds for the entropy of the magnetic system [16] which actually is a thermodynamic potential. In Fig. 4.9 the entropy $S(T, \delta(T))$ is depicted for $\alpha = 0.35$. The consistency with the entropy bounds was already mentioned in [16] for temperatures above $35K$. The experimentally determined bounds are also respected for temperatures between T_{SP} and $35K$, below the critical temperature we observe deviations of about 5% with respect to the upper bound for $K = 11J$. Decreasing the elastic constant to $K = 10.2J$ with the consequences stated above the bounds are respected in the entire temperature range.

Now, the low temperature regime is accessible for the first time by means of the TMRG. To derive the experimentally observed thermodynamics we have to set $K = 11J$ $(10.2J)$ which implies a maximum dimerization of $\delta(T = 0) \approx 2.6\%$ (2.9%) [see inset of fig. 4.9] and $\Delta_{01} \approx 40K$ $(43K)$. This compares well with recent results of Büchner *et al.* [79]. They conclude a minimum dimerization of 3% based on measurements of the pressure dependence of the exchange couplings together with the structural distortion. Interestingly, the larger saturation dimerization leads to a singlet-triplet gap close to the average gap $\overline{\Delta}_{01} \approx 44K$, which may be used within the one dimensional approach regarding the interchain interaction (b direction) approximately [63].[7]

Nevertheless, these elastic constants deviate from earlier $T = 0$ calculations, where $K = 18J$ $(\delta(T = 0) \approx 1.4\%)$ is found to describe the zero temperature physics correctly [18]. In particular, the experimentally observed gap and the critical magnetic field at the D/I transition are reproduced for $K = 18J$. We have to use a smaller value for K to obtain accordance with the experimental transition temperature. The apparent discrepancy of our finite T calculations and the results in [18] may be explained by residual interchain interactions as discussed above.

[7] For a detailed discussion of the influence of an interchain coupling the reader is referred to section 5.3.1.

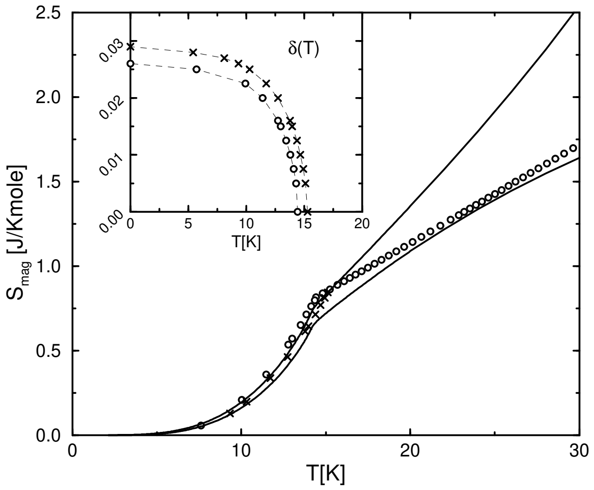

Figure 4.9: Entropy for $CuGeO_3$. Comparison of experimentally determined bounds (solid lines) with DMRG results using $K = 11J$ (circles) and $K = 10.2J$ (crosses). The inset shows the spontaneous dimerization for both cases.

With respect to $CuGeO_3$ frustration values other than $\alpha = 0.35$ had been suggested, in particular $\alpha = 0$ [CF theory] and $\alpha = \alpha_c$. Since experimental and theoretical magnetical susceptibilities do not fit in the entire temperature range for $\alpha \neq 0.35$ we fix J by the requirement that the experimental magnetic susceptibility equals that of the strictly one-dimensional model at the critical point leading to $J = 130K$ ($\alpha = 0$), $J = 150K$ ($\alpha = \alpha_c$), and $J = 350K$ (free fermions)[8]. The circles in Fig. 4.6 denote the values of $T \cdot A(T)$ at the experimentally determined spin-Peierls temperature. For the unfrustrated model the value $T_{\rm SP} \cdot A_{\alpha=0}(T_{\rm SP})$ almost coincides with the results of CF. However, the

[8]A Hartree-Fock approximation of the unfrustrated Heisenberg model (exchange coupling J) is equivalent to the free fermion model with renormalized energy $\epsilon_k = pJ\cos k$ where $p = 1 - \frac{2}{L}\sum_{k'}\langle c^\dagger_{k'} c_{k'}\rangle \cos k'$ [80–82]. It is $p \approx 1.64$ for $T \ll J$.

agreement happens only fortuitously since χ_0 [cf. section 4.3] is a zero temperature quantity. For other frustration parameters qualitative and quantitative deviations from the CF-line appear, especially in the favoured case $\alpha = 0.35$. Not only the divergence of the response function but also the quantitative values for $T_{\rm SP} \cdot A(T_{\rm SP})$ differ significantly from each other. We must conclude that it is risky to deduce quantitative results from the bosonization approach as already pointed out by CF. For applications to $CuGeO_3$ it is furthermore uncertain if the pure Heisenberg chain can even yield the qualitative results correctly.

4.6 Dependence of the miroscopic couplings on the pressure

There is experimental evidence that external pressure affects the magnetic properties of $CuGeO_3$ which manifests in the magnetic susceptibility data and the increase of the critical temperature. The authors of Ref. [83] deduced a value $\frac{dT_{\text{SP}}}{dp} \approx 4.8$ K/GPa. Earlier investigations of the magnetic properties confirmed a change of the NN exchange constant. The authors of Ref. [16] deduced a value of $\frac{d\ln J}{dp} = -7.0(5)\%/\text{GPa}$ using the relation between magnetostriction and pressure dependences of J and α where the dependence of the magnetic susceptibilty χ on J and α plays a crucial role. More quantitively, from our TMRG data we find $\frac{\partial\chi}{\partial\ln J} \gg \frac{\partial\chi}{\partial\ln\alpha}$ at constant temperature. These two quantities appear in the following expression, $\frac{d\chi}{dp} = \sum_i \frac{\partial\chi}{\partial\ln x_i}\frac{\partial\ln x_i}{\partial p}$, where $x_1 = J$ and $x_2 = \alpha$. Therefore, we conclude the value for the pressure dependence of J to be more reliable than that of α.

Writing the elastic energy in terms of the microscopic parameters [cf. eq. (4.6)] we note the important fact $K = \mathcal{C}J^2$ where $\mathcal{C}$ is independent of the magnetic properties. The spin-Peierls temperature as a function of J explicitly reads

$$T_{\text{SP}} = JA^{-1}(\mathcal{C}J) \tag{4.13}$$

inverting eq. (4.12). Applying that result to the findings of CF we have $dT_{\text{SP}}/dp = 0$ as a direct consequence which is also clear because of the fact that the energy scale of the spin system completely drops out due to scale invariance within the bosonization approach. From (4.13) it is straightforward to deduce the dependence of the spin-Peierls temperature on the variation of the spin coupling constants. Fixing the spin-Peierls temperature at the experimental value for $CuGeO_3$ implies constants $\mathcal{C}_0 \approx 0.019$ K^{-1} ($\alpha = 0$), $\mathcal{C}_{\alpha_c} \approx 0.040$ K^{-1} ($\alpha = \alpha_c$), $\mathcal{C}_{0.35} \approx 0.070$ K^{-1} ($\alpha = 0.35$), and $\mathcal{C}_{\text{ff}} \approx 0.0027$ K^{-1} (free fermions). The relation is valid for every fixed value of α. We first focus on the system with $\alpha_0 = 0.35$ at ambient pressure.

Using the experimentally determined change of the critical temperature and the deduced dependence of J on hydrostatic pressure we

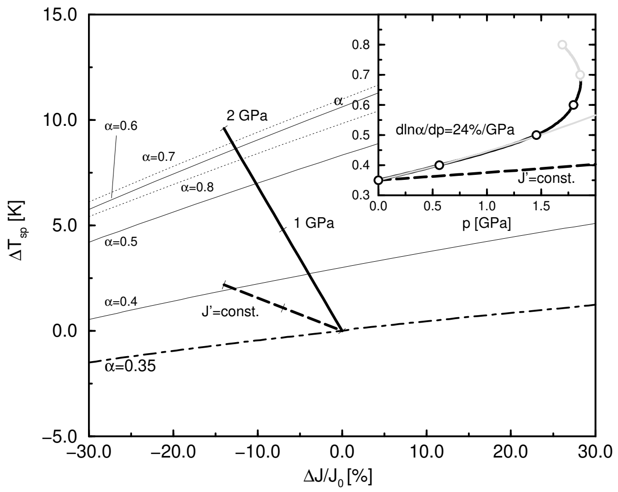

Figure 4.10: Variation of the spin-Peierls temperature versus the relative change of the magnetic exchange coupling. The lines show TMRG results for different constant α's and fixed $\mathcal{C}_{0.35}$. The thick black line displays the experimental behaviour as an implicit function of pressure. The dashed (dashed-dotted) line shows the theoretical results for $dJ'/dp = 0$ ($d\alpha/dp = 0$). The corresponding dependence of α on the pressure is shown in the inset.

obtain the relation $T_{\text{SP}}(J)$ [thick black lines in Fig. 4.10]. Due to the particular geometry involved in the super-exchange mechanism we expect the magnetic exchange energies to respond much more sensitively to the pressure than the phonon frequencies or the spin-phonon coupling constants. We therefore consider $\mathcal{C}$ as being independent of the pressure. The applicability of this assumption for $CuGeO_3$ will not hold in the regime of higher pressures. The numerical results with $\mathcal{C} = \mathcal{C}_{0.35}$ are shown in Fig. 4.10. Obviously, a constant value of $\alpha = 0.35$ [dashed-dotted line] cannot explain the observed behaviour, even yielding a change of the critical temperature to the opposite direction. For geometrical reasons we expect the NNN coupling J' to be non-decreasing. Assuming J' = constant to be realized, the increase of T_{SP} is too small by a factor of approximately 4 [as displayed by the thick dashed line in Fig. 4.10]. Consequently, the main effect must be a strong increase of J'. The deduced dependence of α on the hydrostatic pressure fits well with $\frac{d\ln\alpha}{dp} = 24 \pm 2\%/\text{GPa}$ (or $\frac{d\ln J'}{dp} = 17 \pm 2\%/\text{GPa}$, respectively) up to about 1.4 GPa as displayed in the inset of Fig. 4.10. The error was determined assuming that the value of $\frac{dT_{\text{SP}}}{dp}$ involves an error of $\pm 0.5K/\text{GPa}$, where the uncertainty in $\frac{d\ln J}{dp}$ only plays a secondary role. In general, already the weak requirement that J is non-increasing with hydrostatic pressure gives a minimum pressure dependence of $\frac{d\ln\alpha}{dp} \geq 20\%/\text{GPa}$. The pressure dependence of α deduced in ref. [16], however, with large error bounds as mentioned above are respected by our results. The divergence of $\frac{d\ln\alpha}{dp}$ at a finite pressure or in other words, an upper limit of the critical temperature, is a physical prediction of the chosen one-dimensional approach. It is mostly based on a limited spontaneous gap as a function of α. We expect a proper agreement with $CuGeO_3$ only in the low pressure region. Potentially, the behaviour of $\alpha(p)$ may be an indicator of a further phase transition occuring at high pressure which has been observed in experiments for $p > 4\text{GPa}$ [83].

	$\frac{d\ln J}{dp}$[%/GPa]	$\frac{d\ln\alpha}{dp}$[%/GPa]	$\frac{dT_{\text{SP}}}{dp}$[K/GPa]
free fermions	≈ -6	(0)	$\approx$**1.8**
$\alpha = 0$	≈ -5	(0)	$\approx$**0.3**
$\alpha_0 = 0.35$	-7.0 ± 0.4	**24±2**	4.8 ± 0.5

Table 4.1: Pressure dependences of the spin system parameters and the spin-Peierls temperature as explained in the text. Numbers in bold faces denote results obtained by TMRG calculations, all other quantities were used as input data. Note that models based on free fermions or unfrustrated Heisenberg chains cannot explain the rather large pressure dependence of the critical temperature.

The unfrustrated Heisenberg model and the free fermion model can serve as a basis for a similiar analysis. Evaluating the magnetic susceptibility data of Takahashi et al. [83] we derive $\frac{d\ln J}{dp} \approx -5\%/\mathrm{GPa}$ ($\alpha = 0$) and $\frac{d\ln J}{dp} \approx -6\%/\mathrm{GPa}$ (free fermions). In contrast to the frustrated case, a change of α under pressure for these initially unfrustrated models is not reasonable. The deduced theoretical dependence of the spin-Peierls temperature on the pressure is too small by a factor of about 3 for free fermions (or equivalent Hartree-Fock calculations), in the case of the unfrustrated Heisenberg model even by a factor of ≈ 15 [see Tab. 4.1]. We conclude that neither the unfrustrated Heisenberg model nor Hartree-Fock results are able to describe the physics of $CuGeO_3$ correctly. In constrast to this a Heisenberg model with parameters $\alpha_0 = 0.35$ and $\frac{d\ln\alpha}{dp} = 24\%/\mathrm{GPa}$ turns out to reproduce the experimental findings up to about 1.4 GPa.

Another interesting quantity is the ratio of the singlet-triplet gap to the spin-Peierls temperature, known as "BCS-ratio". Combining the TMRG data for A with zero temperature DMRG calculations for the singlet-triplet gap as a function of α and the dimerization a relation between Δ_{01} and T_{SP} can be derived. The results are shown in the bottom section of Fig. 4.11. Using the scaling of A [see section 4.3], the definition of the critical temperature and the dependence of the ground state energy on small saturation dimerizations $\delta_0 = \delta(T = 0)$, one finds $\delta_0 \simeq {T_{\text{SP}}}^{3/2} \exp(-\frac{\Delta_{01}^0}{2}/T_{\text{SP}})$[9], ignoring logarithmic corrections for $\alpha < \alpha_c$. Here, Δ_{01}^0 denotes the singlet-triplet gap for a vanishing dimerization, which is zero for $\alpha \leq \alpha_c$. In the next step we apply $\Delta_{01} - \Delta_{01}^0 \simeq \delta_0^{2/3}$ [52, 84, 85] to derive an explicit asymptotic relation between the gap and the spin-Peierls temperature,

$$\Delta_{01} - \Delta_{01}^0 \simeq T_{\text{SP}} \exp\left(-\frac{\Delta_{01}^0}{3T_{\text{SP}}}\right), \tag{4.14}$$

again by neglecting logarithmic corrections for $\alpha < \alpha_c$. The thin lines in Fig. 4.11 show fits according to eq. (4.14) in the range up to $T/J = 0.15$. For $\alpha = 0.5$ we used the known value $\Delta_{01}^0 = 0.2338J$ [see section 3.7]. Hence, only a one-parameter fit was performed in the presented

[9] Note that the exp-factor here and also in (4.14) is equal to unity for $\alpha \leq \alpha_c$ as the spin gap Δ_{01}^0 vanishes. The given formula has to be seen as a compact notation valid for all values of α.

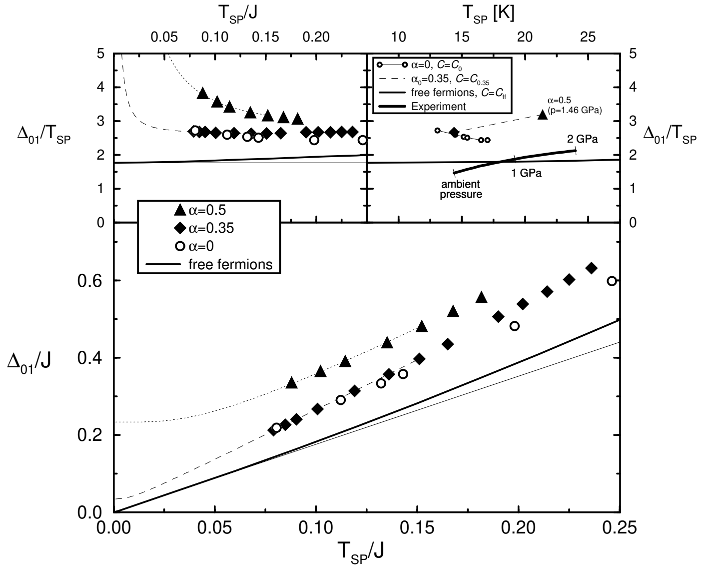

Figure 4.11: Bottom: Singlet-triplet gap Δ_{01} as a function of the spin-Peierls temperature. Symbols denote the DMRG results, the solid line shows the exact result for free fermions. The thin lines show the expected behaviour from the scaling of A [see text]. Top left: Ratio of the spin gap to the spin-Peierls temperature ("BCS ratio"). Top right: BCS ratio, experiment versus theory.

region. For $\alpha = 0.35$ a spontanous gap of $\Delta_{01}^0 = 0.035J$ is used, derived by standard DMRG [89]. For $\alpha = 0$ the predicted linear behaviour [cf. (4.14)] can not be seen due to the logarithmic corrections. A linear extrapolation of our data points shows a positive offset. However, this is consistent with the presence of logarithmic corrections since we expect a zero limit at $T = 0$ with infinite slope. The free fermions show the well known behaviour $\Delta_{01}/T_{\text{SP}} \approx 1.76$. We now derive the BCS-ratio as a function of the spin-Peierls temperature simply by dividing by T_{SP} [upper left of Fig. 4.11]. We observe that the Heisenberg like models have a distinctly larger BCS-ratio than the free fermion model.

For comparison with experiment we again fix the constant $\mathcal{C}$. Furthermore, the pressure dependence of J and the frustration derived in this section are taken into account here. The results are shown in the top right of Fig. 4.11. Interestingly, the experimental result [83] compares well with the low temperature asymptotics for free fermions, but shows a pronounced increase with pressure which cannot be reproduced. From section 4.5 we already know for Heisenberg models that the gap and therefore the BCS-ratio is larger than the experimentally observed one. This happens due to the strictly one-dimensional treatment of $CuGeO_3$, i.e. the neglect of the dispersion perpendicular to the chain which will lower the true gap. The unfrustrated chain even yields a qualitatively incorrect tendency of a decreasing BCS-ratio under pressure. The appropriately frustrated system is at least able to explain the increase.

4.7 Sinusoidal modulation and the U/I phase transition

We consider the model as given in eq. (4.4). In order to model the U/I phase transition we choose an arbitrary sinusoidal modulation of the magnetic couplings with momentum k, i.e.

$$\delta_i = \delta \cos(ki), \tag{4.15}$$

where $0 < k \leq \pi$. The free energy can be expanded in terms of the δ_i as already done for the special case $k = \pi$ in section 4.3. For finite temperature we can write

$$f = f_{\delta=0} + \underbrace{\frac{1}{2}\sum_{i,j} \frac{\partial^2 f}{\partial\delta_i \partial\delta_j}\delta_i\delta_j}_{=\Delta_2 f} + \mathcal{O}(\delta^4). \tag{4.16}$$

The system becomes unstable towards a certain mode k if the condition $\Delta_2 f(k) = 0$ for $\delta \neq 0$ holds indicating a transition from the uniform to the modulated phase with momentum k and modulation δ. The second order change in the free energy can be traced back to the dimer-dimer correlation function. We define the imaginary time dependent dimer operator, $\hat{\epsilon}_{r,\tau} = e^{\tau\mathcal{H}}\hat{\mathbf{S}}_r\hat{\mathbf{S}}_{r+1}e^{-\tau\mathcal{H}}$. The linked part of the correlation function reads $G_T(r,\tau) = \langle \mathcal{T}\hat{\epsilon}_{r,\tau}\hat{\epsilon}_{0,0}\rangle - \langle\hat{\epsilon}_{0,0}\rangle^2$. Using the Fourier transformation with respect to time and spacial degrees of freedom we find [see appendix A]

$$\Delta_2 f(k) = \frac{1}{4}(1+\delta_{k,\pi})\left(K - J^2 G_T(k)\right)\delta^2, \tag{4.17}$$

where $G_T(k)$ is the static dimer-dimer correlation function with momentum k at temperature T. Physically, the response is caused by phonons creating spin-spin excitations. In a picture of dynamical phonons the response function can be regarded as a graph expansion. The lowest order graph which describes the static response consists of two elementary vertices,

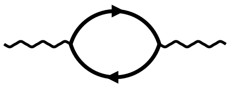

representing a single spin-spin excitation. Revisiting the free energy expansion for the purely dimerized case [see chapter 4.4] we can identify $A(T) = JG_T(\pi)$, confirming the former statement. The change in the free energy actually is discontinuous at $k = \pi$, however, not affecting the condition for the phase transition,

$$\max_{k\in[0,\pi]} G_{T_{\mathrm{SP}}}(k) = \frac{K}{J^2}, \tag{4.18}$$

defining the U-phase boundary. More precisely, for small magnetic fields we expect $G_T(k)$ to have the maximum at $k_{\max} = \pi$ indicating a transition from uniform to dimerized phase. Enlarging the magnetic field stabilizes the incommensurate modulation. By means of eq. (4.18) the maximum of $G_T(k)$ starts moving to smaller momenta.

To visualize the expected behaviour we consider the free fermion model [see appendix B]. The left part of fig. 4.12 shows $G_T(k)$ as a function of k for temperatures $0.25 \leq T/J \leq 0.5$ and a vanishing magnetic field. It is easy to show that the maximum is located at $k_{\max} = \pi$ for every temperature. A different situation arises for

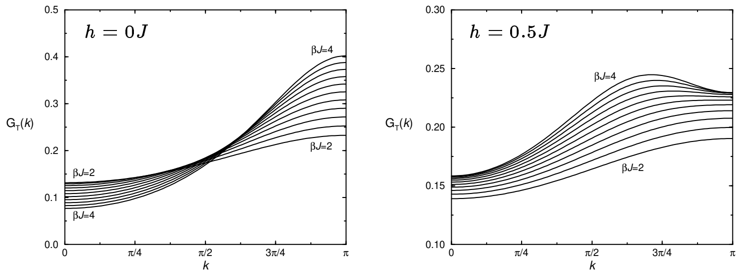

Figure 4.12: Static dimer-dimer correlation function $G_T(k)$ for the free fermion model as a function of k for temperatures $\beta J = 2.0, 2.2, \ldots, 4.0$. The left (right) diagram shows the case $h = 0$ ($h = 0.5J$).

$h \neq 0$, depicted in the right part of fig. 4.12. For large temperatures $G_T(\pi)$ is maximal. At a certain crossover temperture T^* the condition $\frac{\partial^2}{\partial k^2} G_{T^*}(k)|_{k=\pi} = 0$ holds and the maximum starts marching to $k_{\max} < \pi$ by lowering T. More quantitatively, below the crossover temperature we find $k_{\max}(T) - \pi \simeq \sqrt{T^* - T}$ which is generally valid since the dimer-dimer correlation function is analytic in k for finite temperature. In the zero temperature limit the modulation is connected to the fermi momentum by $\lim_{T\to 0} k_{\max}(T) = 2k_{\mathrm{F}} = \pi(1-(2S+1)m)$ where S denotes the spin and m is the zero temperature magnetization. For the free fermion model this can be shown straightforwardly since the magnetic field is acting as a chemical potential [cf. appendix B]. However, in the case of Heisenberg-type models this relation is also expected to hold [19, 51, 86–88].

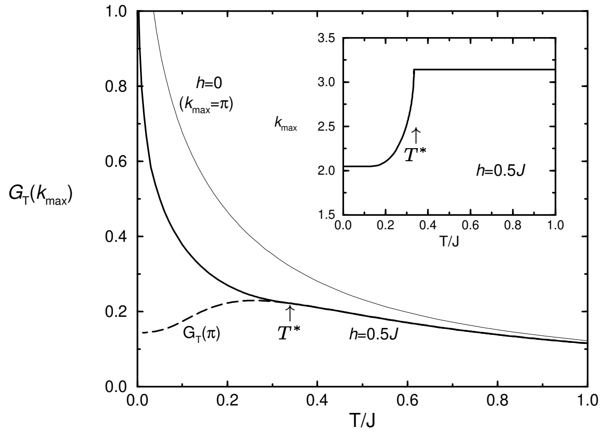

Figure 4.13: Static dimer-dimer correlation function at the modulation maximum $G_T(k_{\rm max})$ for the free fermion model as a function of T. The thick lines correspond to the case $h = 0.5J$ whereas the thin line represents $h = 0$. The function $G_T(\pi)$ is shown as dashed line for $h = 0.5J$. The inset depicts $k_{\rm max}(T)$ for $h = 0.5J$.

Chapter 5

Response functions

As seen in the previous section the static dimer-dimer correlation function is useful for determinig the U-phase boundary within an adiabatic description of the spin-Peierls phase transition. In the low field regime, i.e. U/D transition, the correlation function at momentum π is relevant which can be calculated by means of simple local expectation values [cf. section 4.3]. In contrast, the description of the uniform to incommensurate phase transition necessitates the knowledge of the static dimer-dimer correlation function $G_T(k)$ at every momentum. We do not approach the problem directly from momentum/frequency space, but we start elementary in space and virtual space coordinates. Since correlation lengths of one-dimensional quantum systems are finite at finite temperature a numerical Fourier transformation will turn out to be a suitable tool to treat the problem.

5.1 Correlation functions and TMRG

We consider a spin model with only NN interactions. Firstly, the case of composite spins as in section 3.7 is excluded. Within the Trotter decomposition we define the transfer-matrix [cf. section 3.6] $\mathcal{T}_\Sigma$ ($\mathcal{T}_{\Sigma'}$) of the operator $\sum_\tau \hat{\epsilon}_{0,\tau}$ ($\sum_\tau \hat{\epsilon}_{1,\tau}$) [see appendix A for the definition of the imaginary time evolution]. Due to linearity the decomposition $\mathcal{T}_{\Sigma^{(\prime)}} = \sum_\tau \mathcal{T}_{\hat{\epsilon}_\tau}$ is obviously valid, suppressing the space index, where $\mathcal{T}_{\hat{\epsilon}_\tau}$ is the usual transfer-matrix of a local operator as defined in section 3.6. The information on the virtual space position is still included. We must keep in mind that a transfer-matrix is covering two sites of the spin chain due to the decomposition into even and odd local hamiltonians. Therefore, according to the relation (A.6) we can write for even distances larger than zero

$$\widehat{G}_{\frac{1}{\epsilon M}}(2d, z=0) = \frac{\epsilon}{M}\frac{1}{\Lambda_0^{d+1}}\langle\psi^L|\mathcal{T}_\Sigma \mathcal{T}_M^{d-1}\mathcal{T}_\Sigma|\psi^R\rangle + \mathcal{O}(\epsilon^2), \tag{5.1}$$

whereas the odd distances can be gathered by exchanging the second $\mathcal{T}_\Sigma \to \mathcal{T}_{\Sigma'}$. Additionally, the on-site and the nearest-neighbour correlation have to be treated separately, $\widehat{G}(r, z=0) = \frac{\epsilon}{2M}\frac{1}{\Lambda_0}\langle\psi^L|\mathcal{T}|\psi^R\rangle$ where $\mathcal{T} = M\sum_\tau \mathcal{T}_{\hat{\epsilon}_{0,0}\hat{\epsilon}_{0,\tau}}$ $(r=0)$ or $\mathcal{T} = \sum_{\tau\tau'}\mathcal{T}_{\hat{\epsilon}_{0,\tau}\hat{\epsilon}_{1,\tau'}}$ $(r=1)$, respectively. Again, the corrections in the dimer-dimer correlation for finite Trotter numbers are of order $\mathcal{O}(\epsilon^2)$.

The situation becomes even more complicated in the case of frustrated and/or dimerized spin chains. Due to the combination of two spins each [cf. section 3.7] a transfer-matrix covers four sites of the original spin problem. We therefore have to define at least three transfer-matrices $\mathcal{T}_{\Sigma_i} = \sum_\tau \hat{\epsilon}_{i,\tau}$ for $i = 0, 1, 2$ in order to catch all possible distances where again the distances $r = 0, 1$ have to be treated separately. More explicitly, the dimer-dimer correlation function reads $\widehat{G}(r, z=0) = \frac{\epsilon}{M}\frac{1}{\Lambda_0^{d+1}}\langle\psi^L|A\mathcal{T}_M^{d-1}B|\psi^R\rangle$ where for $r = 4d-2$, $4d-1$, $4d$, $4d+1$ we have to choose for instance $(A, B) = (\mathcal{T}_{\Sigma_2}, \mathcal{T}_{\Sigma_0})$,$(\mathcal{T}_{\Sigma_1}, \mathcal{T}_{\Sigma_0})$, $(\mathcal{T}_{\Sigma_0}, \mathcal{T}_{\Sigma_0})$, $(\mathcal{T}_{\Sigma_0}, \mathcal{T}_{\Sigma_1})$. To enhance the numerical accuracy we can furthermore average over combinations leading to the same distance, e.g. both $(\mathcal{T}_{\Sigma_0}, \mathcal{T}_{\Sigma_1})$ and $(\mathcal{T}_{\Sigma_1}, \mathcal{T}_{\Sigma_2})$ yield $r = 4d+1$. However, at least six transfer-matrices have to be stored which necessitates the sixfold memory size. Moreover, the treatment of the correlation at a distance $r = 4d+x$ requires d additional matrix multiplications as compared to a simple expectation value increasing the required CPU-time enormously, but depending on the maximum r we are interested in.

Another crucial problem arises from the fact that the operators $\mathcal{T}_{\Sigma_i}$ needed to calculate the correlation functions cannot be deduced from the quantum transfer-matrix $\mathcal{T}_M$ in each iteration but have to be extended and renormalized independently. To demonstrate the construction principle and the recursion relations we again switch to the graphical language introduced in chapter 3.

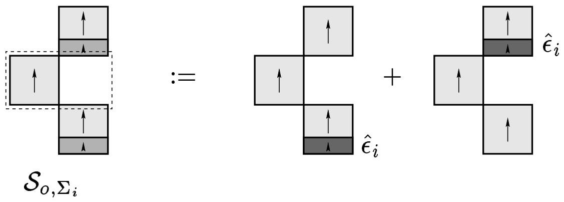

We consider for instance $M = 3$ initially and define the system block operator $\mathcal{S}_{o,\Sigma_i}$ as shown. The environment block $\mathcal{E}_{o,\Sigma_i}$ has to be defined equivalently. Then, by means of the TMRG the transfer-matrix $\mathcal{T}_{\Sigma_i}$ can obviously be constructed graphically as

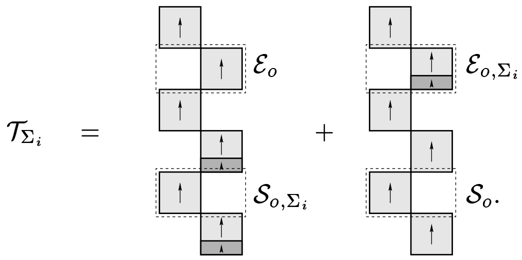

The recursion relation for the system block has to be modified in order to adapt to the structure of $\mathcal{T}_{\Sigma_i}$. First, the blocks in the (a) odd or (b) even case are enlarged as depicted.

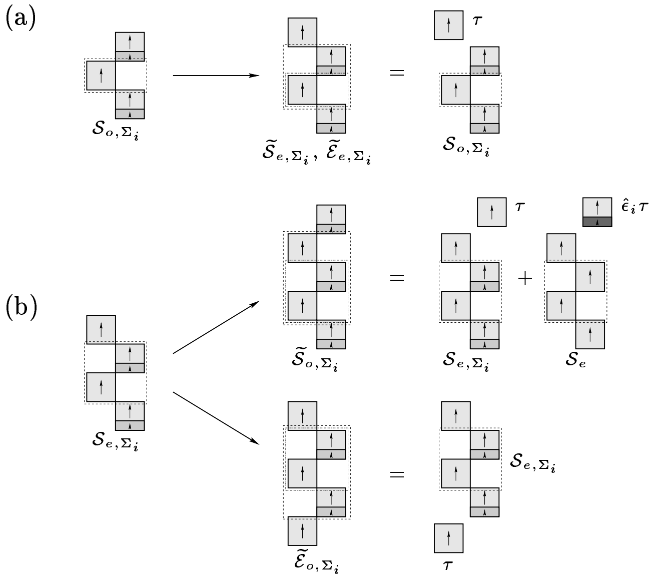

As already known, even blocks convert to odd blocks by adding a slice in virtual space and vice versa. The renormalization, i.e. the projection onto the m states corresponding to the largest eigenvalues of the density matrix, is completely equivalent to the previously discussed procedure [see section 3.3].

In order to calculate $G_T(k)$ we are rather interested in the linked part of the dimer-dimer correlation function which differs from $\widehat{G}_T(r)$ by the temperature dependent constant $c(T) = \frac{1}{T}\langle\hat{\epsilon}\rangle^2$. However, it is not necessary to calculate this constant separately since its value is given by the long distance limit $\lim_{r\to\infty}\widehat{G}_T(r)$. This method has a further advantage in transforming $\widehat{G}_T(r) \to G_T(r)$. Due to the Trotter-Suzuki decomposition even and odd distances (or $r = 4d$, $4d+1$, $4d+2$, $4d+3$ in the case of frustrated models) are treated separately. The inevitable truncation error in the renormalization step leads to slightly different asymptotics including every second (or fourth) site,

$$c_i(T) = \lim_{d\to\infty} \widehat{G}_T(2d+i) \quad \left(\text{or } \lim_{d\to\infty} \widehat{G}_T(4d+i)\right).$$

Since we cannot attain $r = \infty$ practically, we define "infinite distance" r_∞ by the requirement $\widehat{G}_T(r_\infty) = \widehat{G}_T(r_\infty + 2)$ (or $\widehat{G}_T(r_\infty) = \widehat{G}_T(r_\infty+4)$) within numerical precision. Because correlation lenghts are finite at finite temperature the numerical infinity is already attained for relatively small distances. Of course, r_∞ is increasing like the correlation length for lower temperatures. Typically, r_∞ is smaller than 100 for temperatures $T/J \geq 1/20$. The magnitude of $|c_i - c_j|$ basically depends on the number of states kept and the temperature considered. A typical value for $m = 24$ states kept is smaller than 10^{-4} for temperatures down to $T/J = 1/20$. Subsequently, the linked part of the correlation function is constructed as

$$\begin{aligned} G_T(2d+i) &= \widehat{G}_T(2d+i) - c_i(T) \\ &\qquad \left(\text{or } G_T(4d+i) = \widehat{G}_T(4d+i) - c_i(T)\right). \end{aligned}$$

Fig. 5.1 shows TMRG results for $G_T(r)$ (symbols) for the Heisenberg model at the temperature $T = 0.25J$ and for a vanishing external magnetic field. As expected the behaviour exposes to be alternating and decaying exponentially for large r which is imposingly proven by the plot of the function $\ln|G(r)|$ [see inset of Fig. 5.1]. The correlation length can be read off directly from a linear fit. However, the long distance asymptotics does not capture the correlation function entirely. Obviously, the short distance correlations which correspond to high energy excitations deviate from a purely exponential behaviour. Note that the TMRG provides a tool to analyze correlation functions beyond the level of correlation lengths. In contrast to field theoretical approaches we are able to calculate correlation functions at every length scale. Furthermore, absolute values are different from field theories where a global factor remains undetermined [see also section 5.2.1].

Under the influence of an external magnetic field we know that for sufficiently low temperatures the dominant modulation is moving to

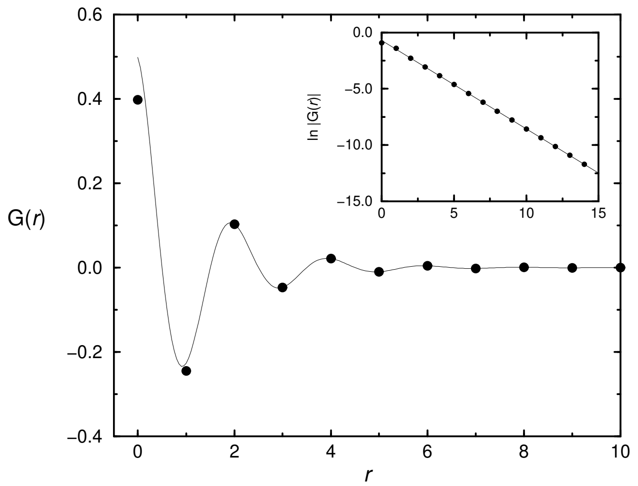

Figure 5.1: Static dimer-dimer correlation function $G(r)$ for the Heisenberg model at $T = 0.25J$ and $h = 0$. Circles denote the TMRG results ($m = 30$, $\epsilon = 0.05$), the solid line represents a fit to long distance asymptotics [see text]. The inset shows $\ln|G(r)|$.

momenta smaller than π. Figure 5.2 shows results for the Heisenberg model at $h = 1J$ and $T = 0.25J$. The more sophisticated asymptotic behaviour is described by

$$G_T^{\mathcal{A}}(r) = Ae^{-|r|/\xi}\cos(\hat{k}|r| + \delta), \tag{5.2}$$

where ξ denotes the correlation length, $\hat{k}$ the dominant modulation momentum[1] and δ a phase shift. This can be understood as follows. Returning to the transfer-matrix method it is easy to show that the asymptotic behaviour of two-point correlation functions depends on the ratio of the maximum eigenvalue Λ_0 and a suitable next leading eigen-

[1]We would like to point out that $\hat{k}$ and $k_{\max}$ [as defined in chapter 4.7] are not identical in general, since the asymptotic form does not capture the entire correlation function.

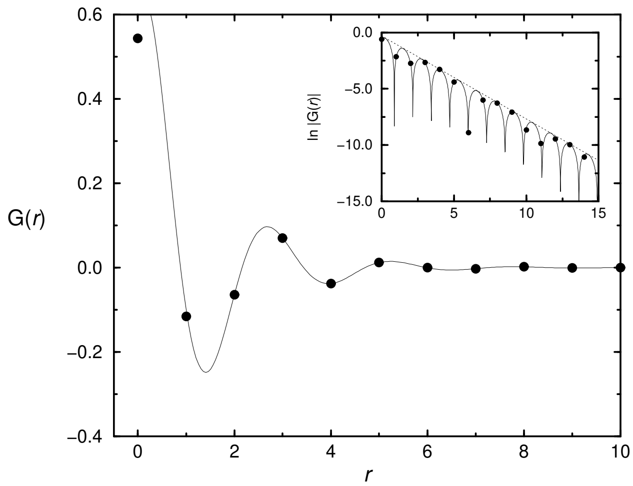

Figure 5.2: Static dimer-dimer correlation function $G(r)$ for the Heisenberg model at $T = 0.25J$ and $h = 1J$. Circles denote the TMRG results ($m = 30$, $\epsilon = 0.05$), the solid line represents a fit to long distance asymptotics [see text]. The inset shows $\ln|G(r)|$, where the dotted line is an envelope of the TMRG data corresponding to the exponential decay.

value Λ_1,

$$G(r) \simeq A\left(\frac{\Lambda_1}{\Lambda_0}\right)^{|r|} \quad \text{for } r \to \infty.$$

It is known that for non-vanishing magnetic field the next leading eigenvalue becomes degenerate and splits up into a complex pair Λ_1, Λ_1^* at a certain crossover temperature. If we write $\Lambda_1 = |\Lambda_1|e^{i\hat{k}}$ the asympotics below the crossover temperature reads

$$G(r) \simeq \frac{A}{2}\left(\frac{|\Lambda_1|}{\Lambda_0}\right)^{|r|}\left(e^{i\delta}e^{i\hat{k}|r|} + e^{-i\delta}e^{-i\hat{k}|r|}\right),$$

where A is chosen to be real and δ denotes the phase of the amplitude. By setting $\xi^{-1} = \ln|\Lambda_1|/\Lambda_0$ we obtain eq. (5.2). This expression is also valid in the case of a vanishing magnetic field by setting $\hat{k} = \pi$ and $\delta = 0$, of course. Again, the correlation length is visual in a logarithmic picture, appearing as an upper envelope of the $\ln|G(r)|$ data [see inset of fig. 5.2]. The parameters in (5.2) can be fitted effectually for $r \gg \xi$. However, the short range correlations are not captured by formula (5.2) being apparent in fig. 5.2. To look ahead, the fitting procedure could be enhanced by using the transfer-matrix. In principle all eigenvalues can be extracted from the transfer matrix $\mathcal{T}_M$. Practically, the present TMRG procedure is designed to optimize a single target state $|\,\psi_0\rangle$. The additional calulation of Λ_1 requires a multi-target state algorithm where the states $|\,\psi_0\rangle$, $|\,\psi_1\rangle$, $|\,\psi_1^*\rangle$ are optimized simultaneously. However, the basic problem is to choose the next leading eigenstate such that $\langle\psi_0^L|\hat{\epsilon}|\psi_1^R\rangle \neq 0$. We do not want to pursue this idea since the accuracy of a multi-parameter fit is sufficient for our purpose.

We like to mention that the typical time to compute a sequence of correlation functions with $m = 30$ and $\epsilon = 0.05$ down to temperatures of about $J/20$ takes approximately 4 days on a 336 MHz UltraSPARC-II workstation. Compared to the original TMRG suitable for calculating local expectation values only, this is an enormous deceleration. The reason, however, is the number of transfer-matrices that have to be renormalized in each step of the TMRG algorithm.

In the next step we want to calculate the Fourier transform of $G_T(r)$,

$$G_T(k) = \sum_{r=-\infty}^{\infty} G_T(r)\cos(kr), \tag{5.3}$$

numerically. One could naively use the pure TMRG data, nevertheless, related to a catchy assessable error especially at low temperatures where correlation lengths are large. As the numerical $G_T(r)$ exactly reaches zero before the maximum numerical precision is bailed out a large part of the tail is neglegted. The results of the Fourier transformation can be enhanced by splitting off the fitted asymptotics [see (5.2)]. Numerically, we build

$$G_T^1(k) = \sum_{r=-r_\infty}^{r_\infty} \left[G_T(r) - G_T^A(r)\right]\cos(kr). \tag{5.4}$$

The value r_∞ is determined as before. In contrast to $G_T(r)$ the function $G_T(r) - G_T^A(r)$ is decaying much faster concerning the length scale as well as the absolute magnitude. The asymptotic function can be transformed exactly yielding

$$G_T^2(k) = \frac{A}{2}\big[\mathcal{G}(\hat{k}+k) + \mathcal{G}(\hat{k}-k)\big], \tag{5.5}$$

where $\mathcal{G}(q)$ is defined by

$$\mathcal{G}(q) = \frac{(\sinh \xi^{-1} + \cos q)\cos\delta - \cos(q-\delta)}{\cosh \xi^{-1} - \cos q}, \tag{5.6}$$

such that the complete Fourier transformation reads $G_T(k) = G_T^1(k) + G_T^2(k)$.

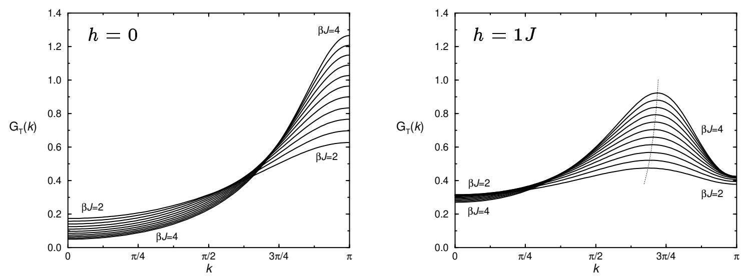

Figure 5.3: Static dimer-dimer correlation function $G_T(k)$ for the Heisenberg model as a function of k for temperatures $\beta J = 2.0, 2.2, \ldots, 4.0$. The left (right) diagram shows the case $h = 0$ ($h = 1J$). The thin dotted line in the right diagram represents the trajectory of the maxima.

Fig. 5.3 shows the function $G_k(T)$ examplarily for the Heisenberg model for a vanishing external magnetic field and $h = 1J$, respectively. As expected, the maximum $G_{k_{\max}}(T)$ increases for decreasing temperature where $k_{\max}$ is smaller than π for strong magnetic fields. Interestingly, the maximum momentum $k_{\max}$ starts at smaller values and increases as the temperature tends to zero. The inset of figure 5.4 shows the explicit evolution of $k_{\max}$ as a function of temperature as

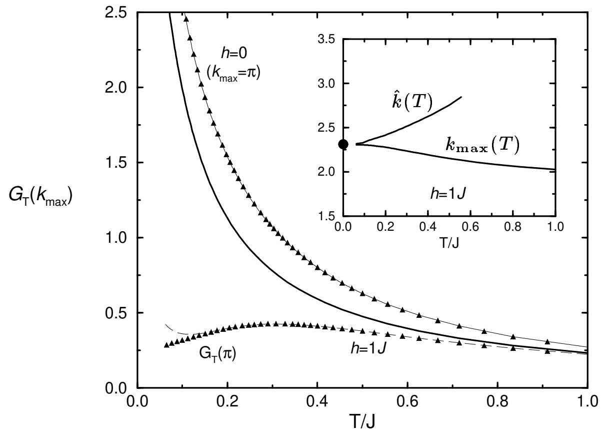

Figure 5.4: Static dimer-dimer correlation function at the modulation maximum $G_T(k_{\max})$ for the Heisenberg model as a function of T. The thick lines correspond to the case $h = 1J$ whereas the thin line represents $h = 0$. The function $G_T(\pi)$ is shown as dashed line for $h = 1J$. The inset depicts $k_{\max}(T)$ and $\hat{k}(T)$ for $h = 1J$ where the circle at $T = 0$ is derived using the zero temperature magnetization [see text]. The triangles at last show the functions $A(T)$ [cf. section 4.3] for parameters $m = 24$, $\epsilon = 0.05$.

well as the dominant modulation momentum $\hat{k}(T)$. Since the correlation length is of order $\mathcal{O}(1/T)$, it is difficult to determine $\hat{k}$ by the multi-parameter fit [cf. eq. (5.2)] for high temperatures. Reliable values are only available for temperatures smaller than $\approx 0.6J$. However, extrapolating $\hat{k}$ and $k_{\max}$ to zero temperature yields $2k_{\mathrm{F}} = 2.31(1)$. As pointed out in section 4.7 the fermi momentum is related to the zero temperature magnetization. From the extrapolated $m_0 = \lim_{T\to 0} m(T)$ we derive $\pi(1-2m_0) = 2.311(1)$ which is in perfect agreement with the momentum extracted directly from the correlation function.

For the Heisenberg model no exact results exist for $A(T)$ [as defined in chapter 4.3] and $G_T(\pi)$, respectively. As we recognized before the response function $A(T)$ is identical to $G_T(\pi)$ (up to a factor J). Both functions are calculated by the TMRG but in a completely different way. The deviations between these two functions for $h = 0$ are less then 1% down to temperatures of $J/10$ whereas a distinct divergence already starts at $T \approx J/10$ for $h = 1$. The analysis in appendix B.2 shows that the correlation functions at momentum π are less reliable at smaller temperatures than the dimerization response function. However, for high magnetic fields we rather have to use the correlation function at a smaller momentum than π which is more accurate [see also appendix B.2]. The deduced SP phase diagram on the basis of dimer-dimer correlation functions therefore proves to be meaningful anyhow.

5.2 Phase diagram

5.2.1 The unfrustrated Heisenberg chain

The first comprehensive decription of the spin-Peierls phase transition was already established by Cross and Fisher (CF) in 1979 [51]. They investigate an unfrustrated Heisenberg chain, i.e. $\alpha = 0$. Two essential simplifications are carried out:

A. The phonons are treated in random-phase-approximation (RPA), equivalent to adiabatical phonons.

B. The relevant response function is calculated within a bosonization approach, i.e. a continuum approximation.

We briefly want to give a sketch of the CF theory in order to illuminate the correspondence to the mean-field approach discussed above. The originator is the phonon propagator $\mathcal{G}^{bb^\dagger}$. Evaluating the Dyson equation at zero frequency yields

$$\mathcal{G}^{bb^\dagger}(k) = \frac{1}{\Omega(k) - \Pi(k)}, \tag{5.7}$$

where $\Omega(k)$ denotes the phonon frequency[2] and $\Pi(k)$ the polarization operator. Within RPA the function $\Pi(k)$ is identical to the previously

[2]For simplicity we restrict ourselves to just one phonon branch.

discussed static dimer-dimer correlation function (up to a constant). In a thermodynamical description of phonons the meaning of $G_T(k)$ is rather a "polarization" which creates particle-hole excitations over a spin-vacuum. The phase transition is indicated by zeros of the denominator of eq. (5.7) complying with eq. (4.18).

Obviously, up to this point, i.e. the consideration of simplification **A**, the CF theory is identical to the approach chosen in the framework of the present thesis. Accordingly, the objective is to calculate the dimer-dimer correlation function. As the TMRG is able to consider the lattice effects of the spin degrees of freedom correctly, CF have to make use of the continuum limit (simplification **B**). The basic argument justifying this approximation is the notion that the long distance asymptotics captures the entire correlation function due to quantum criticality. The CF result reads

$$G_T(k) = \mathcal{C}\,\beta^2 \left(\frac{\pi}{\beta v}\right)^{2x} \left(|I_+(k)|^2 + |I_-(k)|^2\right), \tag{5.8}$$

where v is the fermi velocity and the integrals $I_\pm$ are defined by

$$I_\pm(k) = \frac{1}{2\pi}\int_0^\infty d\lambda \frac{e^{i\frac{(k\pm 2k_\mathrm{F})v}{2\pi T}\lambda}}{(\sinh\lambda)^x}. \tag{5.9}$$

The exponent has the value $x = 1/2$. The magnetic field implicitly enters via the fermi wave vector k_F. For small fields k_F is varying linearly if the excitations are considered as free pseudo-fermions, i.e. $\Delta k_\mathrm{F} = k_\mathrm{F} - \pi \simeq H$. The value $\frac{\Delta k_\mathrm{F}}{2\pi}$ complies with the derivation from half-filling in the fermionic picture. The constant $\mathcal{C}$ in eq. (5.8) is basically the magnetic susceptibility **at** the phase transition temperature and remains undetermined within the continuum approach. CF used $\chi(T=0)$ to fix the value of $\mathcal{C}$. Due to scale invariance the energy scale of the spin system drops out leading to a "universal" phase diagram. Fig. 5.5 shows the experimental data for $CuGeO_3$ (circles) as well as the predicted phase boundaries by CF (thick solid line). We want to focus on the phase transitions from the U-phase into the two different low-temperature phases. In order to obtain a better agreement between the experimental and the theoretical data the susceptibility at T_{SP} might be

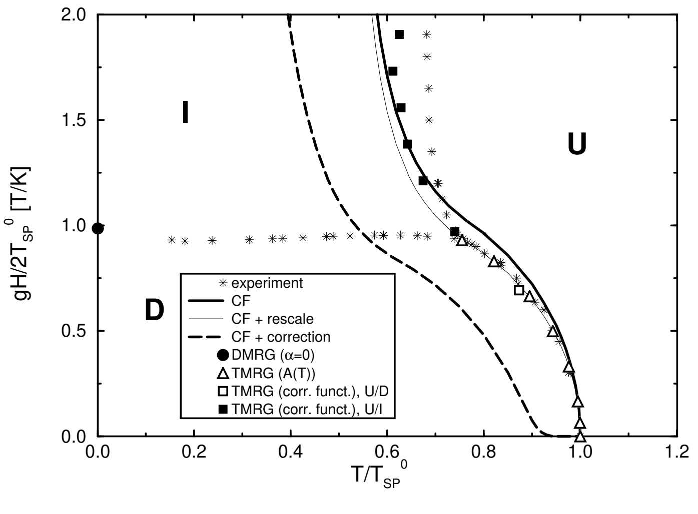

Figure 5.5: Phase diagram of $CuGeO_3$, magnetic field in reduced units versus temperature (stars). The solid line shows the findings of CF (thick=original, thin=rescaled magnetic field) whereas the dashed line represents a CF-like approach with systematical corrections [see text]. The symbols denote the TMRG results for the unfrustrated Heisenberg chain [see text for detailed comments].

used to determine the constant $\mathcal{C}$. Equivalently, the magnetic field can be rescaled by the factor $\chi(T=0)/\chi(T=T^0_{\text{SP}}) \approx 0.89$ (thin solid line). However, the U/I phase boundary does not coincide very convincingly. While the experiment shows a high field asymptotics of $\approx 0.68\,T^0_{\text{SP}}$, the CF theory predicts a value of exactly $T^0_{\text{SP}}/2$. This can be understood as follows. If we return to the pseudo-fermion picture the dimerization corresponds to half-filling. In comparison to the situation in larger magnetic fields the rate of scattering processes is doubled due to umklapp scattering. This effectively yields a λ^2 [cf. eq. 4.6] which is twice as large as for a vanishing field. From eq. (4.12) a bisection of the critical temperature for large fields is implied directly. Of course, these arguments break down if H approaches the critical field of the Heisenberg chain, $H^* = 2J$, as the zero temperature magnetization saturates. Experimentally large fields $(H/J < 0.3)^3$, however, are small compared to H^*.

Reanalyzing eq. (5.8) within conformal field theory the exponent x appears in a more general meaning, namely as scaling dimension. The explicit dependence of x on the external magnetic field was investigated by Klümper [52]. The results are depicted in the right figure. Obviously, the value $x = 1/2$ is only correct for a vanishing field. Even worse, the function $x(H)$ is non-analytic at $H = 0$ and starts increasing with infinite slope. This actually turns out to be a logarithmic singularity. Although the fields of experimental interest are relatively small the observed behaviour of the scaling dimension incapacitates the theory with a constant x even qualitatively. These findings are a non-trivial correction to the CF theory. Including the scaling dimension being correctly adjusted to its field dependence in eq. (5.8) the phase diagram changes drastically [see dashed line in figure 5.5]. As thermodynamic quantities are analytical at finite temperature we expect the U/D phase boundary to develop like $T_{\mathrm{SP}}(H) - T^0_{\mathrm{SP}} \simeq H^2$ which is a feature of the original CF theory. Due to the singularity in x for a vanishing field the critical temperature decreases exponentially. One could argue that the region for extremely low fields is not visual in experiment, but even by rescaling temperatures a correspondence between theory and experimental data cannot be achieved.

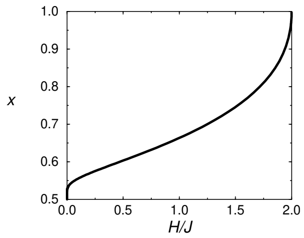

Using the TMRG we are able to avoid a continuum limit. The response functions can directly be calculated treating lattice correlation functions as discussed in section 5.1. However, the static treatment of the lattice degrees of freedom cannot be obviated. Since the

[3]The magnetic field of the model, H (in units of J), and the experimental one, H_{exp} (in Teslar), are connected by $H_{\mathrm{exp}} = \frac{J}{g\mu_{\mathrm{B}}} H \approx 1.49 \left[\frac{\mathrm{Tesla}}{\mathrm{K}}\right] \frac{J}{g} H$.

energy scale of the spin system enters [cf. section 4.3], the phase diagram is not universal in this sense. We again set $J = 130$ K which leads to agreement of the experimental and the theoretical susceptibilty at the phase transition point. The elastic constant is fixed at $K = 2.45J$ in order to set the critical temperature to the experimental value $T^0_{\mathrm{SP}} = 14.4$ K. The resulting phase transition points are shown as triangles in figure 5.5. Using these parameters a zero temperature DMRG calculation [89] yields a critical field of $\frac{gH_c}{2T^0_{\mathrm{SP}}} \approx 0.986$ which is in good agreement with experimental results [see filled circle in fig. 5.5]. The U/D phase transition points are close to the (rescaled) CF line and the experiment, respectively. The open triangles are derived from the function $A(T)$ [cf. eq. (4.12)] with $m = 24$ and $\epsilon = 0.05$. We observe a quadratic change of the critical temperature as expected. The squares show the numerical results derived from correlation functions ($m = 30$, $\epsilon = 0.05$) allowing to access both the U/D (open squares) and the U/I (filled squares) transition line.

First of all, the comparison of the $A(T)$- and the correlation function-approach shows a coincidence with respect to the transition from the uniform to the dimerized phase. The attained accuracy seems to be better than predicted by the analysis of the free fermion model [cf. section B.2]. The asymptotic value of the critical temperature for large magnetic fields is slightly different from that of the CF theory but closer to the experimental data for $CuGeO_3$. Referring to the systematic errors detected in section B.2 the TMRG data represent a lower limit for the true transition temperatures of the considered model. We therefore conclude that the CF theory predicts too small spin-Peierls temperatures with respect to the U/I transition. Renewing the discussed dependence of the scaling dimension on the magnetic field the bosonization approach explains the spin-Peierls phase transition in $CuGeO_3$ only coincidentally, as additionally accounted systematic corrections lead to a qualitatively incorrect phase diagram.

5.2.2 Frustrated models

The TMRG is also suitable to investigate the phase diagram of frustrated spin chains. From a theoretical point of view this is the first time that the phase boundaries are directly accessible within an adiabatic approach. We want to concentrate on the model with $\alpha = 0.35$ which fits well with experiment affecting thermodynamics for vanishing magnetic field [cf. chapter 4]. Since the energy scale of the spin

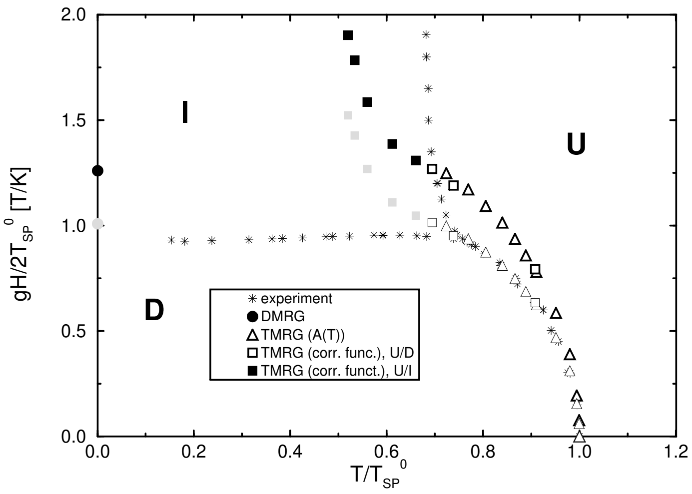

Figure 5.6: Experimental phase diagram of $CuGeO_3$ (stars) and numerical data for the frustrated ($\alpha = 0.35$) Heisenberg chain. The filled circle denotes a zero temperature DMRG result, the triangles show TMRG results derived by $A(T)$ ($m = 24$, $\epsilon = 0.05$) and the squares represent results from correlation function calculations ($m = 30$, $\epsilon = 0.05$). The "light symbols" are formed by rescaling the magnetic field [see text].

system appears in the response functions we fix $J = 160$ K such that thermodynamics is coinciding best. The elastic constant is choosen to be $K = 11J$ in order to set $T^0_{\rm SP} = 14.4$ K [see section 4.5]. The numerical phase diagram compared to the experimental data is depicted in Fig. 5.6. Concerning the D-phase bounds the magnetic field at the transition points is systematically enlarged. In other words, the critical temperature does not decrease rapidly enough with growing field. In the face of the exceeding coincidence of the thermodynamical data for the model with $\alpha = 0.35$ it is surprising that the unfrustrated Heisenberg chain yields a much better correspondence with respect to the influence of a magnetic field on the phase transition. This also holds for the U/I transition where the frustrated model predicts an asymptotic critical temperature lower than in experiment. The results for the frustrated Heisenberg model particularly show that the spin-Peierls phase diagram is explicitly depending on the frustration which contradicts to a conjecture in ref. [58].

We shall discuss in the next chapter how a rescaling of the magnetic field can be justified. The light symbols show the TMRG results with a scaling $H \to 0.8H$ such that the U/D transition lines coincide. This automatically leads to a better agreement of the critical field at zero temperature [see filled gray circle]. Nevertheless, a discrepancy at the U/I phase boundary remains which will also be discussed in section 5.3.

5.3 Corrections on the phase boundaries

5.3.1 Interchain coupling

The intrachain coupling J is the dominant magnetic interaction in $CuGeO_3$ apart from a frustration. Anyhow, there is evidence that two adjacent chains in direction of the crystal b-axes are coupled antiferromagnetically with a coupling constant J_b which is about 10% of the intrachain coupling constant J. Moreover, high temperature expansions suggest an interchain frustration along the b-direction [90, 91]. We just want to discuss qualitative changes arising from interactions perpendicular to the Cu^{2+}-chains here.

At the U/I phase boundary a modulation with a certain momentum $k < \pi$ is stabilized because the gain of magnetic energy surmounts the cost of elastic energy. In contrast, the modulation in the D-phase is $k = \pi$. Although the behaviour at the transition points appears very similar, the ground state properties in the D- and the I-phase, respectively, are significantly different. While the ground state in the D-phase is a singlet the lowest energy state in the I-phase is magnetized [71]. For a vanishing magnetic field a certain gap Δ_{01} between the $S = 0$ ground state and the triplet excitation is present. The triplet excitation can be considered as breaking a local singlet which creates a pair of spinons each with spin 1/2. These elementary excitations are bound by a confining potential [85,92,93]. In the $S = 1$ state they are coupled to a triplet. By applying a magnetic field the triplet state gains the Zeeman energy $E_{\mathrm{Zeeman}} = g\mu_{\mathrm{B}}H$ which causes a transition from D to I at zero temperature at the latest if the gap has been closed, i.e. $\Delta_{01} = E_{\mathrm{Zeeman}}$. Actually, the D/I phase transition takes place earlier, i.e. for lower fields, as a new modulation pattern adapts. The energy of this state is below that of the first excitation of a fixed dimerized chain. However, the critical field is related to the spin-gap.

As pointed out in section 4.5 the singlet-triplet gap calculated within an one-dimensional approach using a frustrated Heisenberg chain with $\alpha = 0.35$ is larger than the experimentally observed one. Theoretically, we find $\Delta_{01}^{\mathrm{th}} \approx 40$ K while experiments yield $\Delta_{01}^{\mathrm{exp}} \approx 23$ K for a vanishing external field. This problem can be resolved by a simple argument. Experiments measure the minimum gap with respect to dispersion along all axes. By assuming a purely one-dimensional model the dispersions perpendicular to the chain are constrained to be constant. Under this assumption it is appropriate to choose the constant to be the average with respect to the perpendicular modes. As shown in ref. [63] the average singlet-triplet gap amounts to $\overline{\Delta}_{01}^{\mathrm{exp}} \approx 44$ K which compares fairly well with the prediction made by the frustrated Heisenberg model. Since the critical field is rather depending on the minimum spin-gap than on the average one would also have to rescale the extrinsic magnetic field.

The authors of ref. [94] recently showed that the phase diagram of $CuGeO_3$ is universal with respect to external pressure if the magnetic field is rescaled by $H \to H/\Delta_{01}$ where Δ_{01} denotes the singlet-triplet gap for a vanishing magnetic field. More abstractly, the magnetic gap changes in consequence of modified microscopic parameters. This suggests rescaling the field with the factor $\Delta_{01}^{\mathrm{exp}}/\Delta_{01}^{\mathrm{th}} \approx 0.58$ in our case. However, this factor does not lead to an agreement affecting all possible transitions. A rescaling which matches the U/D transition also improves the critical field at zero temperature. Therefore, we have to scale $H \to 0.8H$ [cf. fig. 5.6]. Unfortunately, there is no comprehensible justification for using this factor. The theoretical U/I transition line remains shifted to lower temperatures. Since the ground state in the I-phase is magnetized an incommensurate modulation is accessorily stabilized by a magnetic interchain coupling. Translated to the phase diagram the U/I (D/I) phase boundary is shifted to higher temperatures (lower fields) whereas the effect on the U/D transition is expected to be much weaker. The present inconsistency may be resolved potentially by a detailed investigation of the consequences of an interchain coupling at finite temperatures.

The effect of an interchain coupling should also be taken into account for the unfrustrated Heisenberg chain as we observe a discrepancy between the experimental spin-gap and the theoretical prediction as well. Analogously, the field appearing in an H/T phase diagram has to be rescaled by a certain factor which obviously would destroy any coincidence [cf. fig. 5.5].

5.3.2 Higher order spin-phonon coupling

Up to now only the coupling of phonons to the magnetic NN interaction has been considered. The magnetic modulation is proportional to the distance of each two adjacent copper atoms in lowest order, i.e. $\delta_i \propto \mathbf{u}_i - \mathbf{u}_{i+1}$. A shortening of the distance reduces the bond angle and therefore the magnetic coupling constant [cf. section 4.1]. Hence, the proportionality constant is negative. Since the NNN exchange is subjected to lattice modulation as well, we have to allow the phonons to couple to a frustration. For geometrical reasons the expected coupling is proportional to $\mathbf{u}_i - \mathbf{u}_{i+2} \propto \delta_i + \delta_{i+1}$. Therefore, the spin part of the hamiltonian has to be complemented,

$$\mathcal{H} = J \sum_i \Big[(1+\delta_i)\hat{\mathbf{S}}_i \hat{\mathbf{S}}_{i+1} + (\alpha - t(\delta_i + \delta_{i+1}))\hat{\mathbf{S}}_i \hat{\mathbf{S}}_{i+2} \Big] , \qquad (5.10)$$

where t measures the NNN spin-phonon coupling in units of the NN spin-phonon coupling. The frustration is expected to increase for a decreasing distance of next-nearest neighbours which implies a positive t, i.e. $t > 0$. According to section 4.7 and appendix A the relevant response function with respect to the SP phase transition is given by

$$G^{\hat{\Gamma}\hat{\Gamma}}(r,\tau) = \langle\!\langle e^{\tau\mathcal{H}}\hat{\Gamma}_r e^{-\tau\mathcal{H}}\hat{\Gamma}_0\rangle\!\rangle, \quad \hat{\Gamma}_r = \hat{\epsilon}_r - t\,\hat{\eta}_r, \tag{5.11}$$

where $\langle\!\langle\dots\rangle\!\rangle$ denotes the linked part of the correlation function and the NN (NNN) dimer operator is defined by $\hat{\epsilon}_r = \hat{\mathbf{S}}_r\hat{\mathbf{S}}_{r+1}$ ($\hat{\eta}_r = \hat{\mathbf{S}}_r\hat{\mathbf{S}}_{r+2}$). Applying the Fourier transformation with respect to time and spatial coordinates and setting the frequency to zero yields

$$\begin{aligned} G^{\hat{\Gamma}\hat{\Gamma}}(k) = {} & G^{\hat{\epsilon}\hat{\epsilon}}(k) \\ & -4\,t\cos(k/2)\underbrace{\mathcal{R}\{e^{ik/2}G^{\hat{\epsilon}\hat{\eta}}(k)\}}_{=:G^{\hat{\epsilon}\hat{\eta}}_{\mathcal{R}}(k)} +4\,t^2\cos^2(k/2)G^{\hat{\eta}\hat{\eta}}(k). \end{aligned} \tag{5.12}$$

Obviously, the generalized phase transition condition reads

$$\max_{k\in[0,\pi]} G^{\hat{\Gamma}\hat{\Gamma}}_{T_{\mathrm{SP}}}(k) = \frac{K}{J^2}. \tag{5.13}$$

For the U/D phase transition, i.e. $k = \pi$, the distance and therefore the magnetic coupling of NNN spins remains constant. Consequently, the frustration is not affected by the lattice distortion which is of course reproduced by formula (5.12). In the special case $t = 0$ the previously discussed situation is recovered.

To study the qualitative influence of the NNN spin-phonon coupling on the phase diagram, especially on the U/I phase boundary, we consider the free fermion model which can be treated exactly[4]. The effects in the case of free fermions and Heisenberg-type models are expected to coincide qualitatively. Explicit expressions for $G^{\hat{\epsilon}\hat{\eta}}$ and $G^{\hat{\eta}\hat{\eta}}$ are calculated in appendix B.3. However, the numerical computation

[4] Of course, the correlating operators have to be redefined as $\hat{\epsilon}_r = S^x_r S^x_{r+1} + S^y_r S^y_{r+1}$ and $\hat{\eta}_r = S^x_r S^x_{r+2} + S^y_r S^y_{r+2}$.

of $G^{\hat{\eta}\hat{\eta}}$ is so expendable due to the three dimensional integral that a direct evaluation of eq. (5.13) using implicit derivatives proves to be a computational challenge. As we are interested only in qualitative effects and small NNN spin-phonon coupling constants t with regard to a correction we write

$$\Delta T_{\text{SP}} = C_1 t + \frac{1}{2} C_2 t^2 + \mathcal{O}(t^3). \tag{5.14}$$

Appraising the implicit definition of the spin-Peierls temperature [cf. eq. (5.13)] the coefficients are given by

$$\begin{aligned} C_1 &= 4\cos\left(\tfrac{k_{\max}}{2}\right) G^{\hat{\epsilon}\hat{\eta}}_{\mathcal{R}} \left(\partial_T G^{\hat{\epsilon}\hat{\epsilon}}\right)^{-1}, \\ C_2 &= -C_1^2 \partial_T^2 G^{\hat{\epsilon}\hat{\epsilon}} \left(\partial_T G^{\hat{\epsilon}\hat{\epsilon}}\right)^{-3} + 8C_1 \cos\left(\tfrac{k_{\max}}{2}\right) \partial_T G^{\hat{\epsilon}\hat{\eta}}_{\mathcal{R}} \left(\partial_T G^{\hat{\epsilon}\hat{\epsilon}}\right)^{-2} \\ &\qquad -8\cos^2\left(\tfrac{k_{\max}}{2}\right) G^{\hat{\eta}\hat{\eta}} \left(\partial_T G^{\hat{\epsilon}\hat{\epsilon}}\right)^{-1}, \end{aligned}$$

where all functions have to be taken at temperature $T = T_{\text{SP}}(t=0)$ and $k_{\max}(T)$. Again, $k_{\max}(T)$ defines the momentum which maximizes $G^{\hat{\epsilon}\hat{\epsilon}}_T(k)$ at a fixed temperature T. Note, that $C_1 \propto \cos\left(\frac{k_{\max}}{2}\right)$ and $C_2 \propto \cos^2\left(\frac{k_{\max}}{2}\right)$. Since the deviations from modulation π are small for typical magnetic fields formula (5.14) can be considered as an expansion in the parameter $t \cdot (k - \pi)$. The obvious advantage is that all response functions only have to be calculated at a single temperature and a single momentum $k_{\max}(T)$ for each magnetic field. The maximum of the response function for a vanishing t has already been determined in section 4.7. The considered expansion breaks down at the Lifshitz point as the modulation vector is not analytical with respect to its dependence on the temperature. However, the asymptotics for large fields can be studied by the use of eq. (5.14).

To show the substantial effect of the NNN spin-phonon coupling we consider the free fermion model with an elastic constant of $K = 0.5J$ which yields a zero field spin-Peierls temperature of $T^0_{\text{SP}} \approx 0.18J$. We do not want to compare the phase diagram to $CuGeO_3$ but show qualitative effects. However, the chosen critical temperature is much smaller than the coupling constant of the spin system and in this sense a typical phase transition temperature for the experimental spin-Peierls

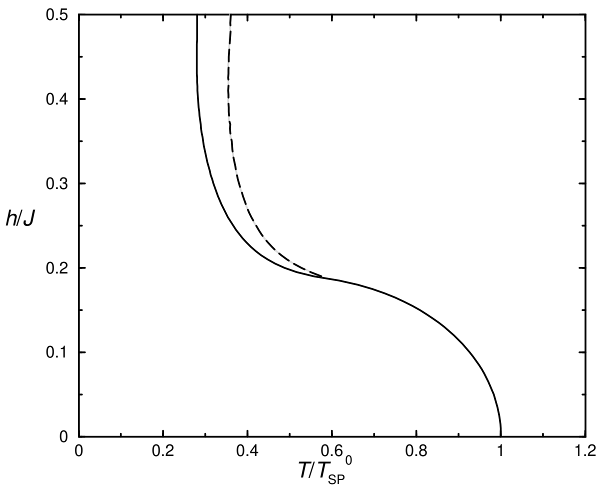

Figure 5.7: Phase diagram for the free fermion model with $K = 0.5J$ [black solid line]. The black dashed line shows the corrections induced by NNN spin-phonon coupling of magnitude $t = 0.05$, i.e. 5% of the NN spin-phonon coupling, in second order expansion. The deviation from the first order [gray line] is nearly imperceptible.

systems. Fig. 5.7 shows the corrected phase diagram exemplarily for the value $t = 0.05$. Thus, the coupling of the phonons to the frustration is assumed to be 5% of the NN spin-phonon coupling. The expansion proves to be suitable as the neglect of the second order term in the t-expansion changes the phase transition line nearly imperceptible. The U/I transition line is distinctly shifted to higher temperatures. This suggests that already a very small coupling of phonons to the next-nearest neighbour interaction has a strong effect on the transition from or into the incommensurate phase. Physically, the incommensurate modulation is stabilized by this additional coupling.

As pointed out above the effect is expected to survive qualitatively in Heisenberg-type models. Therefore, the misfit problem at the U/I transition in the case $\alpha = 0.35$ [cf. section 5.2.2] is possibly explained by the disregard of the higher order spin-phonon coupling. In principle, the correlation functions $G^{\hat{\epsilon}\hat{\eta}}$ and $G^{\hat{\eta}\hat{\eta}}$ are accessible by TMRG calculations, however, connected to a further increase of computational problems. The more complicated response functions can be implemented on the basis of section 5.1, but this requires the storage and renormalization of more transfer-matrices. At the present stage of available workstations the results in a passable time frame would be quite poor. However, since a few effects influence the phase diagram an estimation of the many additional parameters involved is nearly impossible.

Chapter 6

Conclusion

6.1 Summary

The present thesis deals with the spin-Peierls phase transition of frustrated Heisenberg chains at finite temperature. Besides the theoretical investigation of the model involving phonons within an adiabatical approximation the results are applied to the inorganic SP compound $CuGeO_3$ [5,6].

Since Heisenberg-type 1-d quantum spin systems with an additional frustration are not exactly solvable the problem has to be tackled by numerical techniques. The principal tool used is the transfer-matrix DMRG (TMRG), a numerical renormalization group method. As invented by S.R. White in 1992 [4] the fundamental idea is the utilization of a density matrix in order to truncate the Hilbert-space in an iterative enlargement procedure. This concept was extended successfully to the application at finite temperatures [21, 22]. In principle, the 1-d quantum system is mapped onto a 2-d (classical) checkerboard model applying the Trotter-Suzuki decomposition. The thermodynamics is approachable by means of eigenvalues of the quantum transfer-matrix which is handled by the renormalization group. The TMRG exceeds other numerical techniques with respect to accuracy and to the accessible temperature range. Particularly, extremely low temperatures can be reached.

The structure of $CuGeO_3$ showing distinct 1-d structures embedded in the 3-d lattice suggests a modelling by frustrated Heisenberg chains. Motivated by the experimentally observed SP phase transition the instability towards a lattice distortion is investigated. A coupling of the phonons to the magnetic exchange integrals yields a competition between a gain of magnetic energy and a loss of elastic energy. The elastic degrees of freedom are treated within a mean-field approach which cannot be justified a priori. However, it is necessary in order to apply the numerical methods efficiently. In contrast, the spin system can be attended non-perturbatively by the TMRG. Many properties of $CuGeO_3$ prove to be consistent within the scope of adiabatical phonons.

The proper SP transition can be described by means of a suitable response function: the dimer-dimer correlation function. Its physical meaning is basically the inverse of the modulation susceptibility. For a vanishing magnetic field the instablitity towards a dimerization, i.e. an alternation, is expected. Although the response function is a non-local quantity in general it can be derived simply by an analysis of local expectation values in this case.

Depending on the value of the frustration parameter the divergence behaviour for the temperature approaching zero is qualitatively different. For undercritical frustration, i.e. $\alpha < \alpha_c$, the singularity is T^{-1} (neglecting logarithmic corrections) due to quantum critcality. For overcritical frustration, i.e. $\alpha > \alpha_c$, the system shows a spontaneous gap leading to an essential singularity of the type $T^{-3/2}\exp(\Delta/T)$. The appearing effective gap is shown to be half the singlet-triplet gap, i.e. $\Delta = \Delta_{01}/2$, which can be determined also by DMRG. Results of a scaling analysis performed for low temperatures are excellently confirmed by the TMRG.

For the unfrustrated model, i.e. the usual Heisenberg chain, the numerical investigation of the response function improves over the results obtained by Cross and Fisher [51]. Both, the CF and the TMRG treatment use adiabatical phonons. In contrast, the asymptotics of the dimer-dimer correlation function is extended incorrectly to short distances within the continuum limit approach by CF. The TMRG is able to capture correlations on all length scales correctly. It allows to study the deviations between the continuum limit and a lattice treatment of the spin degrees of freedom directly.

As usual for mean-field approaches the order parameter, the magnetic modulation, has to be determined self-consistently equivalent to a minimization of the free energy. Thermodynamical quantities in the dimerized phase are accessible directly at sufficiently low temperatures by means of the TMRG. It is important to mention that the TMRG outranges other numerical techniques as e.g. exact diagonalization. At temperatures necessary to attain the dimerized phase in $CuGeO_3$ the finite size gap is already visible.

With respect to the comparison with $CuGeO_3$ the microscopic parameters have to be fixed suitably. At first, a comparison of magnetic susceptibility data allows to determine the nearest-neighbour coupling constant J as well as the frustration parameter α. Commonly used values are $J = 160$K and $\alpha = 0.35$ [15, 16, 47] which yield an excellent agreement in the entire high temperature (uniform) phase. The elastic constant K can be fixed by the requirement that the predicted spin-Peierls temperature corresponds to the experimentally observed one, $T_{\text{SP}} = 14.4$K. We have to set $K = 11J$. However, a proper agreement of the susceptibility data is obtained for $K = 10.2J$ what enlarges the critical temperature slightly ($T_{\text{SP}} = 15.2$K). This can be explained as a natural effect due to the mean-field approximation yielding a wrong critical exponent. On the other hand, fluctuations appearing as a precursor in the experiment complicate a comparison directly at the phase transition. The entropy for the latter set of interaction parameters also satisfies bounds derived from the experimental specific heat data. This applies to the uniform as well as to the dimerized phase for a vanishing magnetic field.

The zero temperature singlet-triplet gap using these paramters is $\Delta_{01}^{\text{th}} \approx 40$K which is larger than the experimental gap, $\Delta_{01}^{\text{exp}} \approx 23$K. In order to obtain an agreement between the theoretical and the experimental gap an elastic constant of $K = 18J$ has to be used as shown by earlier DMRG calculations [18]. Other zero temperature quantities are also described correctly with this set of parameters. However, the resulting critical temperature is much smaller than in the experiment. The apparent discrepancy may be explained by residual interchain interactions which suggests to average over the dispersions perpendicular to the chain [63].

As the spin system is treated correctly within the TMRG its energy scale appears explicitly in the response functions. This allows to study the pressure dependence of the spin-Peierls temperature of $CuGeO_3$. In contrast, in the continuum limit approximation the energy scale of the spin system completely drops out due to scale invariance. Starting from the dependence of J on the pressure for the frustrated model ($\alpha = 0.35$), $\frac{d \ln J}{dp} \approx -7\%/\mathrm{GPa}$ [16], and the change of T_{SP} the pressure dependence of the frustration parameter can be derived. A strong dependence of α on the pressure is found, $\frac{d \ln \alpha}{dp} \approx 24\%/\mathrm{GPa}$. The unfrustrated Heisenberg model is not able to explain the increase of the critical temperature observed in experiments even qualitatively.

Subsequently, the ratio of the singlet-triplet gap to the critical temperature is analyzed. The increase can be explained qualitatively by the frustrated model accounting the previously deduced pressure dependence of the frustration. However, a quantitative discrepancy remains which again may be resolved by including the interchain coupling. The unfrustrated model cannot affirm even the qualitative behaviour correctly.

The description of the SP phase transition can be generalized to an arbitrary sinusoidal modulation by considering momentum dependent dimer-dimer correlation functions. Technically, this is more demanding than the calculation of the dimerization response function required to investigate the U/D phase transition. A modified TMRG algorithm is developed allowing to calculate dimer-dimer correlation functions for zero frequency and arbitrary distances at finite temperatures. After tracing the linked part of this correlation function a numerical Fourier transformation is performed yielding the relevant response function at arbitrary momenta. This enables to access both the U/D and the U/I phase transition by evaluating a suitable condition equivalent to a minimization of the free energy.

By analyzing the unfrustrated Heisenberg chain by means of the TMRG a reinspection of the results obtained by CF is possible. Particularily, the deviations due to the continuum approximation can be observed directly. The U/D transition is found to coincide with the findings of CF and, as already known, with the experiment. The TMRG data for the U/I transition improve the agreement with respect to the experiment as compared to the CF theory.

Anyhow, the match of the results by CF with the experimental phase boundaries, particularly the U/D line, is remarkable because of two reasons. First, thermodynamics as well as the dependence of microscopic parameters on external fields clearly favour the presence of a frustration. Second, a review of the findings of CF within the scope of conformal field theory complementing systematical corrections shows drastic qualitative changes. The agreement of the experimental phase diagram and the predictions by the theory are suspended completely in this case.

With respect to $CuGeO_3$ the phase diagram of the model with a frustration of $\alpha = 0.35$ is studied. Compared to the phase diagram of $CuGeO_3$ the critical temperature decreases too slowly as a function of the magnetic field. The theoretically predicted U/I phase transition line is shifted to lower temperatures. In the face of the excellent agreement of the frustrated model with respect to the thermodynamics this result is surprising.

Presumably, this problem can be resolved by analyzing the effects of an interchain coupling. As seen in the context of the zero temperature gap a rescaling of the magnetic energy scale arising from the dispersions perpendicular to the chain is suggested. Consequently, the external magnetic field appearing in the model has to be rescaled as well. Particularly, this affects the U/D phase transition. On the other hand, since the ground state in the I-phase is magnetized an antiferromagnetic interchain coupling stabilizes an incommensurate modulation. Therefore, the proper U/I phase transition takes place at higher temperatures.

Another physical effect can be taken into account. The phonons have to be allowed to couple to the next-nearest-neighbour exchange integral which becomes important with respect to an incommensurate modulation. An exact analysis for the free fermion model shows that already a small coupling to the NNN interaction (as compared with that to the NN interaction) has a serious effect on the U/I transition line. It is relocated to higher temperatures, as desired, in order to yield an agreement between the phase diagrams of the model and that of $CuGeO_3$. The effect is expected to hold qualitatively also for frustrated Heisenberg chains.

6.2 Outlook

Although many properties of $CuGeO_3$ can be explained within the adiabatic approach a study of non-adiabatic phonons at finite temperature is remunerative. It is known that the phonon dynamics introduces coupling constants depending on the temperature [66]. This could resolve the discrepancy between the elastic constants in the zero and the finite temperature survey. It is also expected that dependences of microscopic constants on, for instance, the magnetic field are influenced with regard to an improved agreement of the phase diagram.

The interchain coupling has to be investigated quantitatively at finite temperature. Particularly, this is important in the magnetic regime, i.e. the I-phase, and therefore affects the U/I phase transition. In the same context, the influence of the coupling of phonons to the magnetic next-nearest-neighbour interaction can be studied by means of the TMRG.

Appendix A

Sinusoidal modulation

We consider an arbitrary spin model with hamiltonian $\mathcal{H}_0$ where the phononic degrees of freedom couple to an operator $\hat{\epsilon}_r$, for instance $\hat{\epsilon}_r = \hat{\mathbf{S}}_r \hat{\mathbf{S}}_{r+1}$. The phonons are treated adiabatically yielding a classical elastic energy. The complete hamiltonian therefore reads

$$\mathcal{H} = \mathcal{H}_0 + J \sum_r \delta_r \hat{\epsilon}_r + \frac{K}{2} \sum_r \delta_r^2. \tag{A.1}$$

We are interested in the second order change of the free energy with respect to the modulation $\delta_r = \delta \cos(kr)$. First, the free energy is decomposed by means of the Trotter formula [cf. chapter 3],

$$F_M = -\beta^{-1} \ln \mathrm{Tr} \left(e^{-\frac{\beta}{M}\mathcal{H}_0} \prod_{r,\tau} e^{-J\frac{\beta}{M}\delta_r \hat{\epsilon}_r} \right)^M + \frac{K}{2} \sum_r \delta_r^2, \tag{A.2}$$

where the τ-product runs over the values $0, \frac{\beta}{M}, \frac{2\beta}{M}, \ldots, \frac{(M-1)\beta}{M}$ such that $\lim_{M\to\infty} F_M = F$. The imaginary time evolution of $\hat{\epsilon}_r$ is defined as $\hat{\epsilon}_{r,\tau} = e^{\tau\mathcal{H}} \hat{\epsilon}_r e^{-\tau\mathcal{H}}$. Next, we calculate the second order derivative with respect to δ_r and $\delta_{r'}$,

$$\begin{aligned} \frac{\partial^2 F_M}{\partial\delta_r \partial\delta_{r'}} &= -J^2 \frac{\beta}{M^2} \sum_{\tau,\tau'} \langle \hat{\epsilon}_{r,\tau} \hat{\epsilon}_{r',\tau'} \rangle + \beta \left(\frac{J}{M} \sum_\tau \langle \hat{\epsilon}_{r,\tau} \rangle \right)^2 + K\delta_{r,r'} \\ &= -J^2 \frac{\beta}{M} \sum_\tau \underbrace{\left(\langle (\mathcal{T}) \hat{\epsilon}_{r-r',\tau} \hat{\epsilon}_{0,0} \rangle - \langle \hat{\epsilon}_{0,0} \rangle^2\right)}_{=G_T(r-r',\tau)} + K\delta_{r,r'}, \end{aligned} \tag{A.3}$$

where in the second step the translational invariance of the system was exploited. Additionally, the linked part of the correlation function, $G_T(r,\tau)$, is symmetric with respect to inverting the spatial coordinate. Note, that time ordering does not change the correlation function due to the summation over τ. In the Trotter limit $M \to \infty$ we substitute $\frac{\beta}{M}\sum_\tau \to \int_0^\beta d\tau$. Consequently, the total change of the free energy in second order $\Delta_2 F = \frac{1}{2}\sum_{r,r'} \frac{\partial^2 F}{\partial\delta_r \partial\delta_{r'}}\delta_r\delta_{r'}$ amounts to

$$\Delta_2 F = \frac{1}{2}\Bigg(- J^2 \sum_{r,r'} \int G_T(r-r',\tau) d\tau \cos(kr)\cos(kr') \\ + K\sum_r \cos^2(kr)\Bigg)\delta^2. \tag{A.4}$$

It is easy to check that $\sum_r \cos^2(kr) = \frac{L}{2}(1+\delta_{k,\pi})$ if we assume the momentum as being restricted to $0 < k \le \pi$. The Fourier transformation with respect to spatial and imaginary time coordinats should be defined as usual by $G_T(k,z_n) = \int_0^\beta d\tau \sum_r e^{-ikr} e^{z_n\tau} G_T(r,\tau)$ where z_n are the Matsubara frequencies. $G_T(k,z_n)$ can be continued analytically with respect to frequencies yielding the function $G_T(k,z)$ which has poles at the real axes. Switching to new coordinates $r-r'$, r finally yields the change in the free energy per site,

$$\Delta_2 f = \lim_{L\to\infty}\frac{1}{L}\Delta_2 F = \frac{1}{4}(1+\delta_{k,\pi})(K - J^2 G_T(k,z=0))\,\delta^2. \tag{A.5}$$

Henceforth, the static dimer-dimer correlation function with momentum k will be denoted as $G_T(k) \equiv G_T(k,z=0)$. For implementation into the concept of TMRG we like to point out the following relation,

$$G_T(k) = \sum_{r=-\infty}^{\infty}\Bigg[\underbrace{\epsilon\sum_\tau \langle\hat{\epsilon}_{r-r',\tau}\hat{\epsilon}_{0,0}\rangle - \frac{1}{T}\langle\hat{\epsilon}_{0,0}\rangle^2}_{\widehat{G}_T(r)}\Bigg]\cos(kr) + \mathcal{O}(\epsilon^2), \tag{A.6}$$

being valid for finite Trotter numbers M or finite values of ϵ, respectively, which are related by $T = \frac{1}{\epsilon M}$.

Appendix B

Free fermions

B.1 Dimer-dimer correlation function

The free fermion model is equivalent to the XXZ chain with $\Delta = 0$ by applying the Jordan-Wigner transformation [45, 46]. The hamiltonian expressed in terms of the fermions reads

$$\mathcal{H} = \sum_q \underbrace{(\cos q + h)}_{=e_q} c_q^\dagger c_q \tag{B.1}$$

where $c_q^\dagger$ (c_q) is the usual fermionic creation (annihilation) operator. We set $J = 1$. All thermodynamic potentials and derivatives can be derived simply by evaluating the definitions. We do not want to go into details here.

With regard to the spin-Peierls phase transition the dimer-dimer correlation is of a particular interest where the relevant operator reads $\hat{\epsilon}_r = \hat{S}_r^x \hat{S}_{r+1}^x + \hat{S}_r^y \hat{S}_{r+1}^y = \frac{1}{2}(c_r^\dagger c_{r+1} + c_{r+1}^\dagger c_r)$. In order to compute the dimer-dimer correlation function we have to calculate expectation values of the type $\langle c^\dagger c\, c^\dagger c\rangle$ which decompose into pairs of $\langle c^\dagger c\rangle$ by applying Wick's theorem. It is easy to check that the Fourier transformation of $\langle c_{r,\tau}^\dagger c_0\rangle\langle c_{r',-\tau}^\dagger c_0\rangle$ with respect to spacial and virtual time coordinates yields

$$\int_0^{2\pi} \mathcal{K}(k, z, T; q) e^{-iq(r+r')} dq, \tag{B.2}$$

where the integration kernel is defined by

$$\mathcal{K}(k,z,T;q) = \frac{f(e_{q-k/2}) - f(e_{q+k/2})}{z - (e_{q-k/2} - e_{q+k/2})} \tag{B.3}$$

and $f(x) = (1 + e^{x/T})^{-1}$ denotes the fermi function. Combining all addends, using translational symmetry, i.e. $\langle c_r^\dagger c_{r'} \rangle = \langle c_{r-r'}^\dagger c_0 \rangle$, and time inversion symmetry $\langle c_{r,\tau}^\dagger c_0 \rangle = -\langle c_0 c_{r,-\tau}^\dagger \rangle$, we finally derive

$$G_T(k,z) = \frac{1}{2\pi} \int_0^{2\pi} \mathcal{K}(k,z,T;q) \cos^2 q \, dq \tag{B.4}$$

according to appendix A. Physically, a phonon with momentum k creates a pair of spin/anti-spin excitations with momenta $q \pm \frac{k}{2}$ where each excitation contributes with an amplitude $a(q) = \cos q$.

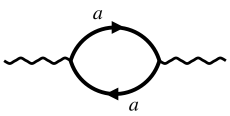

B.2 Accuracy analysis of the TMRG data

The only model available to measure the accuray of the correlation functions is the free fermion model. Its dimer-dimer correlation function has been calculated analytically in the previous section. We like to analyze the function $G_T(h)$ for a vanishing magnetic field, i.e. $h = 0$, and a large magnetic field compared to experiments ($h = 0.5J$).

Fig. B.1 shows the relative errors of $G_T(h)$ deduced from the space-dependent dimer-dimer correlation function. As expected the accuracy is declining for lower temperatures as the cutoff error increases. For a vanishing magnetic field results for different values of ϵ are compared. As stated above, the deviation due to a finite Trotter number in the dimer-dimer correlation functions are of the order $\mathcal{O}(\epsilon^2)$. Consequently, there is a competition between two sources which introduce inaccuracies. The analysis clearly shows that a small value of ϵ has an unfavourable influence on the cutoff error's account. The inaccuracy

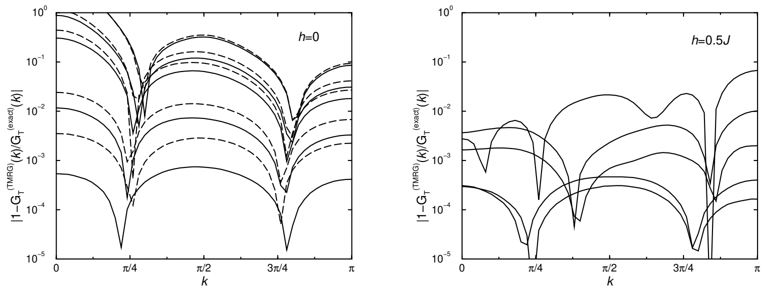

Figure B.1: Relative errors of $G_T(k)$. Left: $h = 0$, fixed temperatures $\beta J = 2, 4, 8, 10, 15$ (from bottom to top). The solid lines correspond to $\epsilon = 0.05$, the dashed lines show $\epsilon = 0.02$. Right: $h = 0.5J$, $\beta J = 2, 4, 8, 10, 15$ (from bottom to top).

is non-systematically depending on the momentum, but showing the tendency of an increase to smaller momenta. However, the interesting momentum with respect to the U/D phase transition for a vanishing magnetic field is $k = \pi$. At this special momentum the deviations are systematical in the sense that the TMRG data are too small compared to the exact results. The temperature dependence of $G_T(\pi)$ is explicitly shown in Fig. B.2 [see open squares]. In a direct composition we show the deviations of the function $A(T)$ [see open triangles/solid line] which is calculated by means of local expectation values [cf. section 4.3]. Obviously, the latter result is at least one order more precise than the dimer-dimer correlation function. We expect this observation also being valid for other models, which is important concerning the deviation of deduced phase transition points. For an applied magnetic field it is more difficult to detect systematical deviations with respect to momentum dependence [see fig. B.1]. Nevertheless, for small temperatures the TMRG results are showing to be systematically too small [see filled squares in fig. B.2]. Additionally, we show the deviations of $A(T)$ which is again more accurate at small temperatures.

Since no exact results are available for other models affecting the dimer-dimer correlation function we have to assume that the accuracies

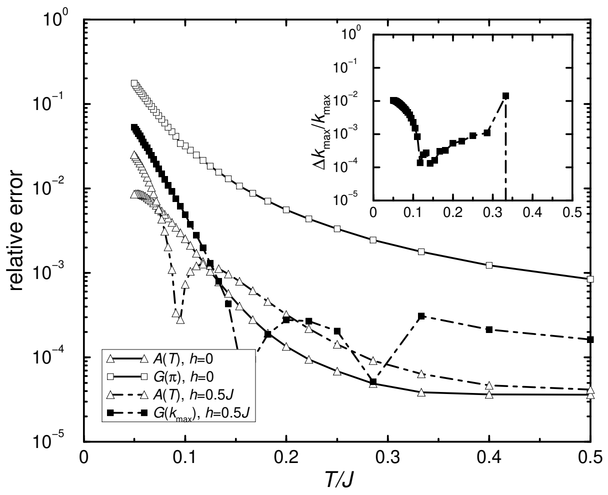

Figure B.2: Temperature dependence of the relative error for different response functions [see legend]. The inset shows the relative error of the momentum $k_{\max}$ which maximizes $G_T(k)$.

are similar for the discussed models. However, an important cross-check is the coincidence of $A(T)$ and $G_T(\pi)$ results which allows to estimate the accuracy especially for the findings based on correlation functions.

The most important application of response functions in this thesis is to calculate critical temperatures which are defined by relations like

$$g(T_c) = \text{const.} \tag{B.5}$$

Therefore, the error of the critical temperature is given by

$$\frac{\Delta T_c}{T_c} \approx \frac{1}{T_c} \left(\left. \frac{\partial \ln g}{\partial T} \right|_{T_c} \right)^{-1} \frac{\Delta g(T_c)}{g(T_c)}. \tag{B.6}$$

As we know the divergence behaviour of the correlation function for different types of models [cf. section 4.3], the relation between the relative error of T_c and that of g can be deduced,

$$\frac{\Delta T_c}{T_c} \simeq \begin{cases} \ln T_c & \text{(free fermions)} \\ 1 & (\alpha < \alpha_c) \\ T_c & (\alpha > \alpha_c) \end{cases} \times \frac{\Delta g(T_c)}{g(T_c)}.$$

This indicates that the free fermion model is the worst case for deducing critical temperatures from response functions while for a overcritically frustrated Heisenberg model the propagated error is suppressed by a factor T. However, Fig. B.2 shows that the inaccuracy is increasing exponentially. Even a linear factor in temperature cannot avoid a divergence of the error but reduces its magnitude in the range of interest.

B.3 Higher order correlation functions

In order to calculate effects arising from the coupling of phonons to the frustration the knowledge of the response functions $G^{\hat{\epsilon}\hat{\eta}}$ and $G^{\hat{\eta}\hat{\eta}}$ is necessary, where $\hat{\epsilon}_r = \hat{S}^x_r \hat{S}^x_{r+1} + \hat{S}^y_r \hat{S}^y_{r+1}$ and $\hat{\eta}_r = \hat{S}^x_r \hat{S}^x_{r+2} + \hat{S}^y_r \hat{S}^y_{r+2}$ [see section 5.3.2]. Since the Jordan-Wigner transformation is non-local the operator $\hat{\eta}_r$ contains contributions of fermions at three different sites,

$$\hat{\eta}_r = -\frac{1}{2}(c^\dagger_r c_{r+2} + c^\dagger_{r+2} c_r) \underbrace{[c^\dagger_{r+1}, c_{r+1}]}_{=2c^\dagger_{r+1}c_{r+1}-1} . \tag{B.7}$$

For future purpose we define Fourier coefficients of the Fermi function,

$$F_n(T) = \frac{1}{2\pi} \int_0^{2\pi} f(e_q) \cos(nq) dq, \tag{B.8}$$

which are depending on the temperature generically. To simplify further notations we additionally define the symbol

$$\mathcal{K}[h(q)] = \frac{1}{2\pi} \int_0^{2\pi} \mathcal{K}(k, z, T; q) h(q) dq. \tag{B.9}$$

Using this abbreviation the dimer-dimer correlation function of nearest neighbours [see section B.1] can be rewritten as $G^{\hat{\epsilon}\hat{\epsilon}} = \mathcal{K}[\cos^2 q]$.

To calculate $G^{\hat{\epsilon}\hat{\eta}}$ we have to treat two different types of terms, $\langle c^\dagger c\; c^\dagger c\rangle$ and $\langle c^\dagger c\; c^\dagger c\; c^\dagger c\rangle$. Expectation values of the first type operators can be traced back to section B.1. The second type of expression decomposes into threefold products of two-fermion Green functions. One out of the three always has to be calculated for a fixed distance and an equal time leading to a simple factor F_n [see definition (B.8)], after applying a Fourier transformation. The remaining two non-trivial two-particle Green functions are subjected to the previous scheme. After some algebra we finally derive

$$G_T^{\hat{\epsilon}\hat{\eta}}(k,z) = e^{-ik/2}\mathcal{K}\big[\underbrace{\cos q}_{a(q)}\big(\underbrace{(1+2F_0)\cos 2q - 4F_1\cos\tfrac{k}{2}\cos q + 2F_2}_{b(q)}\big)\big]. \tag{B.10}$$

In contrast to the NN dimer-dimer correlation function $G^{\hat{\epsilon}\hat{\epsilon}}$ the two excitations contribute with different amplitudes $a(q)$, $b(q)$.

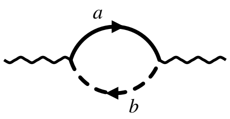

A more complicated situation arises in the case $G^{\hat{\eta}\hat{\eta}}$. The product of two operators $\hat{\eta}$ contains contractions of eight operators $c^{(\dagger)}$ where all pairs have a non-trivial time and distance dependence. Physically, these kinds of terms are interpreted as excitations involving four quasi particles.

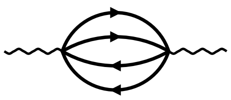

As a direct consequence we have three inner momentum degrees of freedom. We define another integration kernel by

$$\mathbf{K}(z,T;q_1,q_2,q_3,q_4) = \frac{1}{z-(e_{q_1}+e_{q_2})+(e_{q_3}+e_{q_4})} \times \frac{\sinh\frac{(e_{q_1}+e_{q_2})-(e_{q_3}+e_{q_4})}{2T}}{\cosh\frac{e_{q_1}}{2T}\cosh\frac{e_{q_2}}{2T}\cosh\frac{e_{q_3}}{2T}\cosh\frac{e_{q_4}}{2T}}. \tag{B.11}$$

The four quasi particle diagrams finally yield

$$\mathcal{G}_T^1(k,z) = \frac{1}{\pi^3}\int_0^{2\pi}\int_0^{2\pi}\int_0^{2\pi} dq_1 dq_2 dq_3 \cos(q_2+2q_3)\cos 2q_3(\cos q_2 - \cos q_1)$$
$$\times \mathbf{K}(z,T;q_3+\tfrac{q_2-q_1}{2}-\tfrac{k}{4}, q_3-\tfrac{q_2-q_1}{2}-\tfrac{k}{4}, q_3+\tfrac{q_2+q_1}{2}+\tfrac{k}{4}, q_3-\tfrac{q_2+q_1}{2}+\tfrac{k}{4}). \tag{B.12}$$

The remaining terms can be traced back to two-particle graphs already discussed. The two involved excitations contribute with the same amplitude $b(q)$ [see definition in (B.10)],

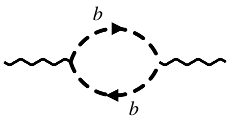

such that

$$\mathcal{G}_T^2(k,z) = \mathcal{K}[b^2(q)]. \tag{B.13}$$

The complete correlation function of NNN dimers therefore reads

$$G_T^{\hat{\eta}\hat{\eta}}(k,z) = \mathcal{G}_T^1(k,z) + \mathcal{G}_T^2(k,z). \tag{B.14}$$

Bibliography

[1] Yu.A. Izyumov and Yu.N. Skryabin, *Statistical Mechanics of Magnetically Ordered Systems* (Consultant Bureau, New York, 1988)

[2] J.L. Cardy, in *Phase Transitions and Critical Phenomena*, Vol. **11**, edited by C. Domb and J.L. Lebowitz (Academic Press, London, 1987)

[3] M. Suzuki, in *Quantum Monte Carlo Methods in Equilibrium and Nonequilibrium Systems*, edited by M. Suzuki (Springer, Berlin, 1987)

[4] S.R. White, Phys. Rev. Lett. **69**, 2863 (1992); Phys. Rev. B **48**, 10345 (1993)

[5] M. Hase, I. Terasaki and K. Uchinokura, Phys. Rev. Lett. **70**, 3651 (1993)

[6] M. Hase *et al.*, Phys. Rev. Lett. **71**, 4095 (1993)

[7] R.E. Peierls, *Quantum Theory of Solids* (Oxford U.P., Oxford, 1955)

[8] I.S. Jacobs *et al.*, Phys. Rev. B **14**, 3036 (1976)

[9] S. Huizinga *et al.*, Phys. Rev. B **19**, 4723 (1979)

[10] D. Bloch *et al.*, Phys. Rev. Lett. **44**, 294 (1980)

[11] D. Bloch *et al.*, Phys. Lett. **82A**, 21 (1981)

[12] T.W. Hijmans, H.B. Brom and L.J. de Jongh, Phys. Rev. Lett. **54**, 1714 (1985)

[13] W.H. Korving *et al.*, Physica B **145**, 299 (1987)

[14] G. Castilla, S. Chakravarty and V.J. Emery, Phys. Rev. Lett. **75**, 1823 (1995)

[15] J. Riera and A. Dobry, Phys. Rev. B **51**, 16098 (1995)

[16] K. Fabricius *et al.*, Phys. Rev. B **57**, 1102 (1998)

[17] G. Bouzerar, A.P. Kampf and F. Schönfeld, condmat/9701176

[18] T. Lorenz *et al.*, Phys. Rev. Lett. **81**, 148 (1998)

[19] G.S. Uhrig, F. Schönfeld and J. Boucher, Europhys. Lett. **41**, 431 (1998)

[20] G.S. Uhrig *et al.*, Phys. Rev. B (in press)

[21] X. Wang and T. Xiang, Phys. Rev B **56**, 5061 (1997)

[22] N. Shibata, J. Phys. Soc. Jap. **66**, 2221 (1997)

[23] see T. Xiang and X. Wang, in *Lecture Notes in Physics* edited by I. Peschel *et al.* (Springer, Berlin, 1999), Vol. 528 and references therein

[24] S. Rommer and S. Östlund, in *Lecture Notes in Physics* edited by I. Peschel *et al.* (Springer, Berlin, 1999), Vol. 528

[25] M.A. Martin-Delgado and G. Sierra, in *Lecture Notes in Physics* edited by I. Peschel *et al.* (Springer, Berlin, 1999), Vol. 528

[26] *Lecture Notes in Physics* edited by I. Peschel *et al.* (Springer, Berlin, 1999), Vol. 528

[27] Part II: Physical Applications, in *Lecture Notes in Physics* edited by I. Peschel *et al.* (Springer, Berlin, 1999), Vol. 528

[28] K.G. Wilson, Phys. Rev. B **4**, 3174 (1971)

[29] *Real-Space Renormalization*, edited by T. W. Burkhardt and J. M. J. van Leeuwen (Springer, Berlin, 1982)

[30] K.G. Wilson and J. Kogut, Phys. Rep. **12**, 75 (1974)

[31] K.G. Wilson, Rev. Mod. Phys. **47**, 773 (1975)

[32] J.W. Bray and S.T. Chui, Phys. Rev. B **19**, 4876 (1979)

[33] T. Xiang and G.A. Gehring, Phys. Rev. B **48**, 303 (1993)

[34] I. Peschel, M. Kaulke and Ö. Legeza, Ann. Physik (Leipzig) **8**, 153 (1999)

[35] R. Noack and S.R. White, in *Lecture Notes in Physics* edited by I. Peschel *et al.* (Springer, Berlin, 1999), Vol. 528

[36] S. Moukouri, and L.G. Caron, Phys. Rev. Lett **77**, 4640 (1996)

[37] E.R. Davidson, J. Comput. Phys. **17**, 87 (1975)

[38] C. Lanczos, J. Res. Natl. Bur. Stand. **45**, 225 (1950)

[39] J.K. Cullum, R.A. Willoughby, *Lanczos Algorithms for Large Symmetric Eigenvalue Computations* (Birkhäuser, Bosten-Basel-Stuttgart, 1985)

[40] H.F. Trotter, Proc. Am. Math. Soc. **10**, 545 (1959)

[41] M. Suzuki, Phys. Rev. B **31**, 2957 (1985)

[42] M. Suzuki, J. Math. Phys. **26**, 601 (1985)

[43] M. Suzuki amd M. Inoue, Prog. Theor. Phys. **78**, 787 (1987)

[44] K. Nomura and M. Yamada, Phys. Rev. B **43**, 8217 (1991)

[45] P. Jordan and E. Wigner, Z. Phys. **47**, 631 (1928)

[46] E. Lieb, T. Schultz and D. Mattis, Ann. Phys. **16**, 407 (1961)

[47] K. Okamoto and K. Nomura, Phys. Lett. A **169**, 433 (1993)

[48] S. Eggert, Phys. Rev. B **54**, R9612 (1996)

[49] C.K. Majumdar and D.K. Ghosh, J. Math. Phys. **10**, 1388 (1969)

[50] C.K. Majumdar, J. Phys. C **3**, 911 (1970)

[51] M.C. Cross, Phys. Rev. B **20**, 4606 (1979); M.C. Cross and D.S. Fisher, Phys. Rev. B **19**, 402 (1979)

[52] A. Klümper, Eur. Phys. J B **5**, 677 (1998)

[53] K. Maisinger and U. Schollwöck, Phys. Rev. Lett. **81**, 445 (1998)

[54] A. Klümper, Z. Phys. B **91**, 507 (1993)

[55] W.J. Caspers, K.M. Emmett and W. Magnus, J. Phys. A **17**, 2687 (1984)

[56] G.S. Uhrig and E. Müller-Hartmann, unpublished

[57] Y. Ginetti, Bull. Soc. Chim. Belg. **63**, 209 (1954)

[58] T. Lorenz, PhD thesis, Universität zu Köln, 1998

[59] W. Geertsma and D. Khomskii, Phys. Rev. B **54**, 3011 (1996)

[60] D. Khomskii, W. Geertsma, and M. Mostovoy, Czech. Journ. Phys. **46**, 3239 (1996)

[61] N. Nishi *et al.*, Phys. Rev. B **50**, 6508 (1994)

[62] L.P. Regnault *et. al*, Phys Rev. B **53**, 5579 (1996)

[63] G.S. Uhrig, Phys. Rev. Lett. **79**, 163 (1997)

[64] B. Büchner and T. Lorenz, private communications

[65] R. Werner, C. Gross and M. Braden, cont-mat/9810038

[66] G.S. Uhrig, Phys. Rev. B **57**, R14004 (1998)

[67] M.E. Fisher, in *Lecture Notes in Physics*, edited by F.J.W. Hahne (Springer, Berlin, 1982), Vol. 186

[68] R. Chitra *et al.*, Phys. Rev. B **52**, 6581 (1995)

[69] S.R. White and I. Affleck, Phys. Rev. B **54**, 9862 (1996)

[70] C. Knetter and G.S. Uhrig, Eur. Phys. J. B **13**, 209 (2000)

[71] F. Schönfeld, G. Bouzerar, G.S. Uhrig and E. Müller-Hartmann, Eur. Phys. J. B **5**,521 (1998)

[72] K. Hirota *et al.*, Phys. Rev. Lett. **73**, 736 (1994)

[73] T. Lorenz *et al.*, Phys. Rev. B **55**, 5914 (1997)

[74] J.P. Pouget *et al.*, Phys. Rev. Lett. **72**, 4037 (1994)

[75] B. Büchner, private communications

[76] S.M. Bhattacharjee, T. Nattermann and C. Ronnewinkel, Phys. Rev. B **58**, 2658 (1998)

[77] Q.J. Harris *et al.*, Phys. Rev. B **50**, 12606 (1994)

[78] U. Ammerahl *et al.*, Z. Phys. B **102**, 71 (1997)

[79] B. Büchner, H. Fehske, A. P. Kampf and G. Wellein, cond-mat/9806022

[80] E. Pytte, Phys. Rev. B **10**, 4637 (1974)

[81] L.N. Bulaevski, Zh. Eksp. Teor, Fiz. **43**, 968 (1962); Sov. Phys. JETP **17**, 684 (1963)

[82] G. Beni, J. Chem. Phys. **58**, 3200 (1973)

[83] H. Takahashi, N. Môri, O. Fujita, J. Akimitsu and T. Matsumoto, Sol. State Commun. B **95**, 817 (1995)

[84] I. Affleck, D. Gepner, H.J. Schulz, and T. Ziman, J. Phys. A **22**, 511 (1989)

[85] G.S. Uhrig, F. Schönfeld, M. Laukamp, and E. Dagotto, Eur. Phys. J. B **7**, 67 (1999)

[86] R. Chitra and T. Giamarchi, Phys. Rev. B **55**, 5861 (1997)

[87] G. Müller, H. Thomas, H. Beck and J.C. Bonner, Phys. Rev. B **24**, 1429 (1981)

[88] D. Poilblanc *et al.*, Phys. Rev. B **55**, R11941 (1997)

[89] F. Schönfeld, private communications

[90] C. Knetter, Diploma thesis, University of Cologne (1999)

[91] C. Knetter and G. Uhrig, in preparation

[92] J.C. Talstra, S.P. Strong and P.W. Anderson, Phys. Rev. Lett. *74*, 5256 (1995)

[93] J.C. Talstra and S.P. Strong, Phys. Rev. B *56*, 6094 (1997)

[94] J. Zeman *et al.*, cond-mat/9908145

Zusammenfassung

Die vorliegende Arbeit beschäftigt sich mit dem Spin-Peierls (SP) Phasenübergang von frustrierten Heisenberg-Ketten bei endlicher Temperatur. Dabei handelt es sich um eine strukturelle Instabilität, die durch eine Spin-Phonon-Wechselwirkung getrieben wird. Neben theoretischen Untersuchungen eindimensionaler (1-d) frustrierter Heisenberg-Modelle steht vor allem der Vergleich mit der anorganischen SP Substanz Kupfergermanat ($CuGeO_3$) im Vordergrund.

Bereits in den 70er Jahren wurde der SP Phasenübergang in organischen Substanzen beobachtet. Charakteristisch für alle SP Substanzen sind drei verschiedene Phasen. Die Hochtemperatur-Phase zeichnet sich durch eine uniforme (U) Struktur des Gitters aus. Bei tiefen Temperaturen liegen in Abhängigkeit von der Stärke des Magnetfeldes eine Dimerisierung (D), also eine Verdopplung der Einheitszelle, bzw. eine inkommensurable (I) Modulation vor. Die Schwierigkeiten bei der Synthese von organischen Kristallen in hinreichend guter Qualität erschweren jedoch experimentelle Untersuchungen. Das Interesse an diesem Phänomen kam 1993 mit der Entdeckung des SP Phasenübergangs in der anorganischen Substanz $CuGeO_3$ durch Hase *et al.* [5, 6] wieder verstärkt auf. Aufgrund der relativ einfachen Kristallstruktur lassen sich qualitativ hochwertige Einkristalle herstellen. Seither wurde eine Vielzahl von experimentellen Untersuchungen vorgenommen. Die kritische Temperatur von $CuGeO_3$ bei verschwindendem Magnetfeld liegt bei $T^0_{\text{SP}} = 14.4\text{K}$ und manifestiert sich experimentell z.B. in einem steilen Abfall der magnetischen Suszeptibilität.

Eine theoretische Beschreibung von $CuGeO_3$ gelingt mit Hilfe von

frustrierten Heisenberg-Ketten. Streuexperimente mit Neutronen zeigen nämlich ausgeprägte 1-d Strukturen. Die Cu^{2+}-Ionen, die den Spin-1/2 tragen, bilden dabei Ketten in Richtung der c-Achse des Kristalls. Über einen Super-Austausch Mechanismus wird eine antiferromagnetische Wechselwirkung J zwischen nächsten Nachbarn (NN) vermittelt. Vergleiche von thermodynamischen Daten zeigen zudem, daß eine antiferromagnetische Kopplung von übernächsten Nachbarn vorliegt, die üblicherweise als Frustration (α) bezeichnet wird. Die Kopplung der magnetischen Momente zwischen den Ketten ist um eine bzw. zwei Größenordnungen schwächer. Die (dreidimensionalen) Phononen werden im Rahmen dieser Arbeit in adiabatischer Näherung behandelt. Dies ist a priori nicht gerechtfertigt, da die Energieskalen des Spin- und des Phononensystems in etwa vergleichbar sind, wird aber durch die Konsistenz diverser theoretischer Untersuchungen mit dem Experiment gestützt.

Die zugrundeliegenden 1-d Modelle werden vornehmlich mit einer Variante der Dichte-Matrix-Renormierungs-Gruppe (DMRG), die auf S.R. White [4] zurückgeht, untersucht. Dabei handelt es sich um ein numerisches Renormierungs-Gruppen Verfahren, das von Wang und Xiang [21] bzw. Shibata [22] später für die Anwendung bei endlicher Temperatur modifiziert wurde. Die Grundidee besteht darin, die Quantenkette unter Benutzung der Trotter-Suzuki-Formel auf ein zweidimensionales, klassisches Schachbrett-Modell abzubilden. Die gesamte Thermodynamik ist determiniert durch den größten Eigenwert der Quanten-Transfermatrix, der durch Anwendung der DMRG bestimmt wird. Diese Variante bezeichnet man als Transfermatrix DMRG (TMRG). Im Vergleich mit anderen numerischen Zugängen wie exakter Diagonalisierung oder Quanten-Monte-Carlo-Verfahren kann die TMRG extrem niedrige Temperaturen bei hoher Genauigkeit erreichen.

Der eigentliche SP Phasenübergang wird durch eine geeignete Response-Funktion, der Dimer-Dimer-Korrelations-Funktion, beschrieben. Physikalisch stellt diese die Inverse der statischen Dimerisierungs-Suszeptibilität dar. Für verschwindendes Magnetfeld wird eine Instabilität gegenüber einer Dimerisierung, also einer Alternierung der Kopplungskonstanten, erwartet. Obwohl die Korrelationsfunktion eine nicht-lokale

Größe ist, kann die Response-Funktion in diesem Fall einfach mit Hilfe von lokalen Erwartungswerten berechnet werden.

Die Response-Funktion divergiert bei Annäherung der Temperatur an den Nullpunkt. Auf der Basis einer Skalenanalyse wird gezeigt, daß die Art der Divergenz stark von der Größe des Frustrationsparameters abhängt. Im Falle einer unterkritischen Frustration, d.h. $\alpha < \alpha_c$, ist die Singularität wegen der lückenlosen Anregungen vom Typ T^{-1}, abgesehen von logarithmischen Korrekturen. Für überkritische Frustration, d.h. $\alpha > \alpha_c$, hingegen zeigt das System eine spontane Lücke, die zu einer wesentlichen Singularität der Art $T^{-3/2}\exp(\Delta/T)$ führt. Die dabei erscheinende Energieskala Δ erweist sich als die halbe Singulett-Triplett-Lücke, die spektroskopisch von Bedeutung ist. Die Vorhersagen der Skalenanalyse können durch die Ergebnisse mittels TMRG hervorragend bestätigt werden.

Die TMRG-Rechnungen für das unfrustrierte Heisenberg-Modell verfeinern die Ergebnisse von Cross und Fisher (CF) [51]. Im Bezug auf die adiabatische Behandlung des Phononsystems sind die CF-Theorie und die TMRG-Rechnungen identisch. Das Spin-System wird jedoch abweichend betrachtet. Die CF-Theorie bedient sich dabei der Bosonisierung, einer Kontinuumsnäherung. Die Asymptotik der Dimer-Dimer-Korrelationsfunktion wird nicht korrekt zu kurzen Distanzen hin fortgesetzt. Im Rahmen der TMRG-Untersuchung ist dagegen ein korrektes Einbeziehen des Gitters und damit eine Berechnung der Korrelationsfunktion auf allen Längenskalen möglich. Insofern erlaubt die numerische Analyse ein direktes Beobachten der durch die Kontinuums-Näherung eingebrachten Abweichungen.

Im Hinblick auf den Vergleich der theoretischen Vorhersagen mit den Messergebnissen an $CuGeO_3$ müssen die mikroskopischen Parameter geeignet gewählt werden. Ein Vergleich der magnetischen Suszeptibilität ergibt eine hervorragende Übereinstimmung für den Parametersatz $J = 160$K, $\alpha = 0.35$ [15, 16, 47] über den gesamten Temperaturbereich in der U-Phase. Die elastische Konstante K wird so gewählt, daß die SP Temperaturen bei verschwindendem äußeren Magnetfeld identisch sind, was auf $K = 11J$ führt. Eine wirkliche Übereinstimmung der thermodynamischen Daten, z.B. der magnetischen Suszeptibilität, in der dimerisierten Phase wird allerdings nur für $K = 10.2J$ erzielt. Dabei vergrößert sich die (scharfe) Phasenübergangs-Temperatur in der Theorie jedoch auf $T_{\mathrm{SP}} = 15.2\mathrm{K}$, wofür es zwei Erklärungen gibt. Zum einen liefert die Mean-Field-Approximation den falschen kritischen Exponenten für den Ordnungsparameter. Dieser weicht mit $\beta = 1/2$ von dem im Experiment beobachteten isingartigen Exponenten $\beta = 1/3$ ab, woraus das sichtbare Verhalten resultiert. Zum anderen erschweren im Experiment auftretende Precursor-Effekte einen Vergleich der Daten unmittelbar am Phasenübergang. Der gewählte Parametersatz ist ebenfalls in der Lage, den aus der experimentellen spezifischen Wärme abgeleiteten Entropieverlauf zu erklären. Es ist anzumerken, daß eine Übereinstimmung sowohl der Suszeptibilität als auch der Entropie für keine andere Frustration, insbesondere auch nicht für das unfrustrierte Heisenberg-Modell, erreichbar ist.

Die aus dem voliegenden Parametersatz abgeleitete Singulett-Triplett-Lücke liegt mit $\Delta_{01}^{\mathrm{th}} \approx 40\mathrm{K}$ über der experimentellen spektroskopischen Lücke von $\Delta_{01}^{\mathrm{exp}} \approx 23\mathrm{K}$. Um hier eine Koinzidenz zu erreichen benötigt man eine elastische Konstante von $K = 18J$. Frühere DMRG-Untersuchungen zeigen, daß in diesem Fall auch andere $T = 0$ Eigenschaften von $CuGeO_3$ erklärt werden können. Die kritische Temperatur für den U/D-Phasenübergang ist dann allerdings deutlich zu klein. Eine mögliche Ursache für diese Diskrepanz stellt die Zwischenkettenkopplung dar. Eine daraus resultierende nicht-verschwindende Dispersion senkrecht zur Kettenrichtung legt nahe, eine gemittelte Lücke anstelle der minimalen (spektroskopischen) Lücke zu verwenden. Dies, durchgeführt für den adäquaten Hochtemperatur-Parametersatz, löst tatsächlich den quantitativen Widerspruch auf. Ein weiterer Effekt ist eine Temperaturabhängigkeit der Kopplungsparameter, die aufgrund der nicht berücksichtigten Fluktuationen der phononischen Freiheitgrade ins Spiel kommt.

Im Gegensatz zum Bosonisierungs-Zugang von CF erscheint in den TMRG-Rechungen die Energieskala des Spin-Systems explizit. Als Folge der Skaleninvarianz fällt diese in der Kontinuumstheorie komplett heraus. Ausgehend von einer aus der magnetischen Suszeptibilität bestimmten Druckabhängigkeit der magnetischen NN Kopplung, $\frac{d\ln J}{dp} \approx$

$-7\%/\mathrm{GPa}$, und der Änderung von T_{SP} unter Druck kann eine überaus starke Druckabhängigkeit der Frustration abgeleitet werden, $\frac{d\ln\alpha}{dp} \approx 24\%/\mathrm{GPa}$. Das unfrustierte Modell kann den experimentell beobachteten Anstieg der kritischen Temperatur auch qualitativ nicht erklären. Unter Verwendung der Druckabhängigkeiten der mikroskopischen Parameter wird anschließend das Verhalten des Verhältnisses aus Lücke und kritischer Temperatur untersucht. Auch hier kann nur das frustrierte Modell den experimentellen Verlauf erklären.

Die Beschreibung des SP Phasenübergangs bei endlicher Temperatur kann unter Verwendung von impulsabhängigen Dimer-Dimer-Korrelationsfunktionen auf eine beliebige sinusoidale Modulation verallgemeinert werden. Damit ist auch der U/I-Phasenübergang zugänglich. Technisch ist dies anspruchsvoller als die Untersuchung des U/D-Übergangs, da dort nur der Gitterimpuls $k = \pi$ eine Rolle spielt. Zunächst wird eine TMRG-Variante entwickelt, die die Berechnung der statischen Dimer-Dimer-Korrelationsfunktion für beliebige Abstände bei endlicher Temperatur erlaubt. Eine numerische Fourier-Transformation führt schließlich auf die impulsabhängige Response-Funktion, die die SP Temperatur implizit definiert.

Die TMRG-Rechungen ermöglichen eine erneute Analyse des Phasendiagramms von CF im Hinblick auf Abweichungen durch die Kontinuumsnäherung. Während die U/D-Grenze der numerischen Rechnungen mit CF und, wie bekannt, mit dem Experiment übereinstimmt, zeigen sich beim U/I-Phasenübergang Abweichungen. Die TMRG-Untersuchungen verbessern dabei die Ergebnisse im Bezug auf das Experiment. In jedem Fall ist diese Übereinstimmung wegen zweier Tatsachen bemerkenswert. Erstens lassen sich die thermodynamischen Daten, wie zuvor gesehen, nicht mit einem unfrustrierten Heisenberg-Modell vereinbaren. Andererseits zeigt eine Analyse auf der Basis der konformen Feldtheorie drastische Änderungen, wenn die korrekte Magnetfeldabhängigkeit der involvierten Skalendimension berücksichtigt wird. In diesem Fall geht auch die qualitative Übereinstimmung mit den TMRG-Ergebnissen verloren.

Im Vergleich mit $CuGeO_3$ wird das Phasendiagramm des geeignet frustrierten, d.h. $\alpha = 0.35$, Heisenberg-Modells untersucht. Es zeigt sich insbesondere, daß die Lage der Phasengrenzen von der Frustration abhängt. Damit ist das Phasendiagramm aus theoretischer Sicht nicht universell. Verglichen mit dem Experiment fällt die Übergangstemperatur des U/D-Übergangs langsamer, während die Asymptotik der U/I-Grenzlinie bei zu tiefen Temperaturen liegt. In Anbetracht der Tatsache, daß das vorliegende Modell thermodynamische Daten hervorragend reproduziert, ist dieser Befund überraschend.

Es gibt eine Reihe denkbarer Ursachen, um die beobachteten Unstimmigkeiten zu verstehen. Im Rahmen des strikt eindimensionalen Zugangs wird die schwache, aber dennoch vorhandene, Zwischenkettenkopplung nicht berücksichtigt. Wie bereits bei der Diskussion der Singulett-Triplett-Lücke erläutert, kann die Dispersion senkrecht zur Kette durch die Bildung des Mittelwertes approximativ einbezogen werden. Dies ist äquivalent zu einer Reskalierung des Magnetfeldes. Andererseits stabilisiert die magnetische Kopplung der Ketten untereinander eine inkommensurable Modulation, da der Grundzustand der I-Phase magnetisiert ist. Der U/I-Phasenübergang wird damit zu höheren Temperaturen hin verschoben. Auf der Basis des eindimensionalen Modells wird zudem der Einfluß einer Kopplung der Phononen an die Wechselwirkung von übernächsten Nachbarn untersucht. Es zeigt sich hierbei ebenso, daß der Übergang von der uniformen in die inkommensurable Phase bereits bei höheren Temperaturen stattfindet. Qualitativ können so die vorliegenden Abweichungen verstanden werden. Eine quantitative Analyse erweist sich aufgrund der zahlreichen unbestimmten Parameter jedoch als schwierig.

Ich versichere, daß ich die von mir vorgelegte Dissertation selbständig angefertigt, die benutzten Quellen und Hilfsmittel vollständig angegeben und die Stellen der Arbeit – einschließlich Tabellen, Karten und Abbildungen –, die anderen Werken im Wortlaut oder dem Sinn nach entnommen sind, in jedem Einzelfall als Entlehnung kenntlich gemacht habe; daß diese Dissertation noch keiner anderen Fakultät oder Universität zur Prüfung vorgelegen hat; daß sie – abgesehen von unten angegebenen Teilpublikationen – noch nicht veröffentlicht worden ist sowie, daß ich eine solche Veröffentlichung vor Abschluß des Promotionsverfahrens nicht vornehmen werde. Die Bestimmungen dieser Promotionsordnung sind mir bekannt. Die von mir vorgelegte Dissertation ist von Herrn Professor Dr. J. Zittartz betreut worden.

Köln, den 3. April 2000

Teilpublikationen:

A. Klümper, R. Raupach, F. Schönfeld, *Finite temperature density-matrix-renormalization-group investigation of the spin-Peierls transition in* $CuGeO_3$, Phys. Rev. B **59**, Seite 3612 (1999)

R. Raupach, A. Klümper, F. Schönfeld, *Pressure dependence and non-universal effects of microscopic couplings on the spin-Peierls transition in* $CuGeO_3$, cond-mat/9908407 (submitted to Eur. Phys. J. B)

R. Raupach, A. Klümper, *On the spin-Peierls phase diagram of frustrated Heisenberg chains*, in preparation

Danksagung

Zunächst danke ich Herrn Prof. Dr. J. Zittartz herzlich für die Vergabe und Betreuung der vorliegenden Arbeit. Das aktuelle und interessante Thema sowie die nötigen Voraussetzungen zur selbständigen, wissenschaftlichen Arbeit haben wesentlich zum Gelingen beigetragen.

Besonderer Dank gilt auch Herrn Prof. Dr. Andreas Klümper, dessen hervorragende Einfälle die Entwicklung dieser Arbeit vorangebracht haben. Die lehrreiche und fruchtbare Zusammenarbeit, unzählige Hinweise und Tips sowie anregende Diskussionen waren stets hilfreich.

Desweiteren danke ich Friedhelm Schönfeld für die angenehme und ideenreiche Zusammenarbeit, Andreas Schadschneider für zahlreiche Informationen und Literaturhinweise sowie Bernd Büchner und Thomas Lorenz für die Bereitstellung der experimentellen Daten und aufschlußreiche Diskussionen.

Ich danke Kai Schneider und Christian Scheeren für das bereitwillige Korrekturlesen und den damit verbundenen Zeitaufwand.

◇

Schließlich möchte ich meiner Familie - insbesondere meinen Eltern, meiner Schwester und meinem Opi - danken, ohne die ich einige schwierige Phasen nicht so einfach gemeistert hätte.

Mein Dank gilt auch Carina für die vielen schönen Momente im Leben jenseits der Arbeit.

Lebenslauf

Persönliche Daten

Name:	Rainer Raupach
Geburtsdatum:	10.01.1972
Geburtsort:	Berlin
Eltern:	Jürgen Raupach und Ulrike Raupach, geb. Bamberger
Familienstand:	ledig
Staatsangehörigkeit:	deutsch

Schulbildung

1978 – 1982	Kath. Grundschule in Odenthal-Blecher
1982 – 1991	Freiherr-vom-Stein-Gymnasium in Leverkusen
Juni 1991	Abitur
Juli 1991 – Sept. 1992	Zivildienst

Hochschulstudium

Okt. 1992	Immatrikulation an der Universität zu Köln, Studiengang Physik (Diplom)
Sept. 1994	Vordiplom
Sept. 1997	Abschluß der Diplomarbeit bei Prof. Dr. J. Zittartz
ab Okt. 1997	Anfertigung der vorliegenden Dissertation unter Anleitung von Prof. Dr. J. Zittartz

Arbeitsverhältnisse am Institut für
Theoretische Physik, Universität zu Köln

Okt. 1995 – Sept. 1997	Studentische Hilfskraft
Okt. 1997 – Okt. 1998	Wissenschaftliche Hilfskraft
seit Nov. 1998	Wissenschaftlicher Mitarbeiter